AD-A113 384 CLARKSON COLL OF TECHNOLOGY POTSDAM NY F/G 20/14
DEFINITION AND LOCATION OF HOMOGENEOUS REGIONS IN RADAR BACKSCA--ETC(U)
FEB 82 B A BLACK, M AROZULLAH, S T CUMMINGS F30602-80-C-0192

UNCLASSIFIED RADC-TR-82-10 NL

1 OF 2
AD A
113384

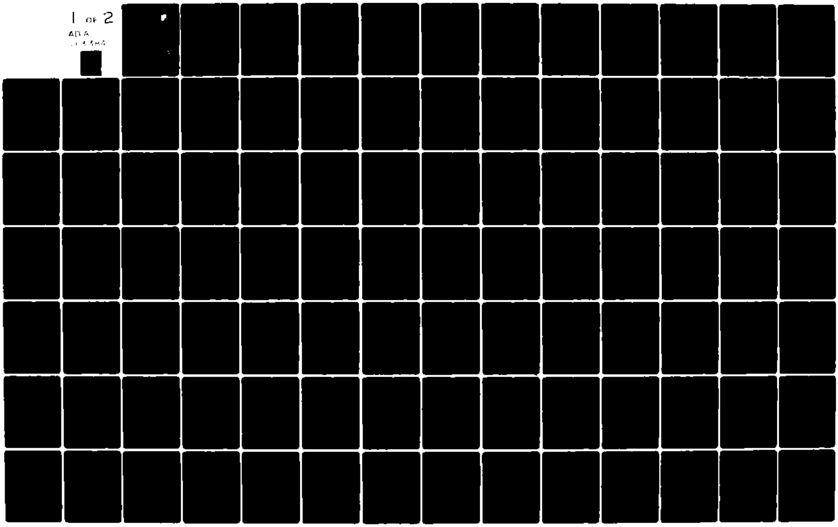

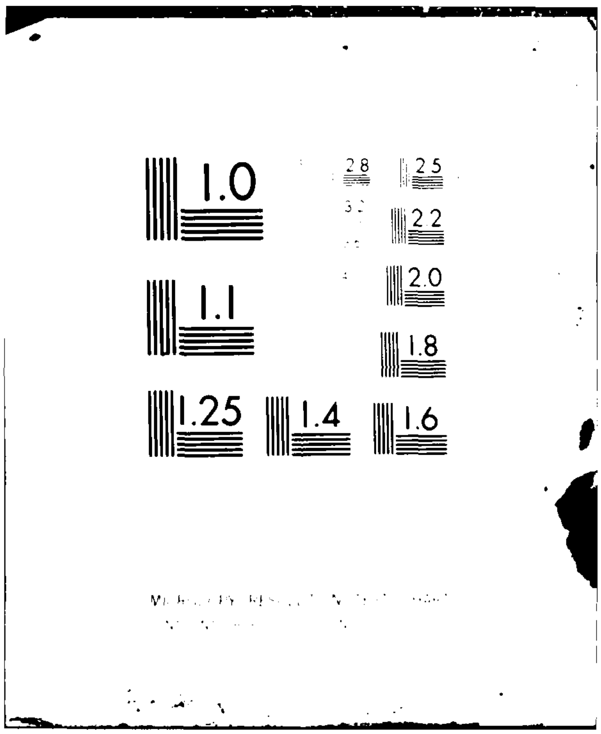
1.0
2.8
2.5
2.2
2.0
1.1
1.8
1.25
1.4
1.6

(12)

RADC-TR-82-10
Phase Report
February 1982

DEFINITION AND LOCATION OF HOMOGENEOUS REGIONS IN RADAR BACKSCATTER

Clarkson College of Technology

Bruce A. Black
Mohammed Arozullah
Steven T. Cummings

ROME AIR DEVELOPMENT CENTER
Air Force Systems Command
Griffiss Air Force Base, New York 13441

This report has been reviewed by the RADC Public Affairs Office (PA) and is releasable to the National Technical Information Service (NTIS). At NTIS it will be releasable to the general public, including foreign nations.

RADC-TR-82-10 has been reviewed and is approved for publication.

APPROVED: William L Simkins, Jr

WILLIAM L. SIMKINS, Jr.
Project Engineer

APPROVED: Frank J Rehm

FRANK J. REHM
Technical Director
Surveillance Division

FOR THE COMMANDER: John P. Huss

JOHN P. HUSS
Acting Chief, Plans Office

If your address has changed or if you wish to be removed from the RADC mailing list, or if the addressee is no longer employed by your organization, please notify RADC (OCTS) Griffiss AFB NY 13441. This will assist us in maintaining a current mailing list.

Do not return copies of this report unless contractual obligations or notices on a specific document requires that it be returned.

UNCLASSIFIED

SECURITY CLASSIFICATION OF THIS PAGE (When Data Entered)

REPORT DOCUMENTATION PAGE		READ INSTRUCTIONS BEFORE COMPLETING FORM
1. REPORT NUMBER RADC-TR-82-10	2. GOVT ACCESSION NO. AD-A113 384	3. RECIPIENT'S CATALOG NUMBER
4. TITLE (and Subtitle) DEFINITION AND LOCATION OF HOMOGENEOUS REGIONS IN RADAR BACKSCATTER		5. TYPE OF REPORT & PERIOD COVERED Phase Report May 1980 - August 1981
		6. PERFORMING ORG. REPORT NUMBER N/A
7. AUTHOR(s) Bruce A. Black Mohammed Arozullah Steven T. Cummings		8. CONTRACT OR GRANT NUMBER(s) F30602-80-C-0192
9. PERFORMING ORGANIZATION NAME AND ADDRESS Clarkson College of Technology Potsdam NY 13626		10. PROGRAM ELEMENT, PROJECT, TASK AREA & WORK UNIT NUMBERS 61102F 2305J909
11. CONTROLLING OFFICE NAME AND ADDRESS Rome Air Development Center (OCTS) Griffiss AFB NY 13441		12. REPORT DATE February 1982
		13. NUMBER OF PAGES 176
14. MONITORING AGENCY NAME & ADDRESS(if different from Controlling Office) Same		15. SECURITY CLASS. (of this report) UNCLASSIFIED
		15a. DECLASSIFICATION/DOWNGRADING SCHEDULE N/A

16. DISTRIBUTION STATEMENT (of this Report)

Approved for public release; distribution unlimited.

17. DISTRIBUTION STATEMENT (of the abstract entered in Block 20, if different from Report)

Same

18. SUPPLEMENTARY NOTES

RADC Project Engineer: William L. Simkins, Jr. (OCTS)

19. KEY WORDS (Continue on reverse side if necessary and identify by block number)

Isodistributive Definition
Rough Clutter Definition
Clutter Intensity and Spectrum

20. ABSTRACT (Continue on reverse side if necessary and identify by block number)

Two definitions of radar clutter homogeneity are presented and tested on clutter data supplied by the Signal Processing Laboratory at Rome Air Development Center. The two-dimensional spectra of clutter regions are individually tested for compliance with the rough clutter definition. The isodistributive definition utilizes a non-parametric (Kruskal-Wallis) statistical test to locate clutter regions whose individual resolution cells possess identical backscatter populations. The regions which

DD FORM 1473, 1 JAN 73 EDITION OF 1 NOV 65 IS OBSOLETE

UNCLASSIFIED

SECURITY CLASSIFICATION OF THIS PAGE (When Data Entered) conform to the rough clutter definition of homogeneity are seen to be areas of low intensity backscatter or areas dominated by thermal noise. The isodistributive regions that are located in the clutter data correspond to the areas between high-intensity regions.

Table of Contents

List of Figures

Chapter One- Introduction and Statement of the Problem

Section 1.1- Introduction

> "The problems of radar clutter have been discussed in all the basic radar texts, and remain the subject of extensive current research. Interest in clutter is almost universal in radar because most of the echo signals received at the radar originate not from the desired target but from surrounding objects or surfaces which tend to mask the target signal. The technologies of MTI, doppler resolution, and high-resolution pulse compression have been driven by the need to separate targets from the clutter background, and the basic decisions in radar system engineering are dependent upon the details of the clutter environment in which the radar is expected to operate."
>
> \- David K. Barton [1]

Clutter has been defined as a conglomeration of unwanted radar echoes [2]. The undesirability of such echoes is related to the application of the radar. To airborne radar in search of aircraft, clouds, terrain, and man-made structures are clutter sources. However, to airborne ground-mapping radar and meteorological radar, targets of interest include terrain and clouds. Aircraft echoes are extraneous returns to these types of radar and are thus clutter. The terms clutter and backscatter will be used interchangably in this report.

The dependence of radar system design upon the statistics of local clutter is the fundamental motivation of the present study. Whereas forecasting techniques which are based on theoretical terrain models exist, it is desirable that more accurate clutter prediction methods be developed and applied to such design problems. In particular, a prognostication of the clutter environment of a land-based, search radar formed on information supplied by topographic maps would be advantageous in both the selection of future radar sites and the eventual design of the radar system.

In the search for a relationship between clutter and topographic features, the ground clutter received by land-based, search radar is of prime concern. The main constituents of ground clutter are terrain echoes, returns from man-made structures, and reflections from bodies of water. This type of clutter may be divided into two categories: 1) returns from point scatterers, and 2) returns from distributed scatterers. A point scatterer is an object whose entire volume may be wholly contained in a single resolution cell of the radar. In contrast to the point scatterer, the distributed scatterer comprises many individual scatterers within a resolution cell so that this type of scatterer is useful in describing objects which are large in comparison to the radar resolution. Common examples of point scatterers and distributed scatterers are water towers and mountainsides, respectively.

Radar design decisions are sensitive to the projected clutter environment. A basic tenet of radar system design is the necessity to reduce clutter echoes while maintaining or enhancing target echoes. The objective of this principle is the optimization of radar performance in regard to target discernment by either human operators or automatic radars. Clutter is a much greater problem in automatic radar than in manned radar. The automatic radar must be designed to self-adjust to the clutter statistics of each resolution cell so as to maintain control over the system's false alarm rate. For this reason, the clutter environment must be known if radar performance is to be satisfactory. Clutter statistics can also greatly influence the selection of the fundamental radar features and parameters that may be employed for clutter reduction. These features include moving target indication (MTI), small resolution cell size, multiple beams in elevation, swept gain, and so on.

An accurate clutter forecast of a future radar site from the surrounding topographic features would supply information to the radar designer which may prove to be indispensible. The determination of clutter forecasting techniques involves the invention of accurate clutter models. Two approaches to determining clutter models may be taken. The first involves the description of terrain to be used as a basis in formulating a scattering model which may include such parameters as ground reflectivity and doppler spread. The scattering model would then be used to predict the clutter environment of existing radar. This prediction would be compared for accuracy to the real clutter environment. The second approach to this problem involves a different tack. Instead of beginning with topographic features and then proposing a clutter model, this second method analyzes clutter returns from areas of unknown topography. Features of the clutter returns are determined and areas described so that relationships between the clutter and the topography of the radar environment may be sought. The advantage of this approach is that preconceived ideas as to the association of topography and clutter can not influence the final determination. This is the approach taken in this thesis.

The traditional approach to clutter analysis has been to measure the backscatter return from different types of terrain [3,4,5]. Quite often, an effective radar cross-section or a reflectivity coefficient was assigned to characterize the terrain types. However, these measurements have yielded results which are sensitive to the physical environment and the system parameters of the radar. For example, the difference in backscatter measurements for a section of terrain measured when dry and then measured again shortly after being irrigated has proven to be as great as 5-7dB [6]. Also, wind velocity, when changed sufficiently, can cause large swings in backscatter measurements taken from vegetated areas such as forests or wheat fields [7].

The inconsistency of terrain backscatter measurements has prodded researchers to attempt to gain a greater understanding of clutter through the analysis of actual returns. Haykin has published papers on the spectral classification of clutter. The spectral analysis employed the maximum entropy method to compute doppler spectra of radar clutter [8]. Also, Haykin has attempted to classify clutter according to a one-dimensional spectral analysis by transforming the clutter into a one-dimensional sequence [9]. In addition to these studies, many researchers have attempted to characterize the statistical nature of clutter [10,11]. The traditionally accepted clutter distribution was the Rayleigh distribution. However, recent publications have opposed this view [12]. The realization that clutter may not be strictly Rayleigh distributed has come from the analysis of clutter data.

Section 1.2- Statement of the Problem

The specific problem which is considered in this thesis is the definition and location of homogeneous regions in radar clutter. The definitions of homogeneity that are presented in this thesis are tested on two data sets.

Section 1.3- Discussion of the Problem

It is necessary to define regions in radar clutter that are, in some sense, homogeneous so that the radar environment, which is generally quite extensive and complex, may be divided into its component parts. The existence of such homogeneous regions seems intrinsic to the topography-clutter relationship problem. However, the relationship may involve correspondence other than that suggested by considering topography alone, since this study considers the clutter itself as the basis of homogeneity. A definition of homogeneity based on clutter returns from the radar environment may not involve the types of homogeneity that topography may infer, e.g., forests, cornfields, and mountains. It is conceivable that a homogeneous region defined on a clutter return map may not be homogeneous with respect to its topography.

The work, which has this thesis as a result, involved the analysis of three data sets supplied by Rome Air Development Center (RADC). The first is a clutter intensity plot of the Utica, New York area. The

Utica clutter map is 81 degrees in azimuth and ranges from 9 kilometers to 27 kilometers from the radar site. The second data set consists of ten statistically independent clutter plots of an area southwest of Rome, New York. These clutter maps were recorded at ten different frequencies. The region is located between azimuths 208 degrees and 232 degrees, and ranges from 14-20 nautical miles in relation to the radar at RADC. This area is dominated by two hills, West Stockbridge Hill and Eaton Hill. The third data set was taken from roughly the same area. It encompasses clutter returns within azimuths 205 degrees and 233 degrees, and ranges 14-20 nautical miles. The third data set was coherently detected so that doppler processing could be performed on the clutter measurements. Two definitions of homogeneity have arisen from the analysis of these three data sets.

The first definition of homogeneity is based on a two-dimensional power spectral analysis of the clutter data. Viewing the clutter returns as a two-dimensional signal in range and azimuth, it was reasoned that any area which yields a white, two-dimensional spectrum should be homogeneous. Such a definition would locate areas which either possess randomly distributed clutter intensities, or a single point scatterer as the main source of radar return. These point scatterers may be located by methods being developed by William Ladew in a concurrent study and thus are removable so that the first definition of homogeneity corresponds only to the random intensity areas.

The second definition of homogeneity requires the ten different frequency sweeps provided by the second data set. It is a definition which is based on regions which possess point-by-point identical populations, i. e., each point in the region represents a random variable with the same distribution as every other point. This definition relies on the Kruskal-Wallis test for identical populations [13].

Two-dimensional spectra were computed for the Utica area and for a mean value version of the West Stockbridge Hill area. This processing has led to the discovery of several areas in the Utica clutter map which are homogeneous under the first definition. The test for identical distributions was applied to the ten statistically independent frequency sweeps of the West Stockbridge Hill area. Many small homogeneous regions and several larger homogeneous regions under the second definition were found to exist. Doppler spectra and the corresponding doppler spreads were computed and plotted so that a doppler spread map could be compared with the homogeneous regions which were located.

The following is an outline of the remainder of this paper. Chapter Two describes the three data sets in detail. Chapters Three and Four motivate and define the two types of homogeneity. Chapter Five is divided into two sections, each discussing the results for one type of homogeneity. Chapter Six contains the relevant conclusions and presents suggestions for future work.

Chapter Two- Description of the Backscatter Data Sets

Section 2.1- The Radar

The ground clutter analyzed in this thesis consists of three data sets. All three sets were recorded with the experimental radar system located in Building 106 at RADC. This radar is an experimental coherent L-band system with real time operator control of a wide range of system parameters. While the basic system is capable of operating over 1175 to 1375 MHz, the standard operating configuration allows frequency agile operation over 1250 to 1280 MHz. Quadrature backscatter data is recorded through a flexible high-speed digital buffer memory. The system parameters that are operator selected and computer controlled are the following:

PRF	166 Hz to 6000 Hz
Bandwidth	60 MHz max. instantaneous (limited by A/D)
Coded waveforms	LFM or up to 1024 chip phase code (8 bit phase quantization)
Matched filtering	off-line array processor provides general purpose matched filtering in near real time
Pulse width	up to 360 microsecond (or 6% duty cycle)
Frequency	programmable or operator controlled
Burst mode	up to 15 pulses per burst
High speed recording buffer	10240 complex words (10 bit I and Q) A/D converters: 60 MHz @ 6 bits 20 MHz @ 8 bits programmable recording window: * start range * stop range * start azimuth * number of pulses per recording

The TWT transmitter can provide a peak power of 160 kW. The antenna used in the L-band system is an FPS-8 antenna with a 2.7 degree one-way azimuthal beamwidth.

Section 2.2- The Utica Data Set

The first set of clutter data consists of envelope-detected values which are quantized to eight bits. There are 81 recorded azimuths with 240 range cells per azimuth. The sector of ground is located between 100 and 180 degrees (0 degrees is true north) and ranges from 9 km to 27 km. This area includes the city of Utica and its surroundings. The significant radar and recording parameters are listed below:

radar frequency: 1265 MHz
radar peak power: 160 kW
radar pulse width: 0.002 msec
radar bandwidth: 1 MHz
A/D sample rate: 2 MHz
record range: 9-27 km
record azimuth: 100-180 degrees
3 dB beamwidth: 3 degrees

The parameters of pulse width, beamwidth, and A/D sample rate may be used to determine the resolution cell size and number of samples per cell. The pulse width τ may be inserted in the following equation to obtain the range resolution R_r:

$$R_r = \frac{c\,\tau}{2} = \frac{(3\text{x}10^8 \text{ m/s})(2\text{x}10^{-6}\text{s})}{2} = 300 \text{ m.} \tag{2.1}$$

where c is the speed of light in free space. The A/D sample rate of 2 MHz yields a value of range difference between samples as in the following equation:

$$R_r' = \frac{3\text{x}10^8 \text{ m/s}}{2\text{x}10^6 \text{ cycles/s}} \text{ x } \frac{1}{2} = 75 \text{ m.} \tag{2.2}$$

This corresponds to 4 samples per range cell since

$$N_R = \frac{300 \text{ m}}{75 \text{ m}} = 4. \tag{2.3}$$

In azimuth, the 3 dB beamwidth is the measure of resolution. The data were recorded in steps of 1 degree in azimuth. Therefore, the azimuthal resolution cell size is 3 samples. The azimuthal resolution cell size in meters varies from

$$R_A\Big|_{9\ \mathrm{km}} = \frac{2\pi d}{360^\circ} \times 3^\circ \simeq 471\mathrm{m}. \tag{2.4}$$

to

$$R_A\Big|_{27\ \mathrm{km}} \simeq 1414\ \mathrm{m}. \tag{2.5}$$

These resolution widths are the arcs subtended by an angle of 3 degrees. At 18 km, the azimuthal resolution is 942 meters. We may use this value as a representative azimuthal resolution size. Therefore, the average resolution cell size for the first set of envelope-detected, magnitude data is 300 m in range and 942 m in azimuth. The resolution cell is oversampled in both range and azimuth, and consists of 4 samples in range and 3 samples in azimuth.

The Utica data set is displayed in Figure 2.1. This radial graph is a simulated PPI display. The darker areas of the plot represent the areas of higher clutter return.

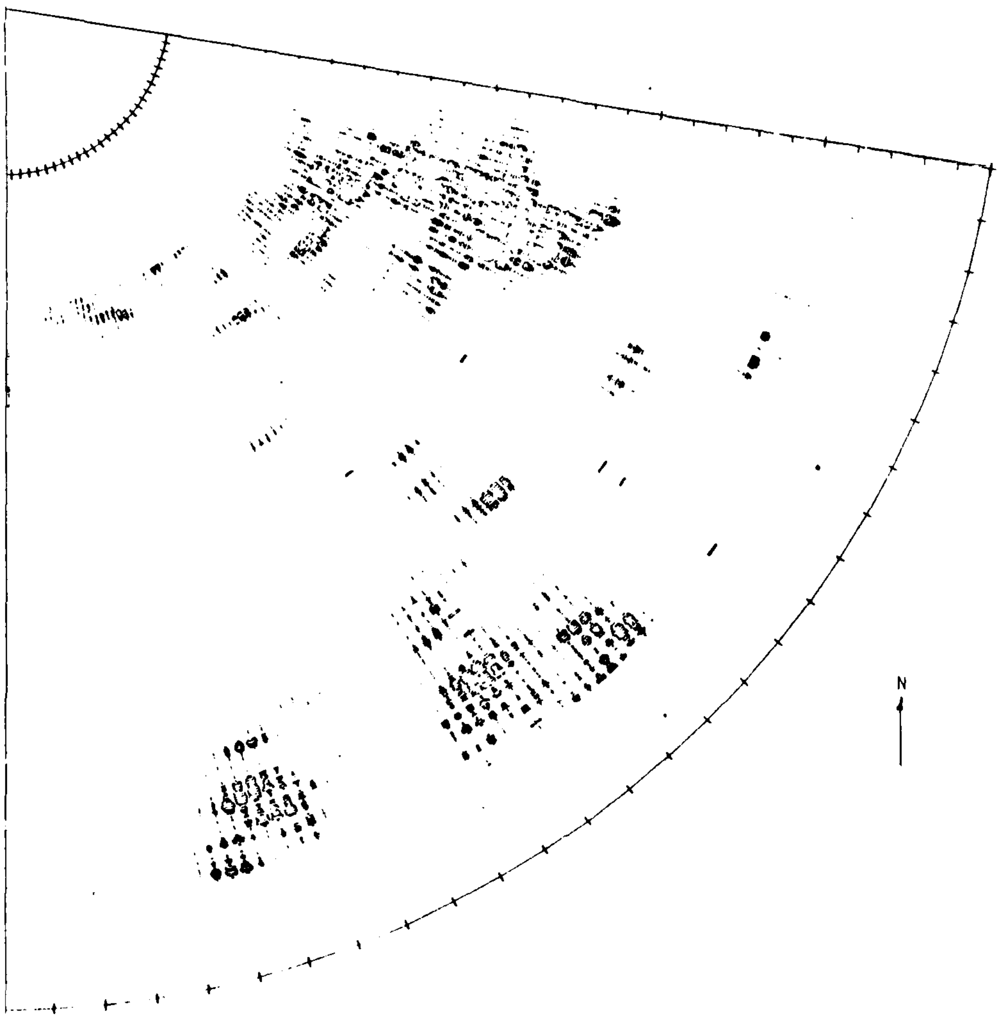

FIGURE 2 1- SIMULATED PPI DISPLAY OF UTICA DATA

Section 2.3- The West Stockbridge Hill Data Set

The second set of data was recorded using a 40 microsecond LFM pulse waveform. The pulse bandwidth was 2.5 MHz. The motivation for using the LFM waveform is that a long pulse with a high level of signal energy may be used to increase detection capability at no expense to range resolution. This is so because the LFM pulse may be compressed by using signal processing techniques to increase resolution. In this case, the compressed pulse width given by the following:

$$\tau_c = \frac{k}{B} \cong \frac{1.41}{2.5}\ \mu s = 0.564\ \mu s, \tag{2.6}$$

where k represents mainlobe broadening and B is the bandwidth of the LFM pulse, corresponds to a range resolution given by:

$$R_r = \frac{c\,\tau_c}{2} = 84.6\ \mathrm{m}. \tag{2.7}$$

As for the first data set, the 3 dB beamwidth, and hence the azimuthal resolution, is 3 degrees. Once again the beam is stepped in 1 degree increments yielding 3 samples per azimuthal resolution cell.

The data were recorded between azimuths 209 and 232 degrees, and ranges 25.9 and 33.9 km. The A/D sample rate was 5 MHz which gives 2 samples per range resolution cell. The overall resolution cell is 3 samples in azimuth and 2 samples in range. The azimuthal resolution width varies from 1356 m at 25.9 km to 1775 m at 33.9 km. The average azimuthal resolution is 1566 m, so that the average resolution cell size for the second data set may be taken to be 60 m in range and 1566 m in azimuth.

The data values were coherently detected and recorded in I (in-phase) and Q (quadrature) format. Quantization was to 23 bits of mantissa and 7 bits of exponent with a sign bit for each. The bit representation is in two's complement. The decimal value of the magnitude of I and Q was the value used in the data analysis.

The unique feature of this second data set is that it provides ten statistically independent radar scans of an area of ground southwest of RADC that includes West Stockbridge Hill and part of Eaton Hill. The statistical independence was obtained by frequency hopping the radar from 1253 MHz to 1280 MHz in steps of 3 MHz. The separation in frequency is sufficient to guarantee statistical independence but is not enough to change the reflectivity coefficients of the ground. Therefore, the ten numerical values associated with each range-azimuth sample may be regarded as ten statistically independent samples of a random variable. To ensure spatial independence for subsequent statistical testing, one range-azimuth sample from each resolution cell was selected. This was done by resampling at one-third the original rate in azimuth and one-fourth the rate in range. Thus, the data per cell are reduced to ten statistically independent samples of a random variable, which is the value of backscatter magnitude return from each cell. This is the data set used to identify homogeneous regions under the second definition of homogeneity.

A version of the West Stockbridge Hill data set is displayed in Figure 2.2. This data set is a mean value per resolution cell representation of the original data set.

Section 2.4- The Coherently Detected Stockbridge Data Set

The third set of data was recorded using a 6.4 microsecond, 5 MHz bandwidth, LFM pulse. The pulse compression was done off-line as for the second data set. The weighting used was Taylor weighting [14] with 6 equi-amplitude sidelobes 40 dB down from the main lobe. A total of ten azimuths were recorded from 205 to 232 degrees in 3 degree increments. This means that each recorded azimuth is independent of every other azimuth. Each azimuth was divided in range into six range windows, each consisting of 50 range samples. The 50 samples were computed from the 50 samples in the window plus 30 samples preceding the window. This computation was performed by the aforementioned pulse compression routine.

Now, each range window in each azimuth is illuminated with 128 pulses at a pulse interval of 6 milliseconds. These pulses are generated and detected coherently so that their echoes may be used to estimate the relative vector-sum velocity of the scatterers in an area of ground corresponding to the resolution cell, which is the same size as for the second data set. The samples per cell, however, are one in

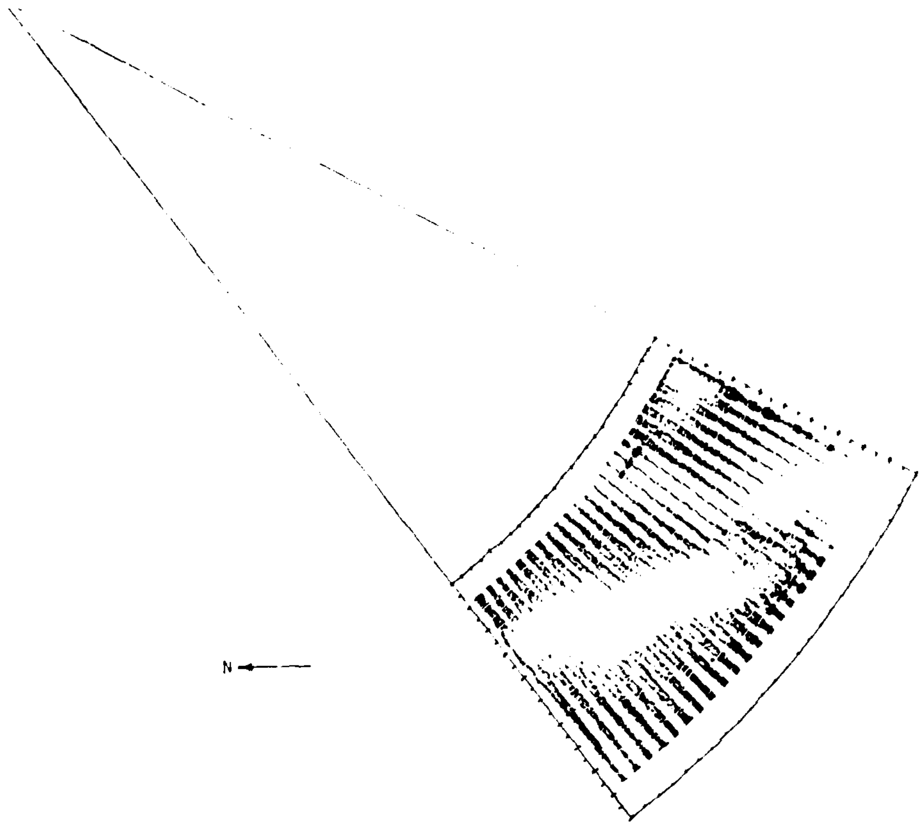

FIGURE 2 1 - SIMULATED PPI DISPLAY OF WEST STOCKBRIDGE HILL MEAN VALUE DATA azimuth and two in range. Each pulse is sampled at every point in the range window so that the data for one range window after compression is a two-dimensional array, 50 samples by 128 samples. The magnitude quantization for the third data set is the same as for the second data set.

Chapter Three- The Rough Clutter Definition

This chapter describes the motivation, methodology, and results for the first definition of homogeneity presented in this thesis.

Section 3.1- The Motivation

Radar ground clutter may be viewed as a two-dimensional signal when the magnitude of the returns are represented as a function of range and azimuth. While the radar is in operation, the antenna is rotated in azimuth, and magnitude return measurements are made at finite range intervals. This scanning process may be regarded as a two-dimensional convolution of the antenna beam pattern with the ground reflectivity. The two-dimensional signal generated by this convolution represents the interaction of the radar beam with the ground surrounding the radar.

Now, if the ground reflectivity within a particular region varies erraticly from resolution cell to resolution cell, one would expect the two-dimensional clutter sequence which represents the area to appear as a rough surface. Furthermore, this type of region should possess a two-dimensional spectrum that is irregularly structured, i. e., the two-dimensional spectrum is an uneven surface which flucuates around a constant level. If the spectra of an infinite number of such sequences were averaged, then this irregular structure would not appear. The averaged spectrum would be perfectly flat, or white. However, since this is not the case, the power spectrum of a single, finite-length segment of a rough clutter region will be an unevenly flucuating surface.

To detect this irregular structure, a test for "whiteness" must be applied to the two-dimensional spectral estimates. A test based on runs-above-and-below the median value was employed for this purpose [15]. A run is defined as a sequence of elements of the same kind, i. e., elements that are above or below the median. Any region whose spectrum passed this test was said to contain rough clutter in that the clutter intensity samples from that region could be represented by a rough two-dimensional surface. The statement of the rough clutter definition is the following:

Definition: A region which yields an irregularly structured two-dimensional spectrum, as determined by the runs-above-and-below the median test, is said to be homogeneous in that the region contains rough clutter.

Section 3.2- The Method of Spectral Estimation

The classical method of spectral estimation [16] is the method used in this thesis. This method involves the choice of a data window, or taper, which reduces the bias of the spectral estimates caused by finite-length data sequences. Next, the autocorrelation estimates of the tapered data sequence are computed. This is done by taking the squared magnitude of the Fourier transform of the tapered data and inverse transforming the resulting sequence. The periodogram is the inverse transform of the autocorrelation sequence. However, to reduce the effects of the unreliable autocorrelation estimates at large values of time delay, a lag window is applied to the autocorrelation sequence.

The two-dimensional extension of the classical method of spectral estimation is based on the two-dimensional discrete Fourier transform (DFT), whose implementation is seen to comprise the iterated application of a one-dimensional fast Fourier transform (FFT) algorithm. The following text presents this statement more formally.

The two-dimensional DFT of a sequence, x(m,n), is given by

$$X(k,\ell) = \sum_{m=0}^{M-1} \sum_{n=0}^{N-1} x\,(m,n) W_M^{km}\, W_N^{\ell n} \tag{3.1}$$

where $W_M = e^{-j\frac{2\pi}{M}}$

$W_N = e^{-j\frac{2\pi}{N}}$.

Now, equation (3.1) may be written as

$$X(k,\ell) = \sum_{n=0}^{N-1} G(k,n) W_N^{\ell n}, \tag{3.2}$$

where $G(k,n) = \sum_{m=0}^{M-1} x(m,n) W_M^{km}$.

The function, G(k,n), is seen to be the result of an application of a two-dimensional transform to each column of $x(m,n)$. Then, by applying the one-dimensional transform to each row of $G(k,n)$, the two-dimensional transform of $x(m,n)$ is obtained.

The above procedure is implemented through the use of an FFT subroutine. The data taper was chosen to be a raised cosine of width equal to 18.75% of the data sequence, or 2 points. (Note: The DC level is removed prior to tapering by subtracting a computed average value for each of the two-dimensional data segments to be transformed.) The taper was applied to each of the four edges of the two-dimensional finite-length sequence which was sixteen points in both dimensions. This size data sequence was chosen after some experimentation as the minimum length that would give reasonably good results. The lag window was chosen to be a Hanning window [16] of width equal to the length of the data sequence. The two-dimensional lag window was generated by rotating the appropriate one-dimensional window about the origin of the two-dimensional lag plane [17].

Section 3.3- The Test for Irregular Structure

The final set of power spectrum estimates are correlated with one another because of the convolution of the actual spectrum and the spectral lag window. Since the runs-above-and-below the median test for randomness assumes independence of samples, this spectral correlation must be dealt with in an appropriate manner. The two-dimensional equivalent noise bandwidth of the lag window was selected as a measure of the spectral correlation [16]. The two-dimensional noise bandwidth calculation is presented in Appendix A. The bandwidth is 3.13 spectral lines. Therefore, the spectra were sampled on the basis of every fourth spectral estimate in both azimuthal and range frequencies. The resulting set of spectral estimates was tested for irregular structure.

The test for irregular structure, or "whiteness", of the two-dimensional spectra is based on the runs-above-and-below the median test given in Hald [14]. The test is one-dimensional by nature and in order to apply it to the two-dimensional spectral data, the two-dimensional spectral estimates must be rearranged into a one-dimensional sequence (whereas this procedure does not affect the level of significance of the test, the sensitivity to alteratives may be affected, as will be discussed later). This was done by appending columns of constant azimuthal frequency to the next column of higher azimuthal frequency. The resulting one-dimensional sequence was tested at the 5% level of significance using the number of runs (>11.9) as the measure of significance. The number of runs which is significant may be computed as in [15]. Because of symmetry in the two-dimensional spectrum, only half the spectral estimates are needed in the test.

Section 3.4- The Calculation of Spectral Spreads

The spectra which are computed in order to locate homogeneous regions have been described by their two-dimensional spectral spreads. The two-dimensional spectral spreads are computed by projecting the spectral lines onto each frequency axis and then performing a variance calculation on the resulting function. This is presented more formally in the following.

The equation for the azimuthal spread is

$$\sigma_A^2 = \frac{\sum_{i=1}^{N} [\sum_{j=1}^{N} X(i,j)](i-1)^2}{\sum_{i=1}^{N} \sum_{j=1}^{N} X(i,j)} \tag{3.3}$$

And, similarly the range spread is

$$\sigma_R^2 = \frac{\sum_{j=1}^{N} [\sum_{i=1}^{N} X(i,j)](j-1)^2}{\sum_{i=1}^{N} \sum_{j=1}^{N} X(i,j)} \tag{3.4}$$

where N is the number of spectral lines along one dimension. The resulting numerical values are in units of spectral lines squared.

Section 3.5- Description of Results

The format of the two-dimensional data plots and spectral plots, which appear at the end of Chapter Five, is given in this section.

First, the three-dimensional representation of the backscatter intensity data sequence (referenced by the minimum range and azimuth sample appearing in the 16 by 16 point region) and the corresponding magnitude spectrum are given. The orientation of the range and azimuthal axes, as well as the range and azimuthal frequency axes, are shown on each plot. The frequency origin is located in the center of the spectral plane in the spectral magnitude plots. The azimuthal frequency increment is (0.5/16 cycles/degree) and the range frequency increment is (2.0/16 cycles/range cell).

Chapter Four- The Isodistributive Definition

This chapter describes the motivation, methodology, and the results for the second definition of homogeneity presented in this thesis.

Section 4.1- The Motivation

The West Stockbridge Hill data set provides ten statistically independent samples of backscatter return from each resolution cell. This type of data allows for the comparison of the underlying probability distributions governing the backscatter return from each cell. Such a comparison necessarily involves the selection and application of some form of statistical testing procedure to a group of resolution cells. The choice of which type of test to use must be based on what the user of the test hopes to accomplish. The objectives of the user, however, need not be overly restrictive as to the capabilities of the test. In the present case, it is desired that the test be capable of finding contiguous groups of resolution cells whose sets of ten backscatter samples are consistent with a null hypothesis of identical populations. As will eventually be seen, the criterion of contiguity is imposed for convenience of processing, and is not a restriction of the selected test.

In defining regions according to their topography, it seems reasonable that a region whose resolution cells contain comparatively similar ground types should be deemed homogeneous. The similarity is at best subjective. It may be that "resolution cells of similar ground types" may include cells which subdivide a forested lot, cultivated land, an urban area, or gently rolling hills. In addition to this, it seems fair to propose that areas of similar ground types will exhibit backscatter return distributions of a kind. However, these simple examples of ground types may not be of a sufficiently specific nature. It is quite probable that such factors as slope, soil type, and other less obvious characteristics of the ground that affect backscatter properties may be significant in determining what regions may be identified as "similar".

Taking the above into account, it is apparent that many different probability distributions might arise in the measurement of backscatter. Therefore, it seems both appropriate and prudent to use a statistical test which does not require prior knowledge of the probability distribution from which the samples to be tested are drawn. It is for this reason that the type of statistical test chosen was a non-parametric test. Furthermore, the specific test used should be a multi-sample test since the number of resolution cells that should be considered in one test run is undetermined a priori. Indeed, it may be necessary to vary the number of included cells so as to locate the largest regions which pass the test. The test described in the next section meets the above requirements and was used to locate regions which correspond to the following definition of homogeneity:

Definition: A contiguous set of resolution cells which exhibit no significant differences in the distribution of clutter are said to be homogeneous.

Section 4.2- The Kruskal-Wallis Test

The non-parametric statistical test chosen was the Kruskal-Wallis test for identical populations which is sensitive to unequal locations [13].

The test is performed by forming a table whose entries are the observations of backscatter. Each column of the table contains the ten backscatter observations of one particular resolution cell. The order in which the backscatter values of a cell are placed in the column is not important, but the backscatter values from a cell must all be entered in one column of the table. Now, the values of backscatter return are replaced in the table by their numerical ranks from lowest to highest with '1' corresponding to the lowest value of backscatter. The ranks are assigned by considering every observation to be from a single pool of samples so that ranks ascend in order from 1 to N, where N is the total number of observations in the group of cells tested. The rank sums for each column of the table are computed and their squares are used in calculating a statistic, H, according to the following equation:

$$H = \frac{12}{N(N+1)} \sum_{i=1}^{C} R_i(\overline{T}_i - \frac{N+1}{2})^2, \qquad (4.1)$$

where N= total number of observations
C= number of columns (or cells)
R_i= number of observations in column i

T_i= rank sum for column i

T_i= T_i/R_i, the mean value of ranks in column i

This equation is reducible to a form more conducive to calculation:

$$H = -3(N+1) + \frac{12}{N(N+1)} \sum_{i=1}^{C} \frac{T_i^2}{R_i} \tag{4.2}$$

The test assumptions that, along with the null hypothesis, are necessary to give the test statistic, H, its null distribution are 1) sampling is random, 2) sampling is with individual replacement, and 3) there are no tied observations.

The Stockbridge Hill data set meets the above assumptions. The data per resolution cell are random samples insofar as all the possible combinations of ten backscatter values have equal a priori probabilities of occurrence in each resolution cell. Hence, the requirement of the first assumption is satisfied. The second assumption is met even though the data are quantized. This is true since any quantum may be repeated. Now, it is possible that quantization could cause problems with the requirement imposed by the third assumption. However, no tied observations, i. e., no observations of equal value, were noted during the actual tests. If such tied observations had occurred, there exist methods for properly handling those instances [18].

An advantage in using H as the test statistic is that its distribution may be closely approximated by the chi-squared distribution in the case where R_i=R, i. e. all the R_i are equal. The approximation improves as R increases. In our case, R=10 and the chi-squared distribution is a very good approximation to the null distribution of H as can be seen in Appendix B which contains an explanation of why the distribution of H may be approximated by the chi-squared distribution.

The Kruskal-Wallis test, as described above, was applied to a version of the West Stockbridge Hill data which was formed by spatially subsampling the original data set. The cells were selected on the basis of every third sample in azimuth and every second sample in range so that one set of ten samples from each resolution cell of the radar appeared in the data. The subsampling was done to ensure spatial independence on the bases of 3 dB beamwidth and range resolution. The resulting data set comprised eight azimuths with 128 range samples per azimuth.

Section 4.3- Description of Results

The regions tested were of varying sizes. First, a group of four resolution cells, two in azimuth and two in range, was selected as a "window". Next, the length in range was doubled three times, so that windows of 2x4, 2x8, and 2x16, were used. The windows were passed over the data in a non-overlapping fashion and the resolution cells appearing in each window were tested against one another for similarity in their backscatter distributions. The results for the windows utilized are shown in Figures 5.2.2-5.2.5. Azimuth is the horizontal axis and range is the vertical axis in these plots. The crossed areas correspond to windows whose enclosed resolution cells passed the Kruskal-Wallis test. These crossed regions represent homogeneous regions under the second definition. Figure 5.2.6 presents the results of a test in which a 2-cell by 2-cell window was slid over the data so that successive tests overlapped in range and azimuth. This is a method for testing all combinations of four contiguous cells in a 2-cell square window. Figure 5.2.6 shows large regions which were selected for testing by looking for concentrations of small homogeneous regions in Figures 5.2.1-5.2.5.

Chapter Five- Presentation and Discussion of Results

Section 5.1- The Rough Clutter Definition

The results for the rough clutter definition of homogeneity are presented in Figures 5.1.3-5.1.83, which are located at the end of this section. In each figure the coordinates (e.g. "5X113") of the area tested are shown. Figure 5.1.1 is a three-dimensional plot of the Utica clutter intensity data. Figure 5.1.2 is a three-dimensional plot of the West Stockbridge Hill mean value data set.

The two-dimensional power spectral estimation routine was applied to areas in the Utica clutter map which were chosen as being characteristic of the overall map. The representative areas selected fall into four categories which are based on their backscatter intensity plots. First, regions of high intensity backscatter are depicted in Figures 5.1.3-5.1.8. Figure 5.1.9-5.1.19 shows eleven areas in which the greater values of intensity are concentrated in a localized "mound". The level of intensity varies over the eleven mounded areas presented. Figures 5.1.20-5.1.26 show areas that represent the low intensity backscatter regions that cover much of the Utica clutter map. Figures 5.1.27-5.1.28 graphically depict the results of the test for irregularly structured spectra. The graphs are representations of the sampled spectra with those values above the median marked by an "A" and those below by a "B". Figures 5.1.30-5.1.81 show the areas, spectra, and corresponding tests for irregularly structured spectra of the West

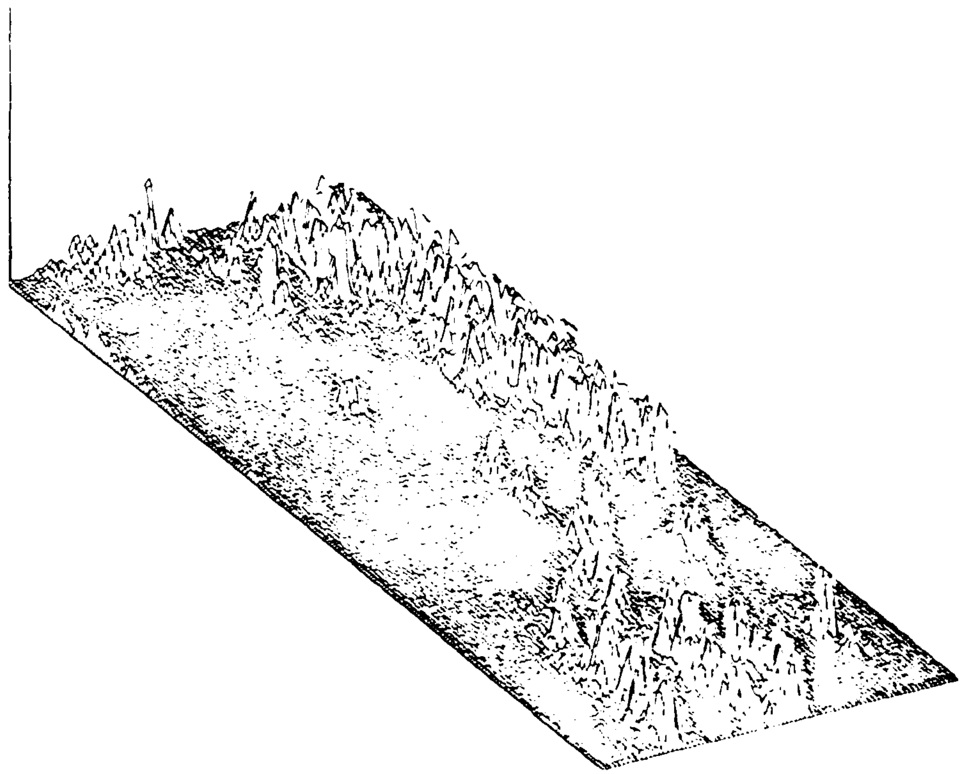

FIGURE 5.1.1- THREE-DIMENSIONAL PLOT OF THE UTICA DATA

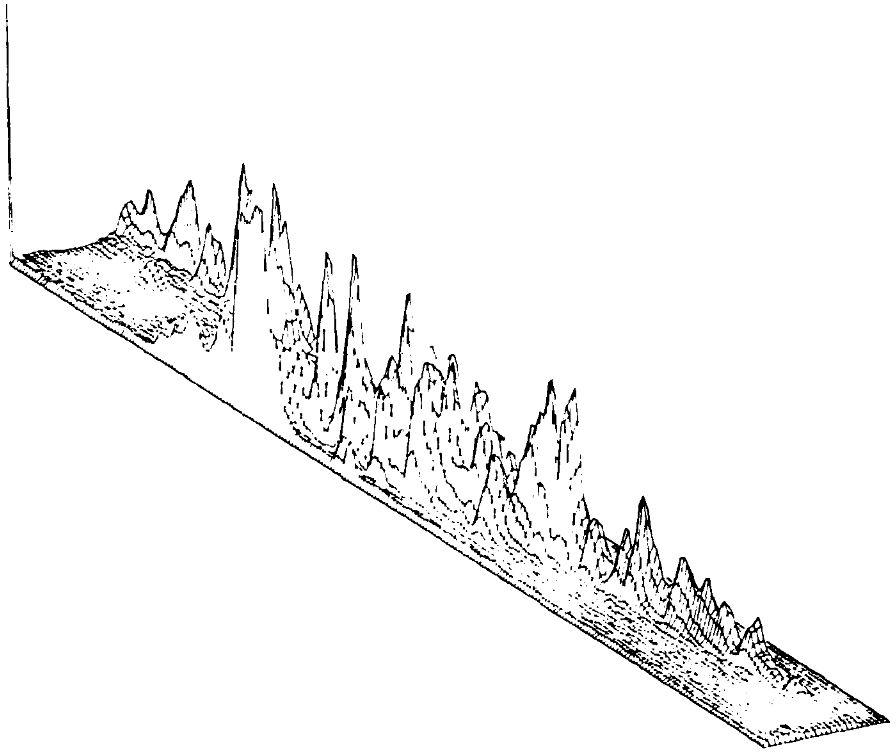

FIGURE 5 1 2- THREE-DIMENSIONAL PLOT OF THE WEST STOCKBRIDGE HILL MEAN VALUE DATA

Stockbridge Hill clutter map.

In Figures 5.1.3-5.1.8, we see six areas of the Utica clutter map which represent the high intensity areas of the map. The intensity for these areas flucuates wildly in both azimuth and range. These regions would appear to be prime candidates for rough clutter. However, as can be seen from the spectral plots, these areas comprise a few significant frequency components. These frequency components suggest a marked periodicity in the intensity sequence. Such an intensity sequence does not fit the rough clutter definition, the test for irregularly structured spectra indicates this fact clearly in that all the high intensity areas fail to be classified as homogeneous under the rough clutter definition.

The mounded (medium intensity) areas are shown in Figures 5.1.9-5.1.19. These areas yield spectra which are generally well-behaved surfaces in that they are relatively smooth. However, two of the spectra for this type of area pass the test for irregular structure. These observations may be attributed to the one-dimensional nature of the runs-above-and-below the median test and statistical chance. The fact that the spectra for the two "homogeneous" mounded areas pass the test for irregular structure is an example of the test's sensitivity to alternatives to randomness. Since these spectra are highly concentrated at low frequencies, short runs above the median are picked up by the test and an erroneous decision is made. Also, some irregular structure at high frequencies increases the likelihood that more than the critical number of runs above-and-below the median will be surpassed.

The flucuating areas in Figures 5.1.9-5.1.12 were thought to be candidates for rough clutter. However, the test for irregularly structured spectra proved this supposition to be inaccurate. None of these areas passed the test for homogeneity under the rough clutter definition. These failures are due to the fact that the flucuations are predominantly low frequency oscillations.

The results for the low intensity areas, shown in Figures 5.1.20-5.1.26 are interesting in that all these areas are homogeneous under the rough clutter definition. All the low intensity spectra passed the test for irregular structure (see Figure 5.1.28). This type of intensity plot is the kind which the rough clutter definition was designed to classify as rough clutter. The backscatter intensity surfaces can be seen to comprise small, uneven disparities from sample to sample. This uneveness is believed to arise from the combination of low intensity returns and the thermal noise in the radar receiver.

The two-dimensional spectral processing has located no rough clutter regions which are also high backscatter intensity areas. Although this fact does not preclude the existence of high intensity rough clutter regions in clutter maps other than those analyzed herein, it has indicated two possible reasons for the absence of such regions in the Utica and West Stockbridge Hill data sets: 1) the resolution cell size attenuates any high frequency components which might be present in the clutter signal, and 2) the data sequences represent areas that are so large that changes in ground elevation dominate the clutter signal and changes in ground cover do not appreciably affect the clutter signal.

To illustrate the effects of the resolution cell on the two-dimensional spectra of clutter regions, the two-dimensional spectrum of an approximation to the beam patterm is shown in Figure 5.1.29. Since the beam pattern is convolved with the ground, the clutter spectrum is multiplied by the beam pattern spectrum. This convolution of the beam with the ground severely attenuates the higher clutter frequencies.

The intensity and spectral plots for West Stockbridge Hill are shown in Figures 5.1.30-5.1.81. The results all show that no regions in the Stockbridge clutter map are homogeneous according to the rough clutter definition. This is because the two hills, Stockbridge and Eaton, dominate the map. The area covered by the spectral estimation is so large in azimuth, 1566 m, and so narrow in range, 480 m, that the hills dominate the frequency content of the clutter signal, so that little variation in the signal occurs in the range dimension, whereas one full period occurs in the azimuthal direction. This essentially yields very narrow, low frequency concentrated spectra.

The above discussion indicates that the area which the spectral estimation considers as a two-dimensional data sequence is too large in space. The handicap of limited radar resolution, coupled with the fact that the two-dimensional FFT performs poorly on short data sequences and thus requires at least sixteen clutter samples in both dimensions for good results, suggests that the area required in the spectral estimation

FIGURE 5.1.29

BEAM PATTERN APPROXIMATION

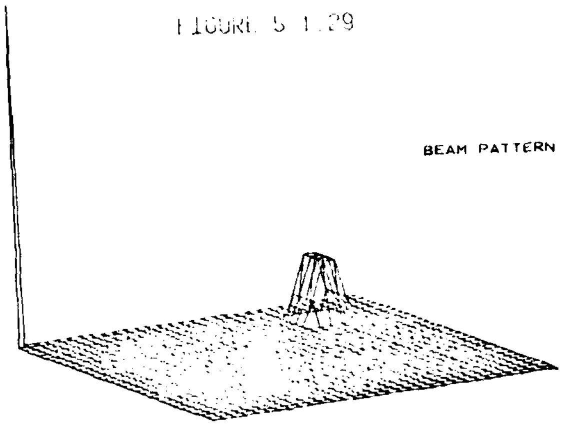

TWO-DIMENSIONAL SPECTRUM OF
BEAM APPROXIMATION

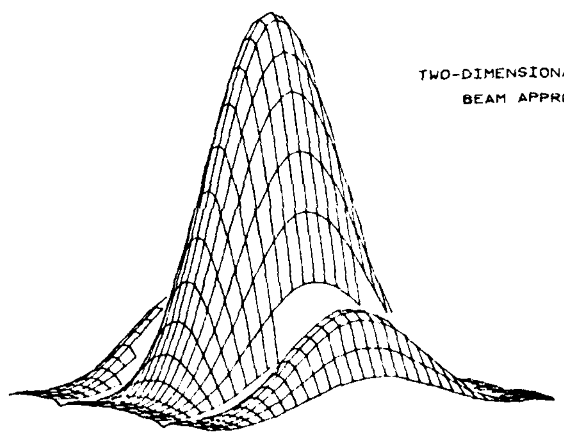

TWO-DIMENSIONAL SPECTRUM OF
BEAM APPROXIMATION IN DB

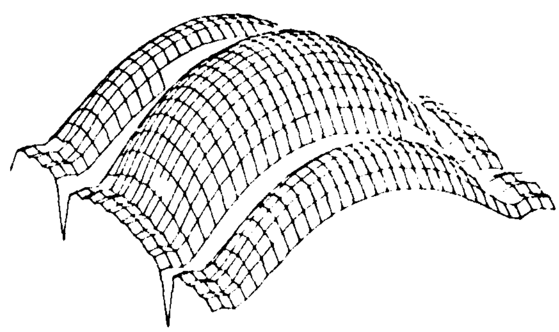

encompasses a ground surface which is simply too extensive and topographically complex to be considered homogeneous by this definition.

In Figures 5.1.82 and 5.1.83 , the scatter diagrams of the Utica and Stockbridge spectral spreads are shown, respectively. The Utica spectral spreads show that the low intensity areas which were found to be homogeneous, tend to cluster at large values of spectral spreads. Thus, the spectral spreads, or bandwidths, are useful in separating these areas from the mounded, or medium intensity, areas which were erroneously classified as homogeneous. The Stockbridge bandwidths do not exhibit any particularly significant clusterings. However, the areas closer to the radar (denoted by the alphanumeric characters ′123456789ABCDEFG′ in increasing distance from the radar) tend towards higher azimuthal bandwidths whereas the areas further from the radar tend towards lower azimuthal bandwidths. This phenomenon may be attributed in part to the increasingly poor azimuthal resolution as range increases. However, one can see that the areas which are farthest from the radar (denoted by ′G′) tend towards higher bandwidths. These areas are partially in the shadow region of the hills as were the homogeneous Utica areas.

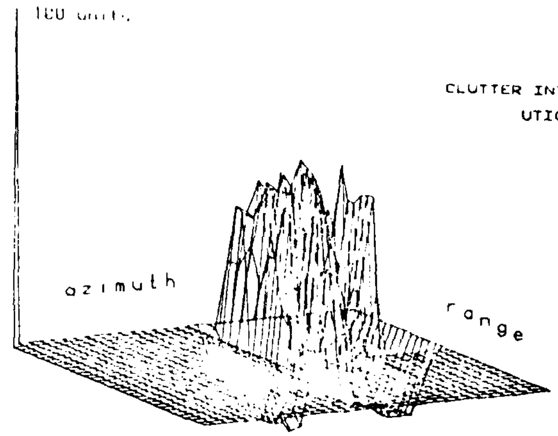

100 units
CLUTTER INTENSITY PLOT OF
UTICA 6X113
azimuth
range

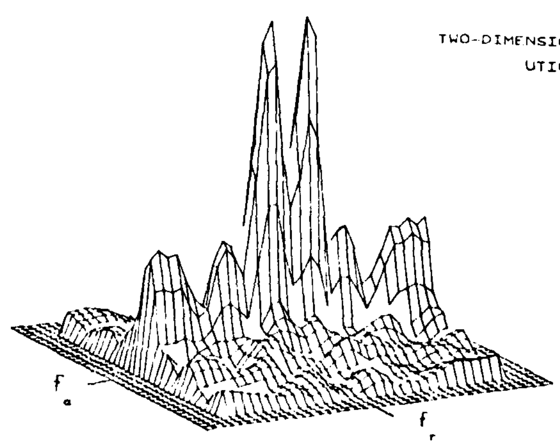

TWO-DIMENSIONAL SPECTRUM OF
UTICA 6X113
f_a
f_r

FIGURE 5 1 3

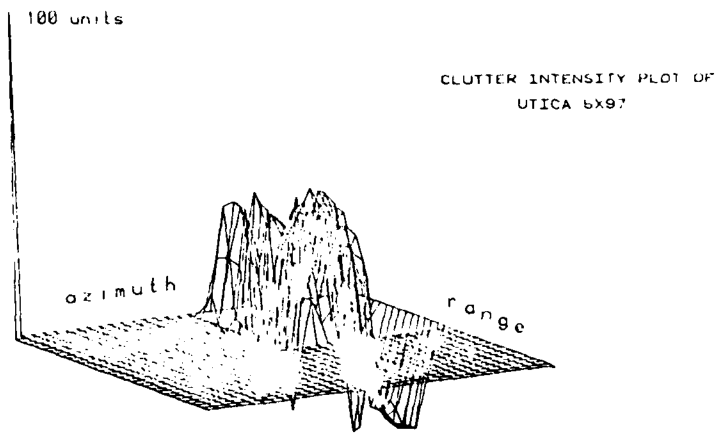
100 units
CLUTTER INTENSITY PLOT OF
UTICA 6X97
azimuth
range

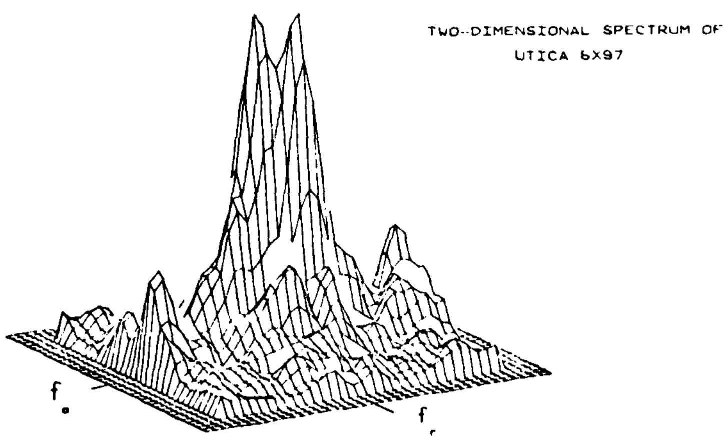
TWO-DIMENSIONAL SPECTRUM OF
UTICA 6X97
f_a
f_r

FIGURE 5 1 4

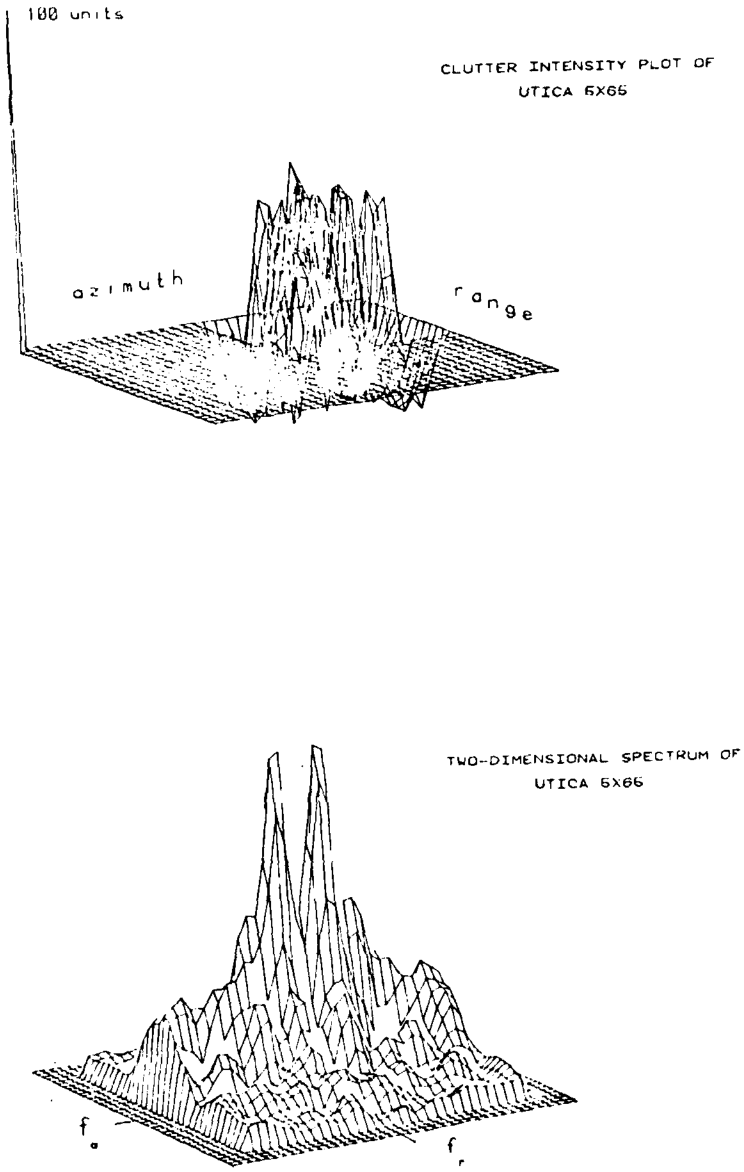
100 units
CLUTTER INTENSITY PLOT OF
UTICA 6X66
azimuth
range
TWO-DIMENSIONAL SPECTRUM OF
UTICA 6X66
f_a
f_r

FIGURE 5 1 5

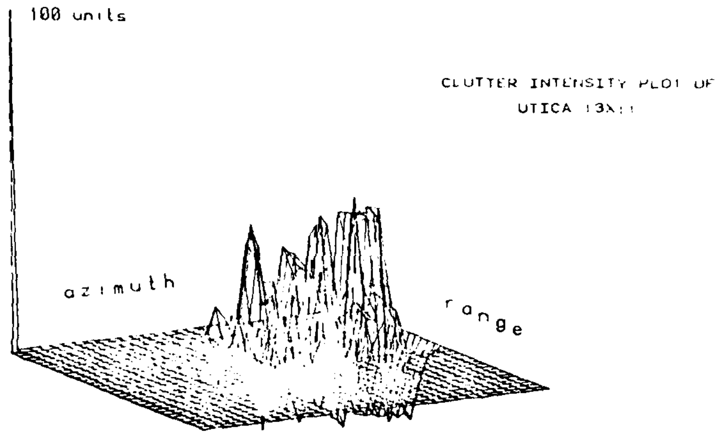
100 units
CLUTTER INTENSITY PLOT OF
UTICA 13X11
azimuth
range

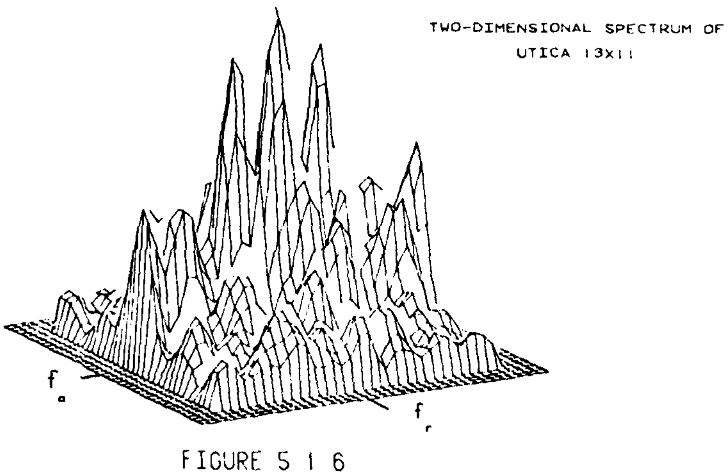
TWO-DIMENSIONAL SPECTRUM OF
UTICA 13X11

FIGURE 5 1 6

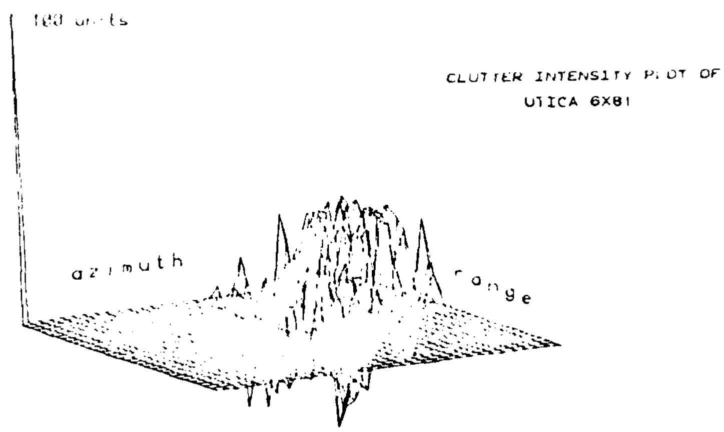

CLUTTER INTENSITY PLOT OF
UTICA 6X81
azimuth
range

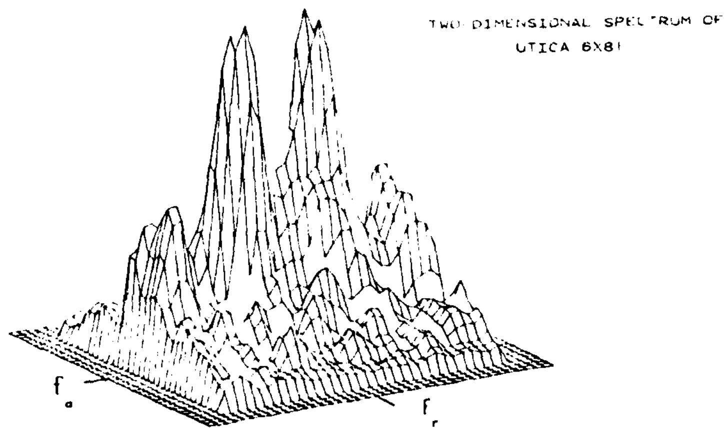

TWO DIMENSIONAL SPECTRUM OF
UTICA 6X81

FIGURE 5 1 7

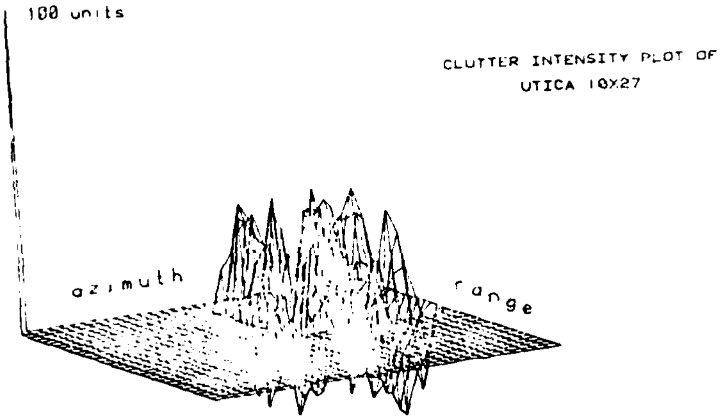
100 units
CLUTTER INTENSITY PLOT OF
UTICA 10X27
azimuth
range

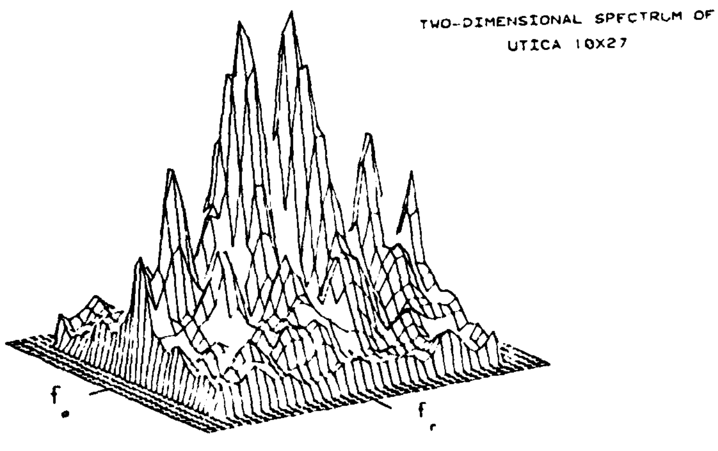
TWO-DIMENSIONAL SPECTRUM OF
UTICA 10X27
f_a
f_r

FIGURE 5.1.8

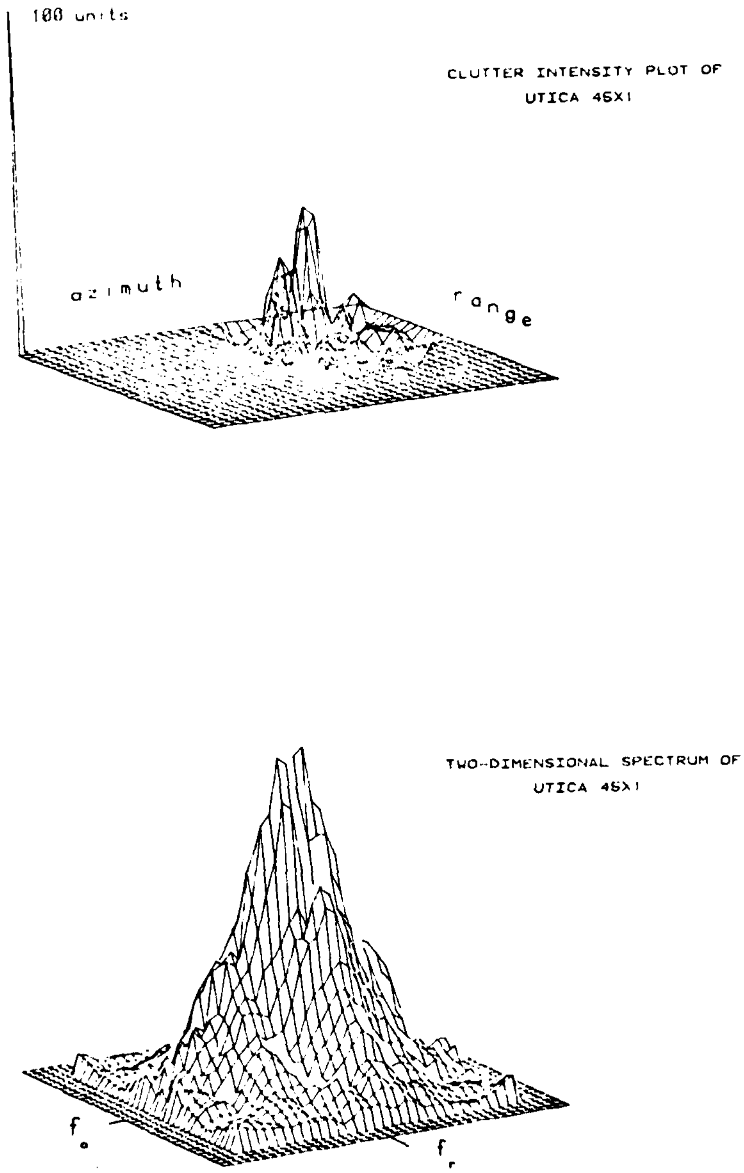
100 units
CLUTTER INTENSITY PLOT OF
UTICA 45X1
azimuth
range
TWO-DIMENSIONAL SPECTRUM OF
UTICA 45X1
f_a
f_r

FIGURE 5 1 9

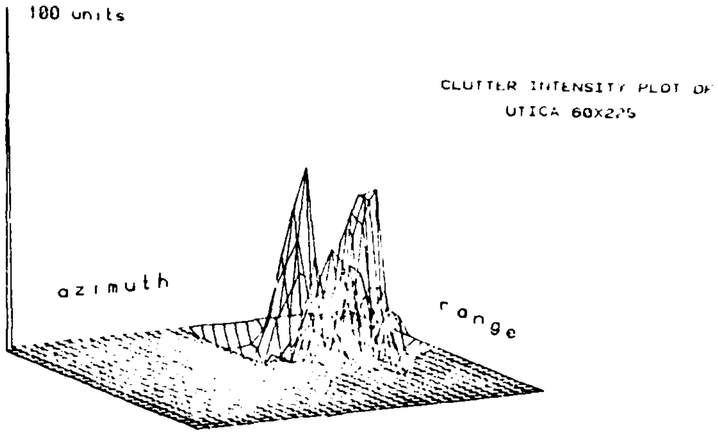
100 units
CLUTTER INTENSITY PLOT OF
UTICA 60X225
azimuth
range

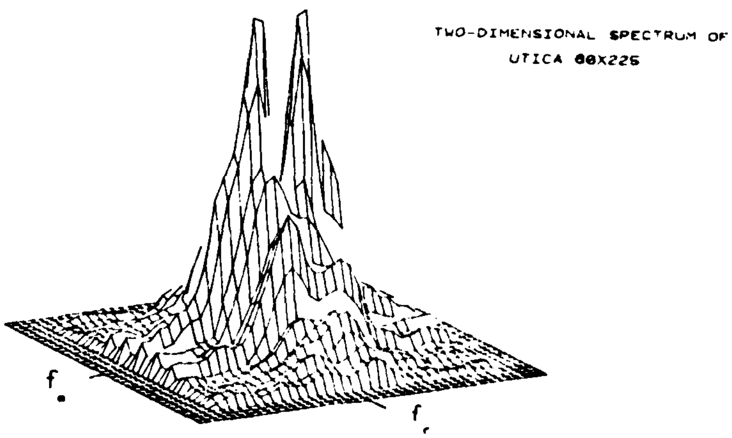
TWO-DIMENSIONAL SPECTRUM OF
UTICA 60X225

FIGURE 5 1 10

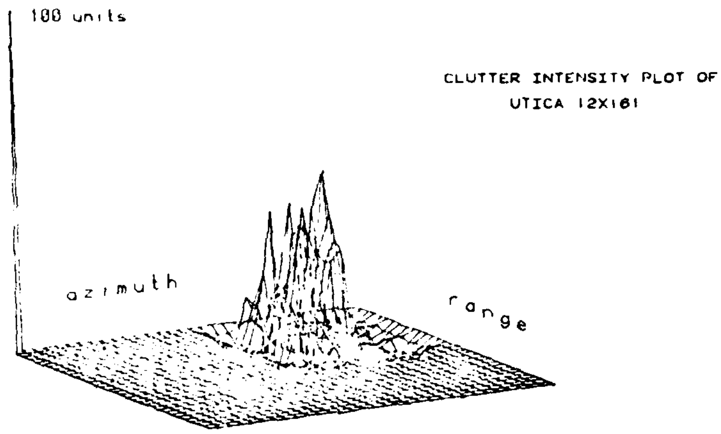
100 units
CLUTTER INTENSITY PLOT OF
UTICA 12X161
azimuth
range

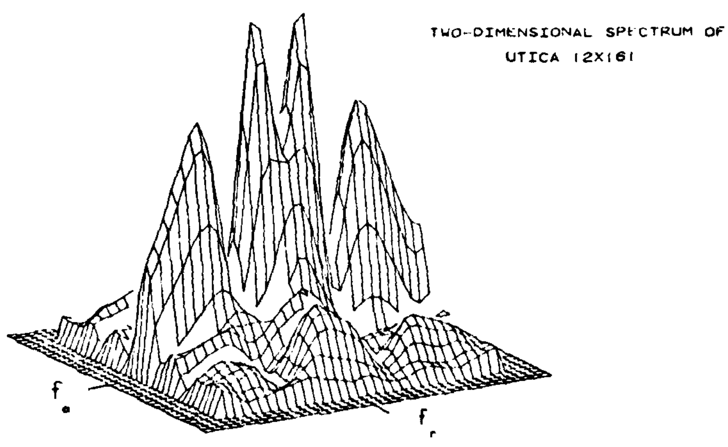
TWO-DIMENSIONAL SPECTRUM OF
UTICA 12X161
f_a
f_r

FIGURE 5.1.11

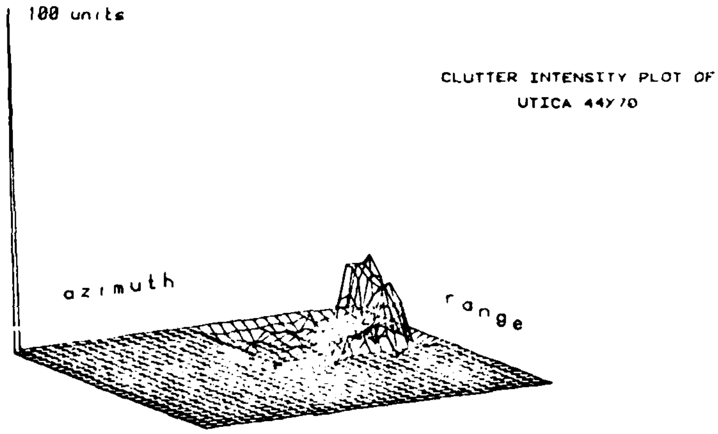
100 units
CLUTTER INTENSITY PLOT OF
UTICA 44X70
azimuth
range

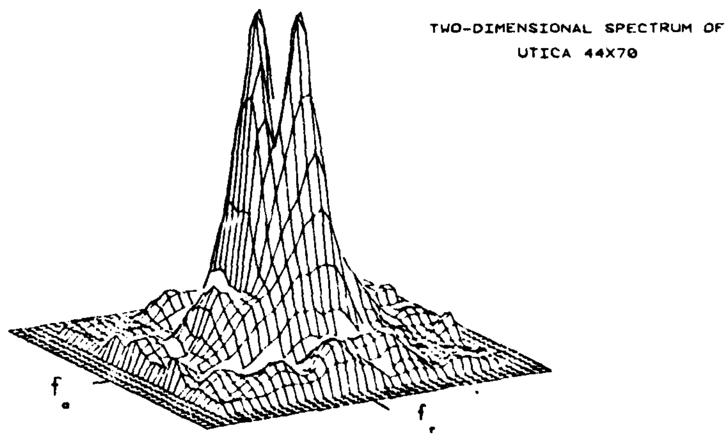
TWO-DIMENSIONAL SPECTRUM OF
UTICA 44X70
f_a
f_r

FIGURE 5 1 12

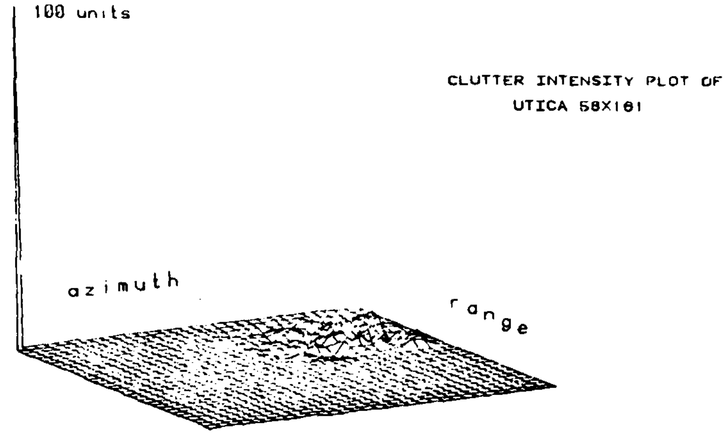
100 units
CLUTTER INTENSITY PLOT OF
UTICA 58X161
azimuth
range

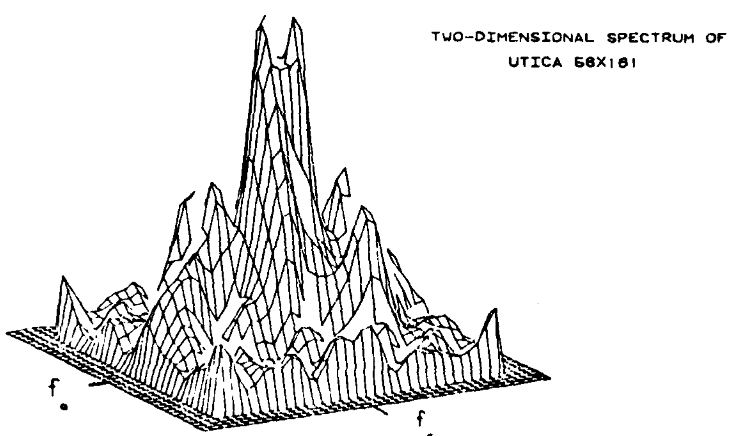
TWO-DIMENSIONAL SPECTRUM OF
UTICA 58X161
f_a
f_r

FIGURE 5 1 13

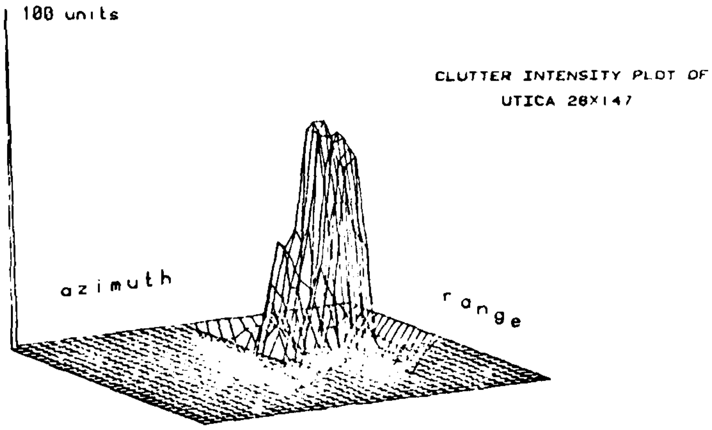
100 units
CLUTTER INTENSITY PLOT OF
UTICA 28X147
azimuth
range

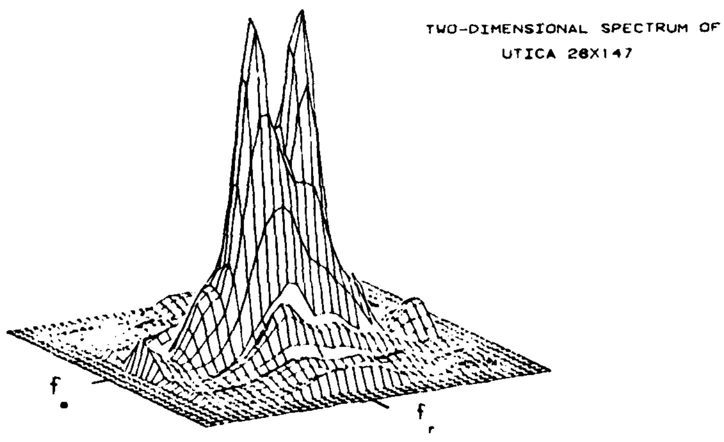
TWO-DIMENSIONAL SPECTRUM OF
UTICA 28X147
f
f

FIGURE 5 1 14

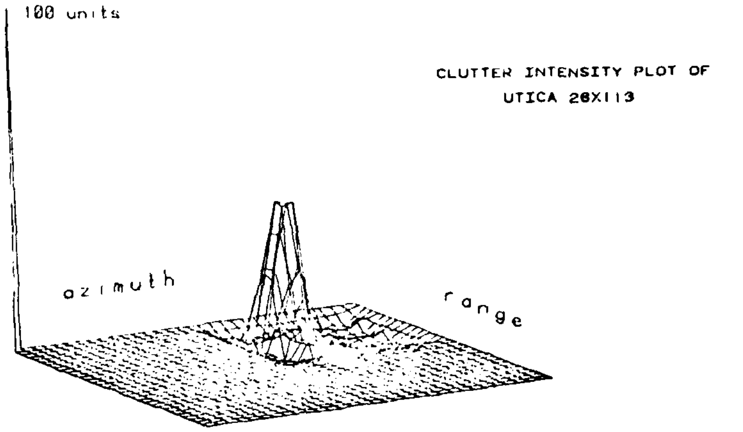
100 units
CLUTTER INTENSITY PLOT OF
UTICA 28X113
azimuth
range

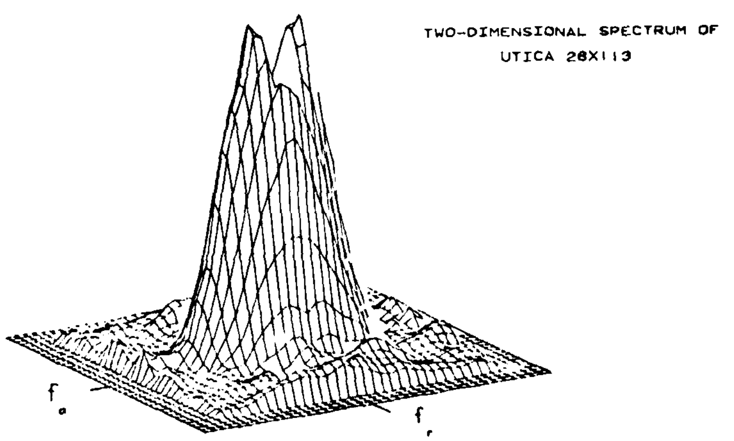
TWO-DIMENSIONAL SPECTRUM OF
UTICA 28X113

FIGURE 5 1 15

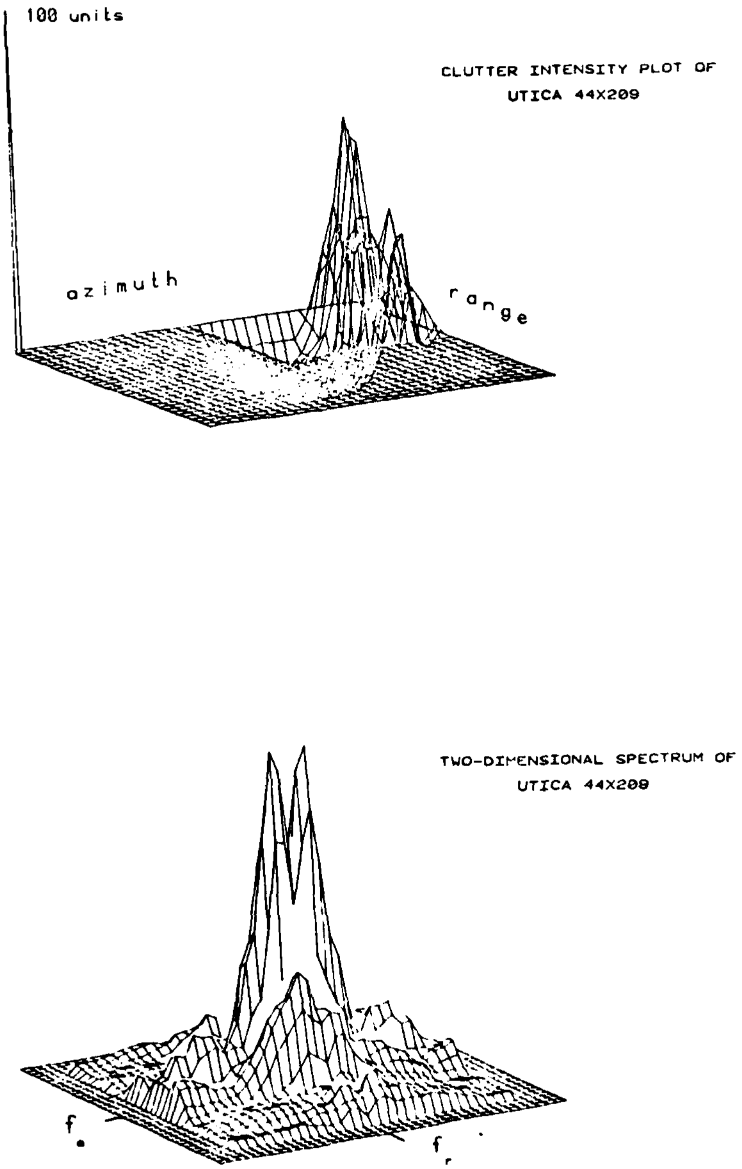

100 units
CLUTTER INTENSITY PLOT OF
UTICA 44X209
azimuth
range
TWO-DIMENSIONAL SPECTRUM OF
UTICA 44X209
f_a
f_r

FIGURE 5 1 16

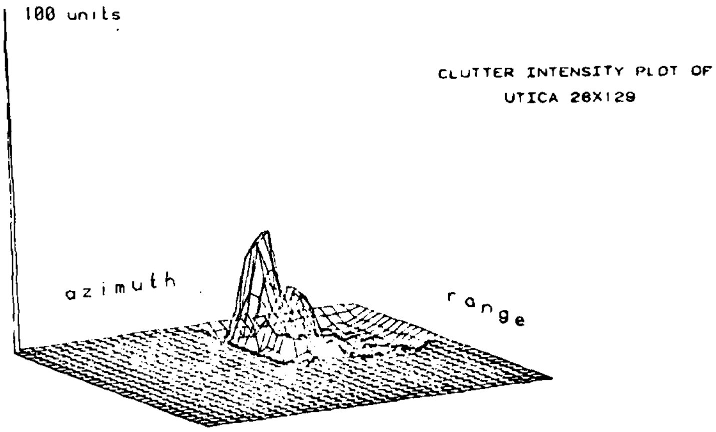
100 units
CLUTTER INTENSITY PLOT OF
UTICA 28X129
azimuth
range

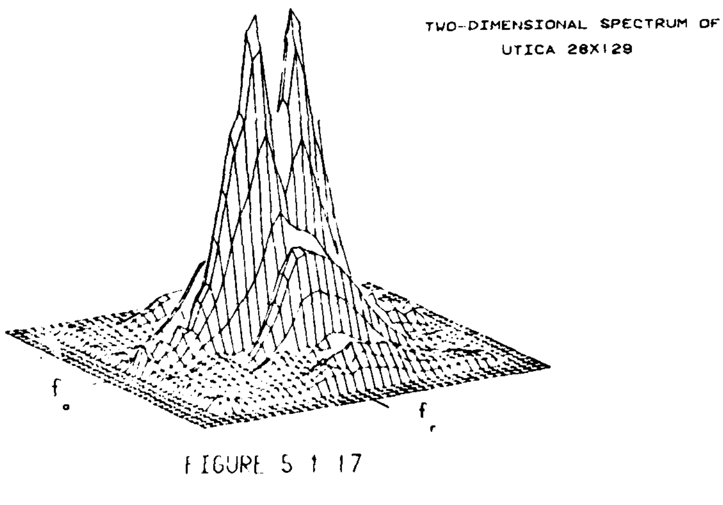
TWO-DIMENSIONAL SPECTRUM OF
UTICA 28X129
f_a
f_r

FIGURE 5.1.17

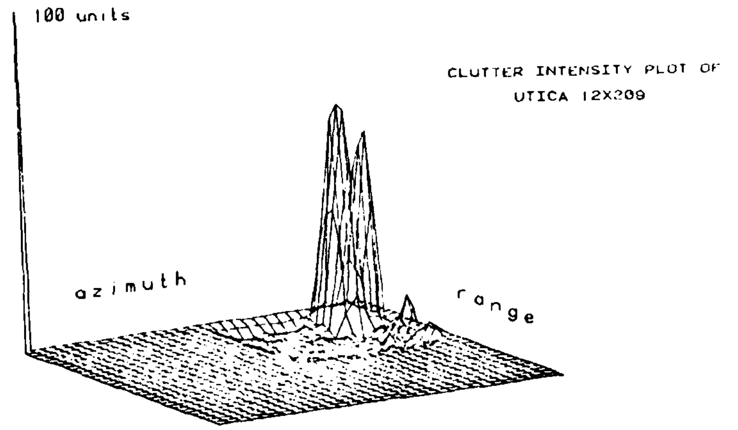
100 units
CLUTTER INTENSITY PLOT OF
UTICA 12X209
azimuth
range

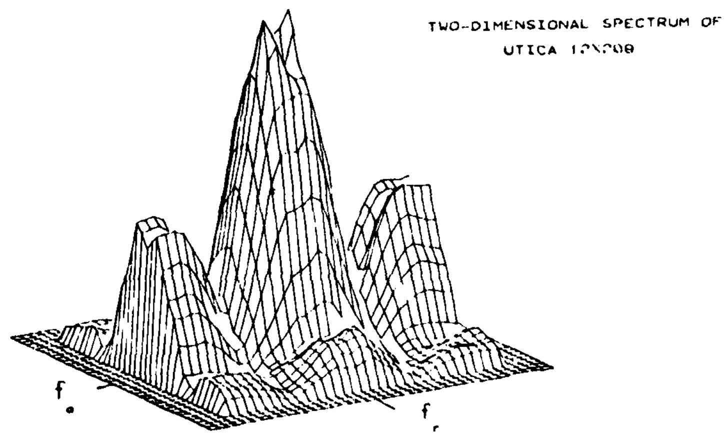
TWO-DIMENSIONAL SPECTRUM OF
f_a
f_r

FIGURE 5 1 18

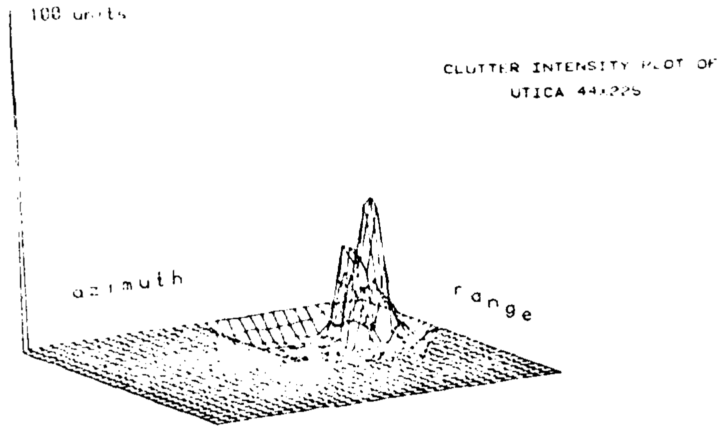
100 units
CLUTTER INTENSITY PLOT OF
UTICA 44X225
azimuth
range

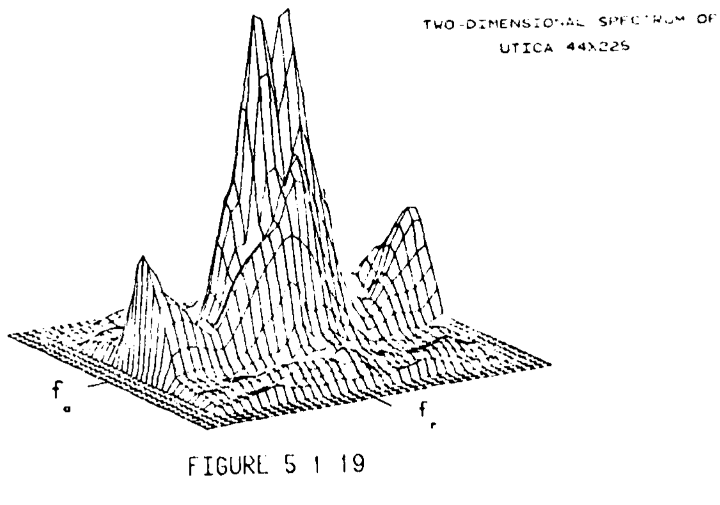
TWO-DIMENSIONAL SPECTRUM OF
UTICA 44X225
f_a
f_r

FIGURE 5 1 19

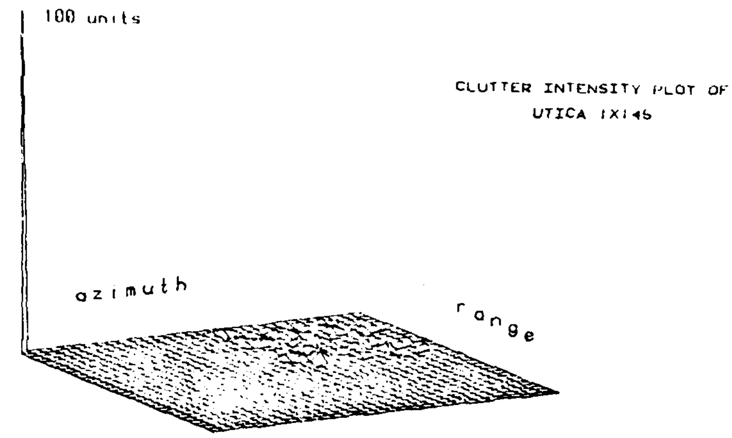
100 units
CLUTTER INTENSITY PLOT OF
UTICA 1X145
azimuth
range

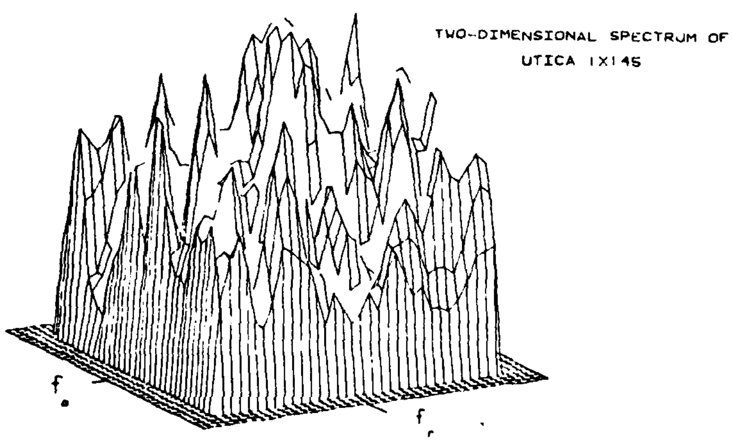
TWO-DIMENSIONAL SPECTRUM OF
UTICA 1X145
f_a
f_r

FIGURE 5 1 20

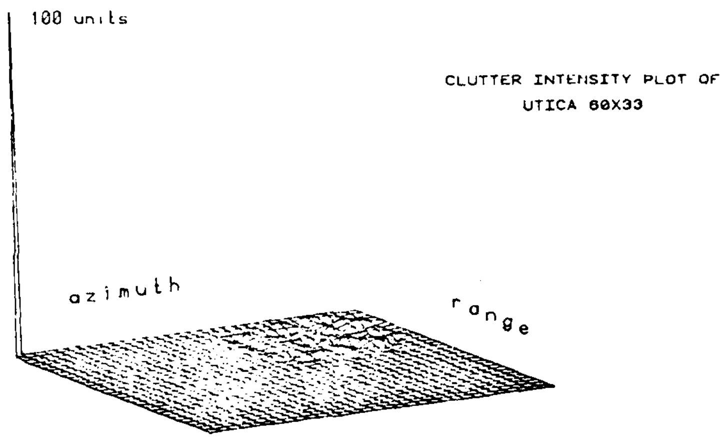
100 units
CLUTTER INTENSITY PLOT OF
UTICA 60X33
azimuth
range

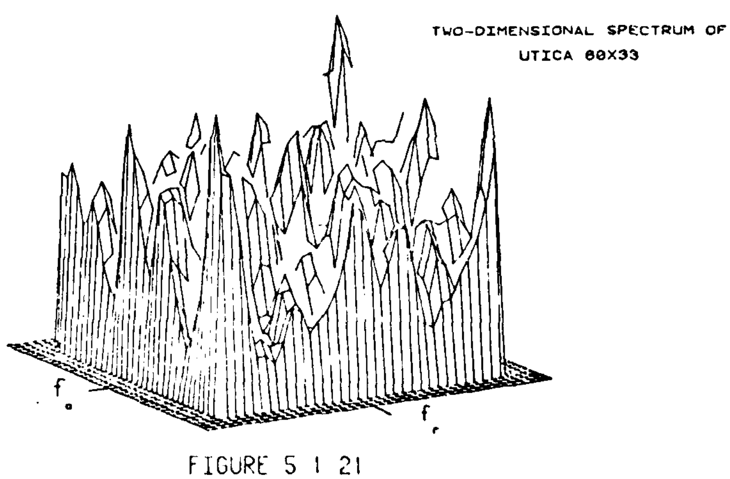
TWO-DIMENSIONAL SPECTRUM OF
UTICA 60X33
f_a
f_r

FIGURE 5 1 21

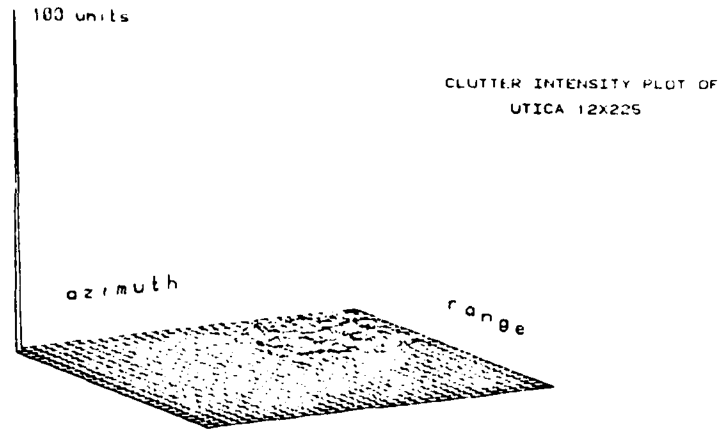
100 units
CLUTTER INTENSITY PLOT OF
UTICA 12X225
azimuth
range

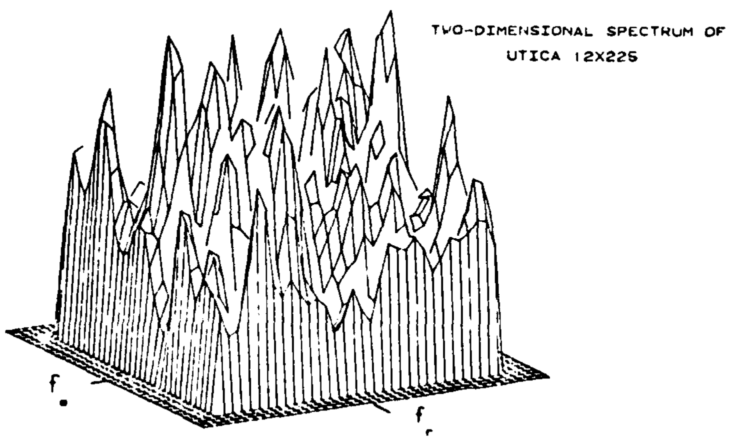
TWO-DIMENSIONAL SPECTRUM OF
UTICA 12X225

FIGURE 5 1 22

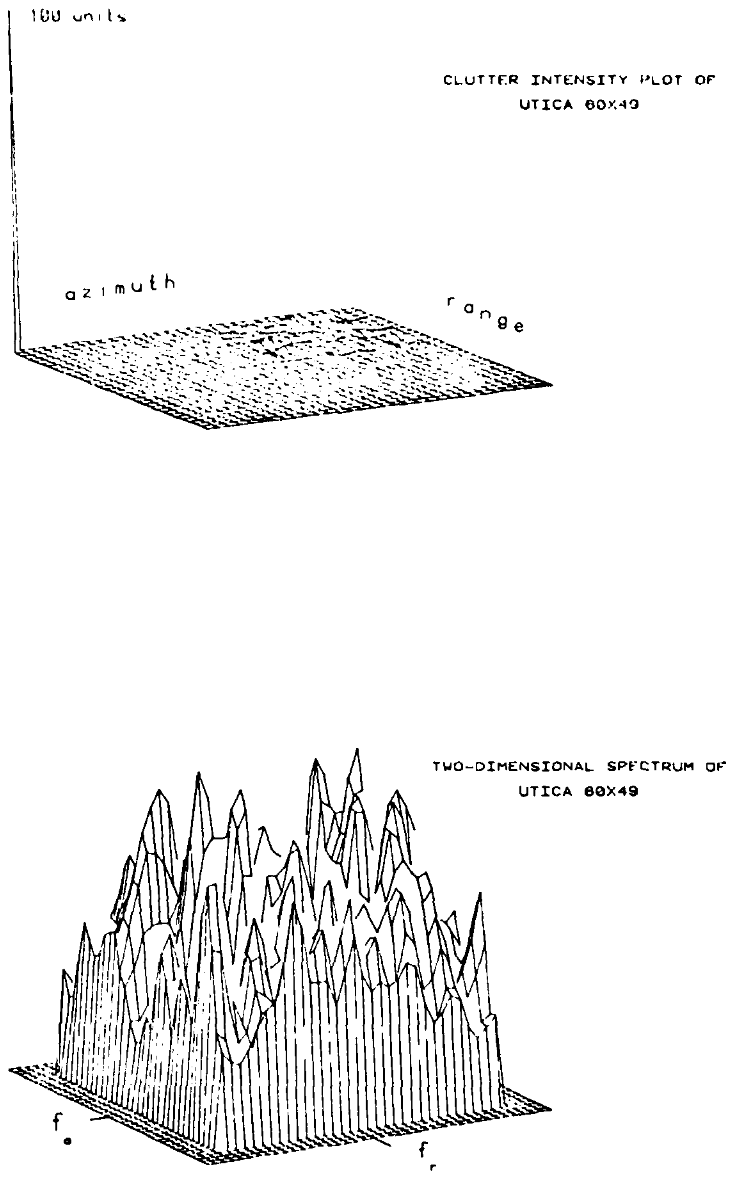
100 units
CLUTTER INTENSITY PLOT OF
UTICA 60X49
azimuth
range
TWO-DIMENSIONAL SPECTRUM OF
UTICA 60X49
f_a
f_r

FIGURE 5 1 23

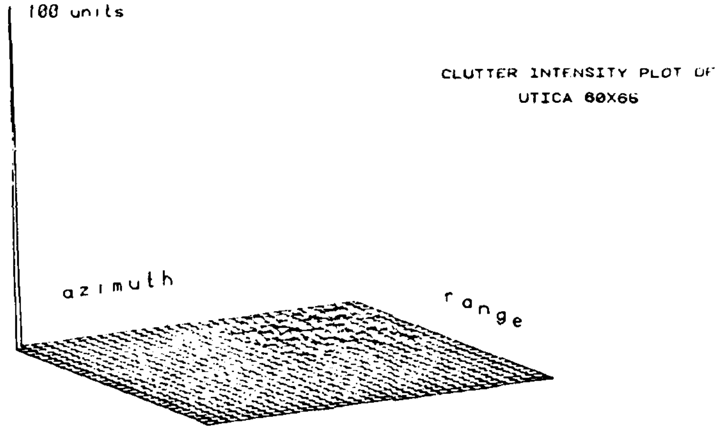
100 units
CLUTTER INTENSITY PLOT OF
UTICA 60X65
azimuth
range

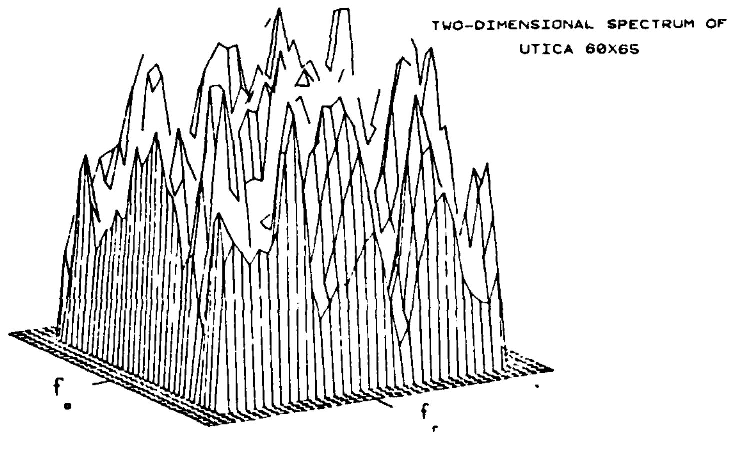
TWO-DIMENSIONAL SPECTRUM OF
UTICA 60X65
f_a
f_r

FIGURE 5 1 24

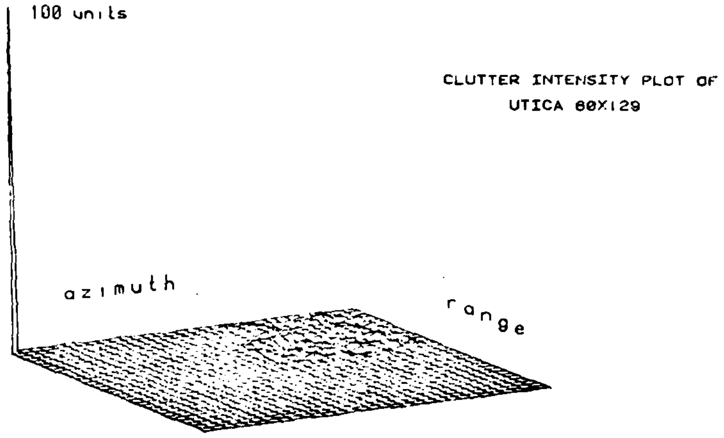
100 units
CLUTTER INTENSITY PLOT OF
UTICA 80X128
azimuth
range

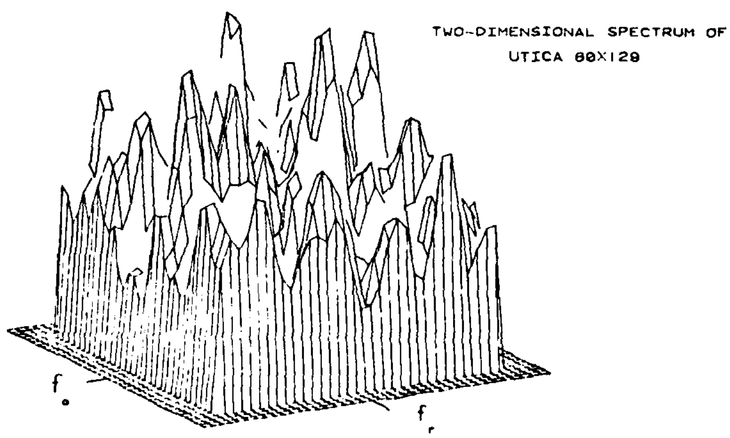
TWO-DIMENSIONAL SPECTRUM OF
UTICA 80X128

FIGURE 5 1 25

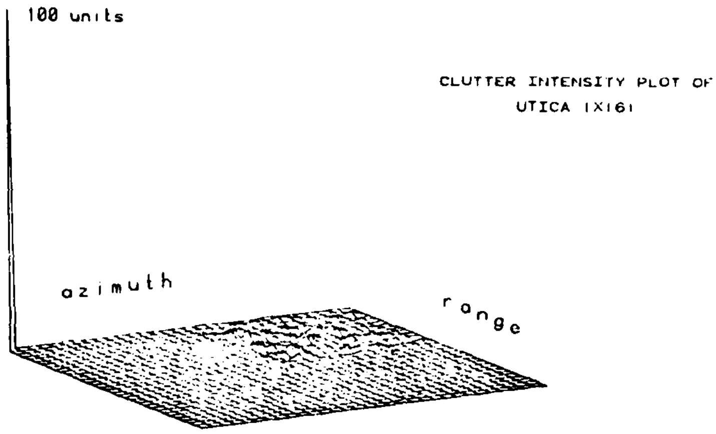
100 units
CLUTTER INTENSITY PLOT OF
UTICA 1X161
azimuth
range

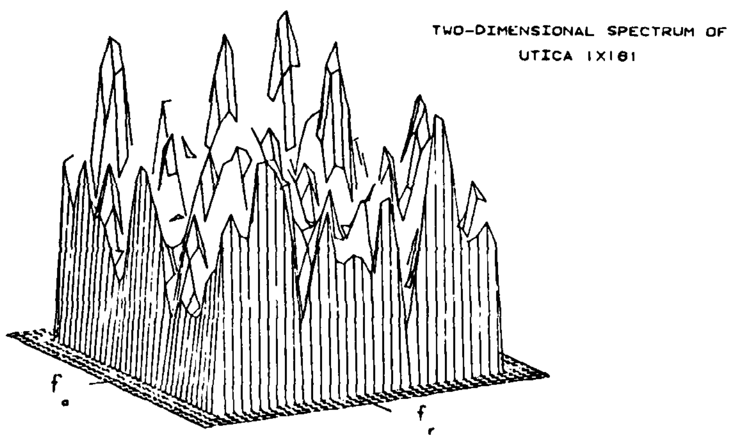
TWO-DIMENSIONAL SPECTRUM OF
UTICA 1X161
f_a
f_r

FIGURE 5.1.26

SAMPLED SPECTRA OF UTICA AREAS

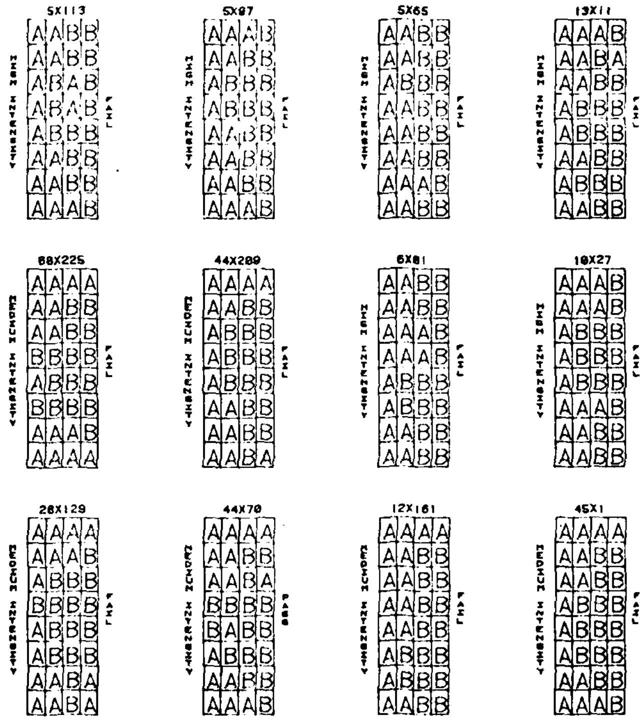

FIGURE 5.1.27

SAMPLED SPECTRA OF UTICA AREAS

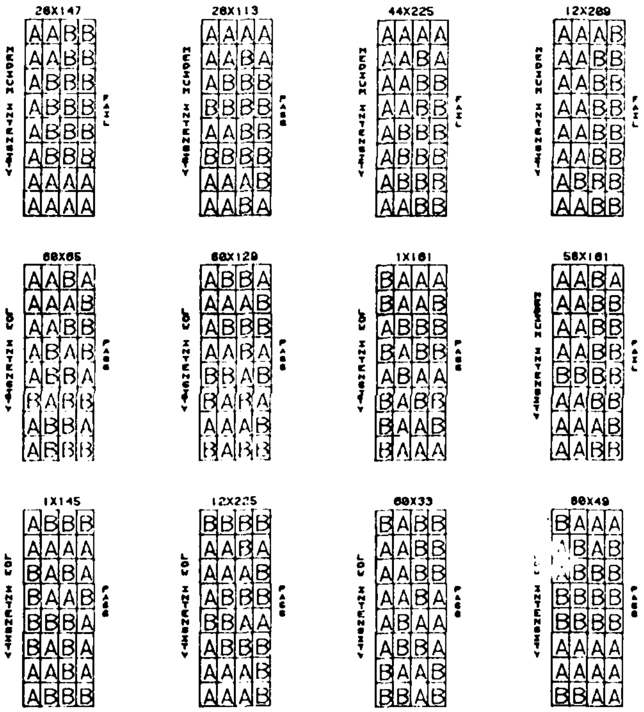

FIGURE 5 1 28

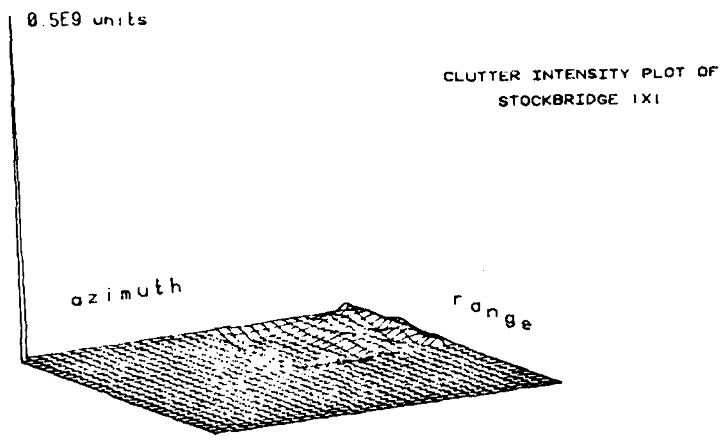
0.5E9 units
CLUTTER INTENSITY PLOT OF
STOCKBRIDGE 1X1
azimuth
range

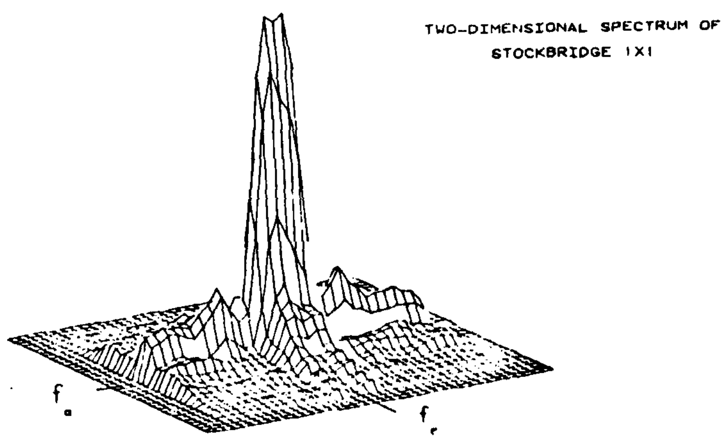
TWO-DIMENSIONAL SPECTRUM OF
STOCKBRIDGE 1X1
f_a
f_r

FIGURE 5 1 30

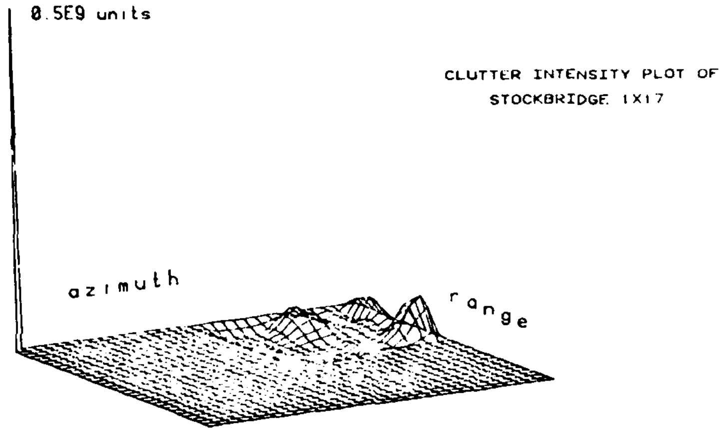
0.5E9 units
CLUTTER INTENSITY PLOT OF
STOCKBRIDGE 1X17
azimuth
range

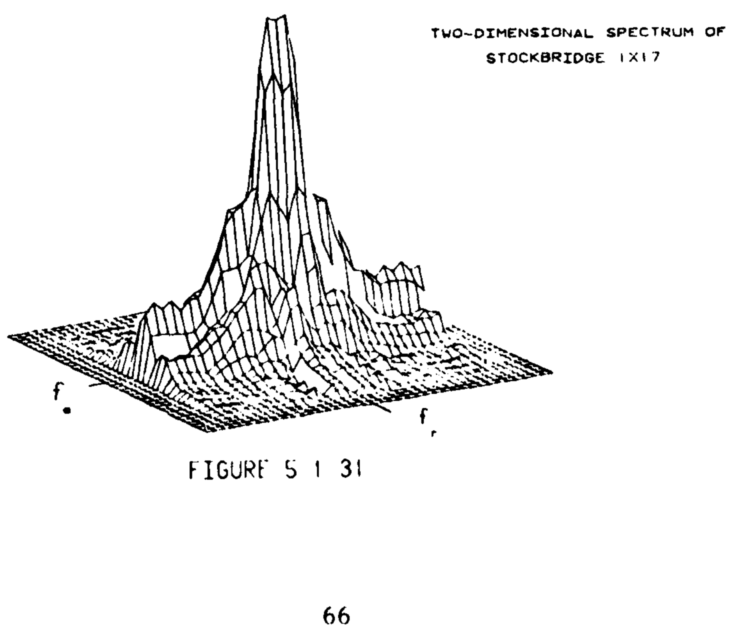
TWO-DIMENSIONAL SPECTRUM OF
STOCKBRIDGE 1X17
f
f

FIGURE 5 1 31

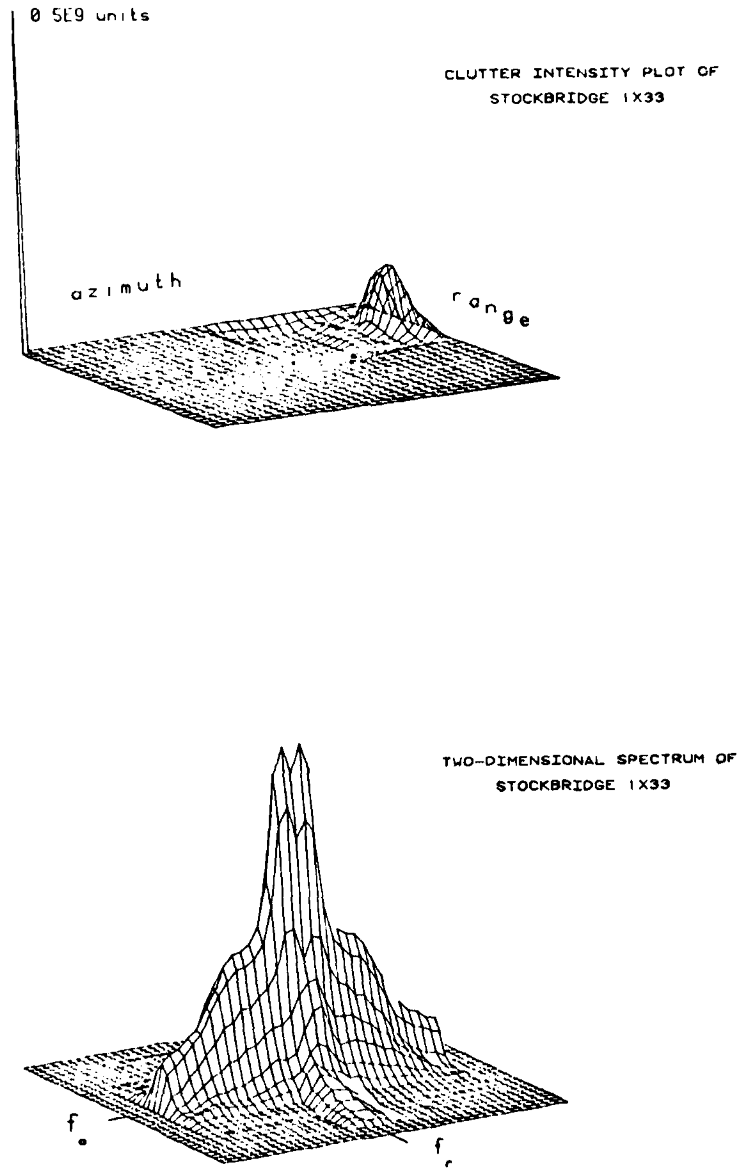
0 5E9 units
CLUTTER INTENSITY PLOT OF
STOCKBRIDGE 1X33
azimuth
range
TWO-DIMENSIONAL SPECTRUM OF
STOCKBRIDGE 1X33
f_a
f_r

FIGURE 5 1 32

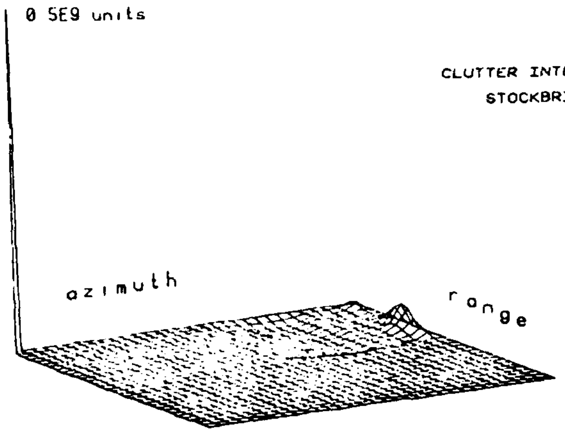

CLUTTER INTENSITY PLOT OF
STOCKBRIDGE 1X49

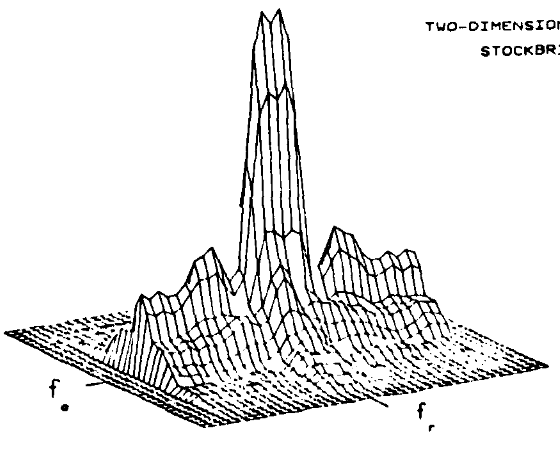

TWO-DIMENSIONAL SPECTRUM OF
STOCKBRIDGE 1X49

FIGURE 5 1 33

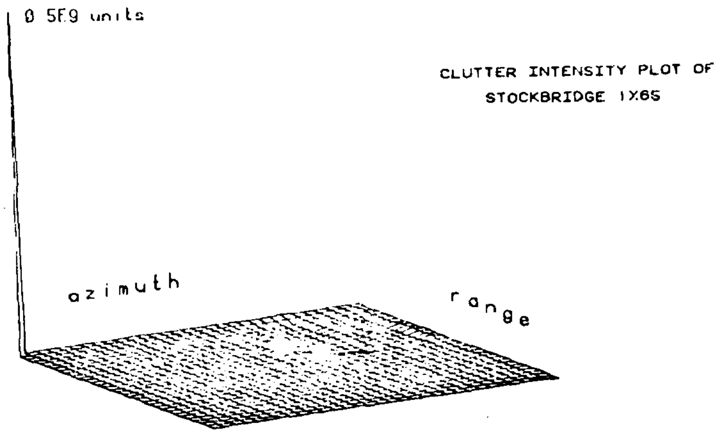
0 5E9 units
CLUTTER INTENSITY PLOT OF
STOCKBRIDGE 1X65
azimuth
range

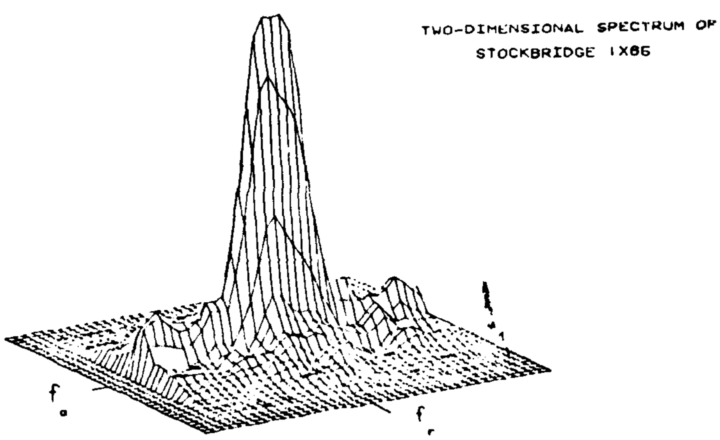
TWO-DIMENSIONAL SPECTRUM OF
STOCKBRIDGE 1X65
f_a
f_r

FIGURE 5 1 34

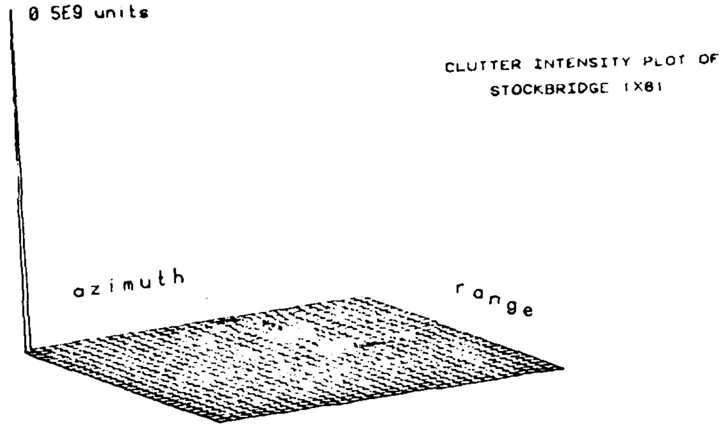
0 5E9 units
CLUTTER INTENSITY PLOT OF
STOCKBRIDGE (X8)
azimuth
range

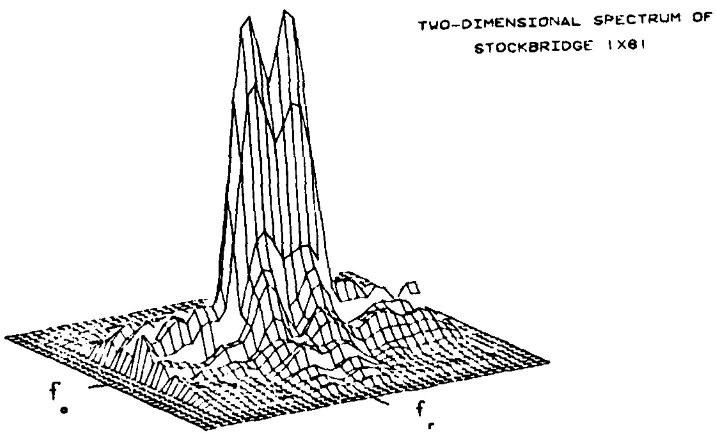
TWO-DIMENSIONAL SPECTRUM OF
STOCKBRIDGE (X8)
f_a
f_r

FIGURE 5.1.35

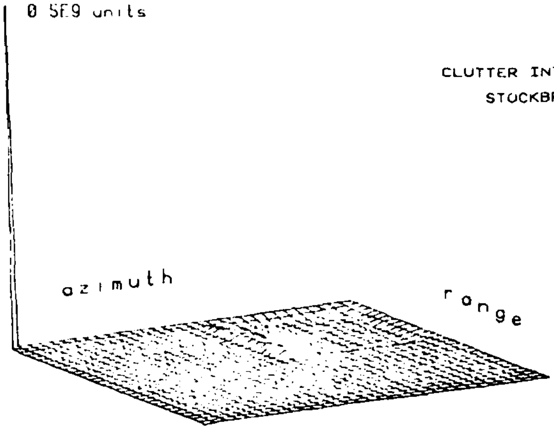

CLUTTER INTENSITY PLOT OF
STOCKBRIDGE 1X97

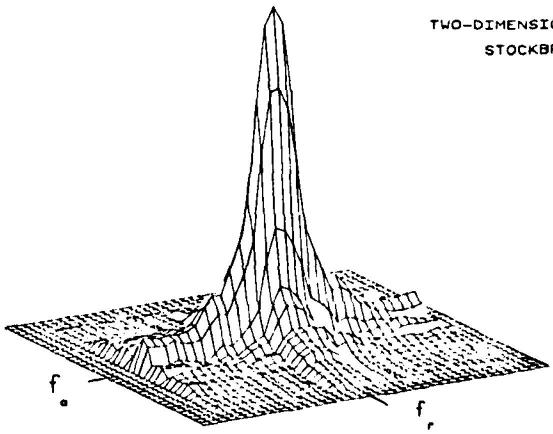

TWO-DIMENSIONAL SPECTRUM OF
STOCKBRIDGE 1X97

FIGURE 5 1 36

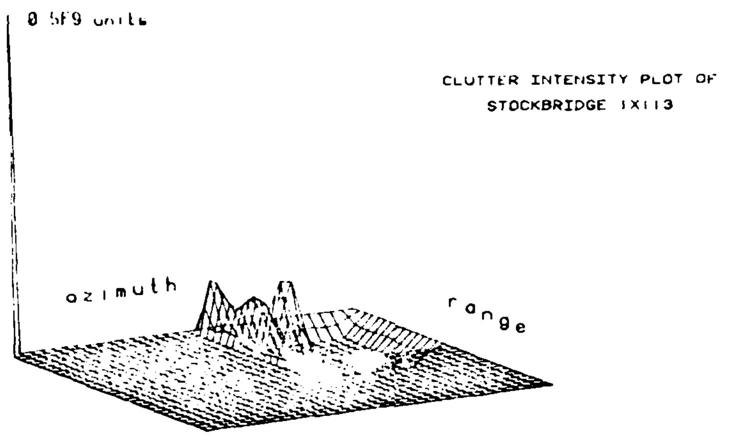
0 5F9 units
CLUTTER INTENSITY PLOT OF
STOCKBRIDGE 1X113
azimuth
range

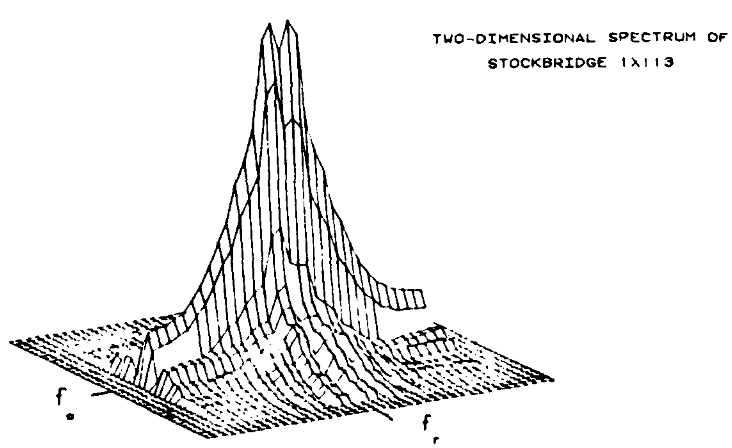
TWO-DIMENSIONAL SPECTRUM OF
STOCKBRIDGE 1X113
f_a
f_r

FIGURE 5 1 37

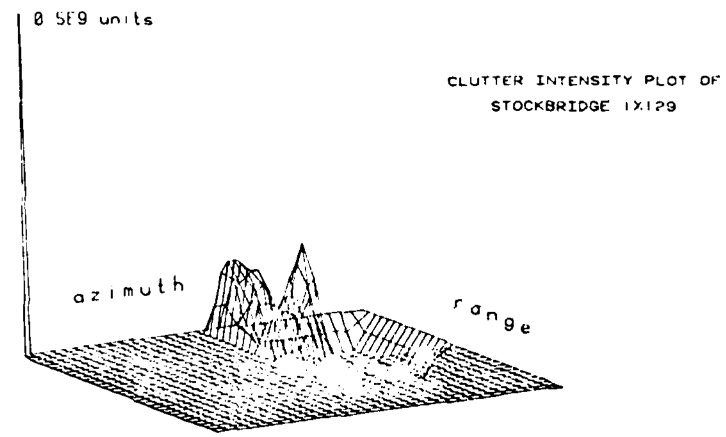
0 5E9 units
CLUTTER INTENSITY PLOT OF
STOCKBRIDGE 1X129
azimuth
range

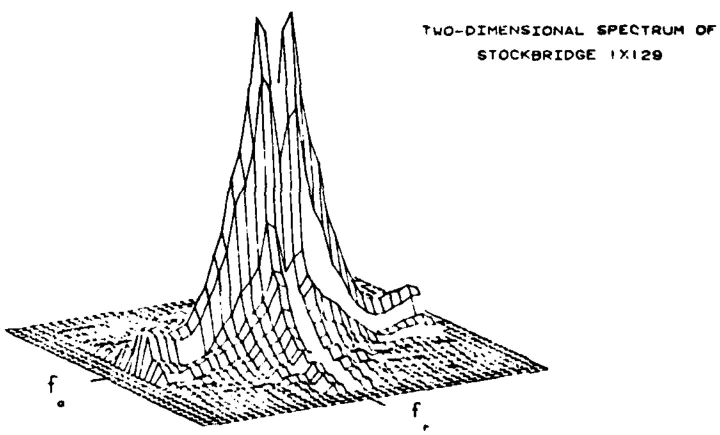
TWO-DIMENSIONAL SPECTRUM OF
STOCKBRIDGE 1X129
f_a
f_r

FIGURE 5 1 38

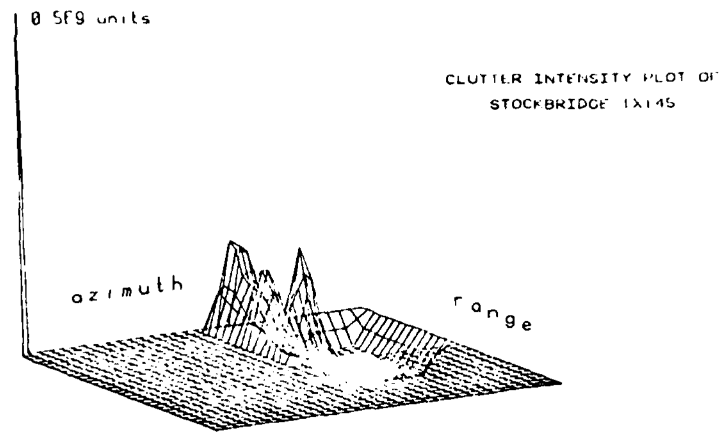
0 SF9 units
CLUTTER INTENSITY PLOT OF
STOCKBRIDGE 1X145
azimuth
range

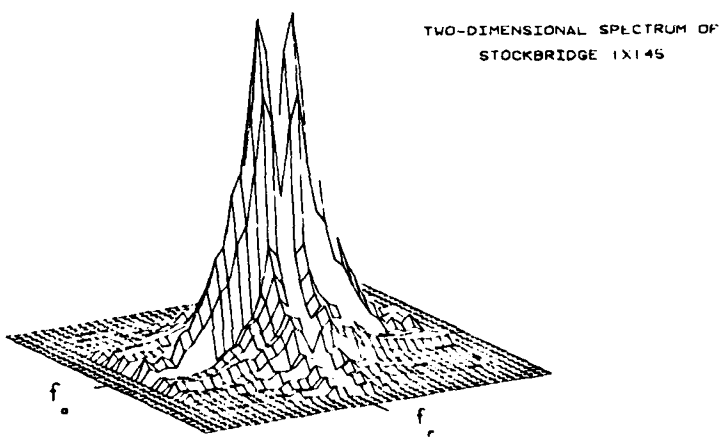
TWO-DIMENSIONAL SPECTRUM OF
STOCKBRIDGE 1X145
f_a
f_r

FIGURE 5 1 39

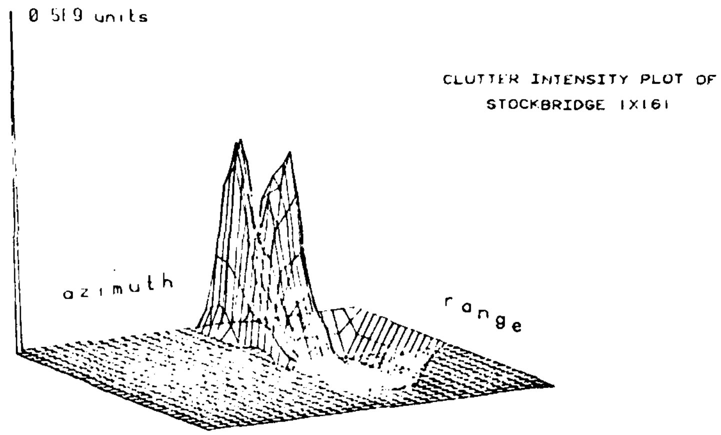
0 519 units
CLUTTER INTENSITY PLOT OF
STOCKBRIDGE IXI6I
azimuth
range

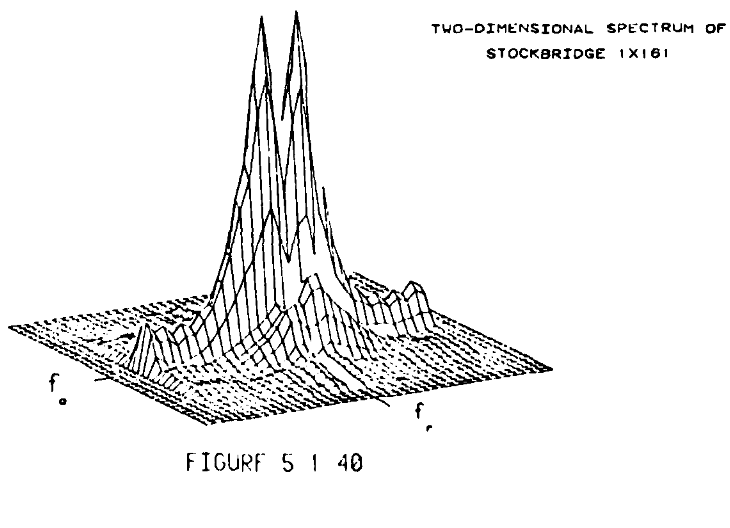
TWO-DIMENSIONAL SPECTRUM OF
STOCKBRIDGE IXI6I
f_a
f_r

FIGURF 5 1 40

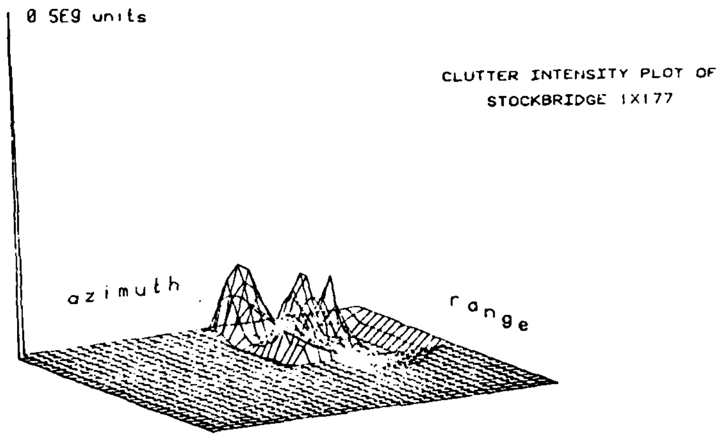
0 SE9 units
CLUTTER INTENSITY PLOT OF
STOCKBRIDGE 1X177
azimuth
range

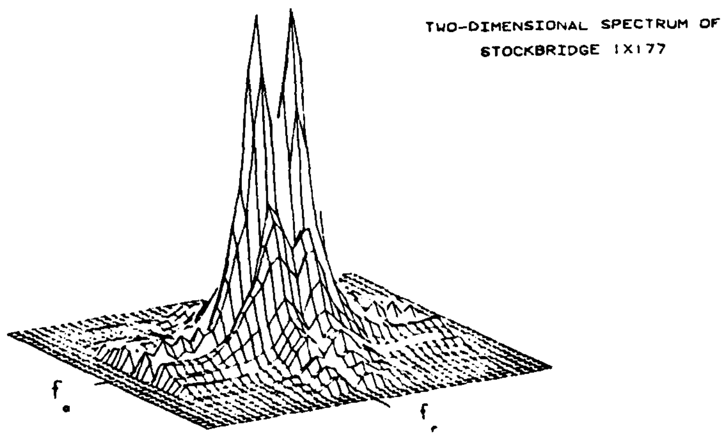
TWO-DIMENSIONAL SPECTRUM OF
STOCKBRIDGE 1X177

FIGURE 5.1.41

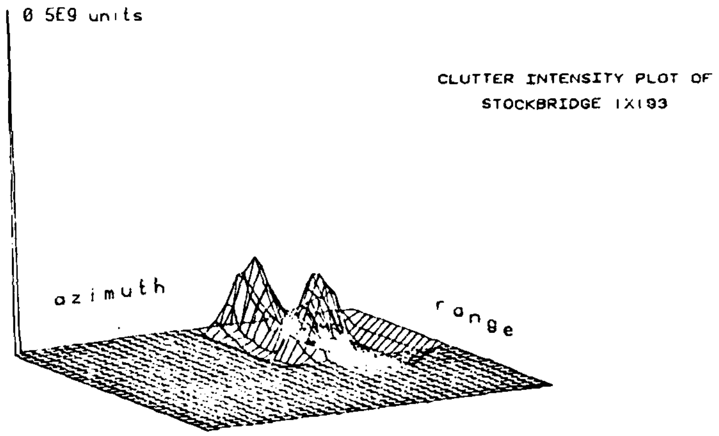
0 5E9 units
CLUTTER INTENSITY PLOT OF
STOCKBRIDGE 1X193
azimuth
range

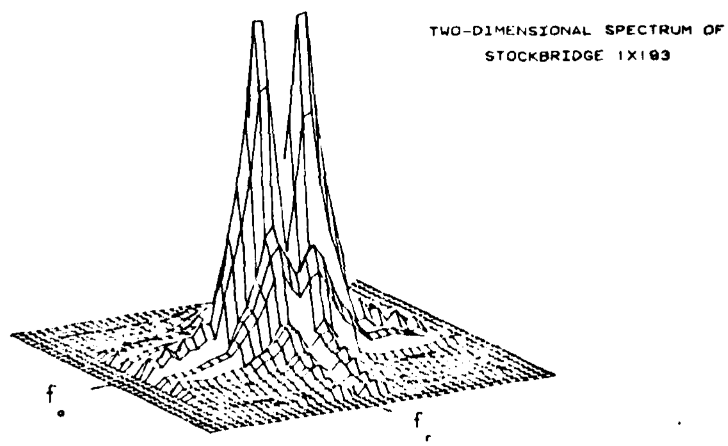
TWO-DIMENSIONAL SPECTRUM OF
STOCKBRIDGE 1X193
f_a
f_r

FIGURE 5 1 42

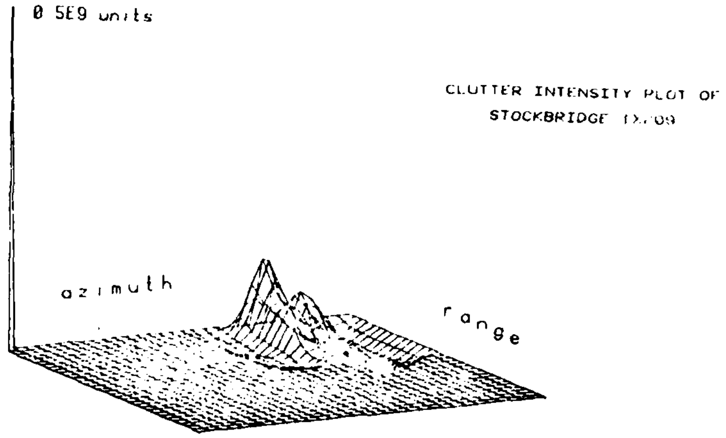
0 5E9 units
CLUTTER INTENSITY PLOT OF
STOCKBRIDGE
azimuth
range

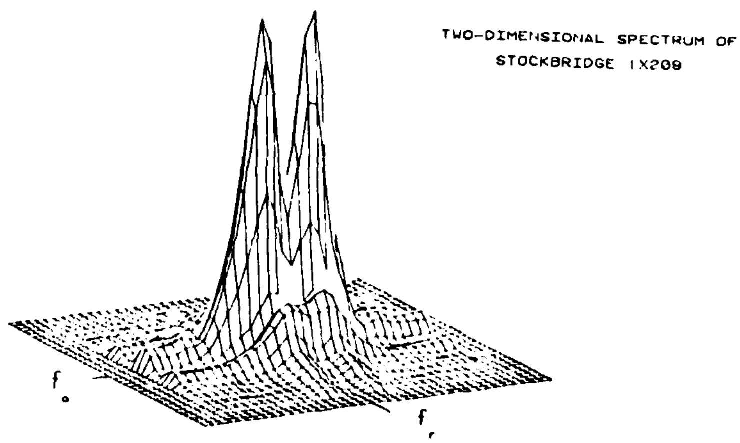
TWO-DIMENSIONAL SPECTRUM OF
STOCKBRIDGE 1X209
f_a
f_r

FIGURE 5 1 43

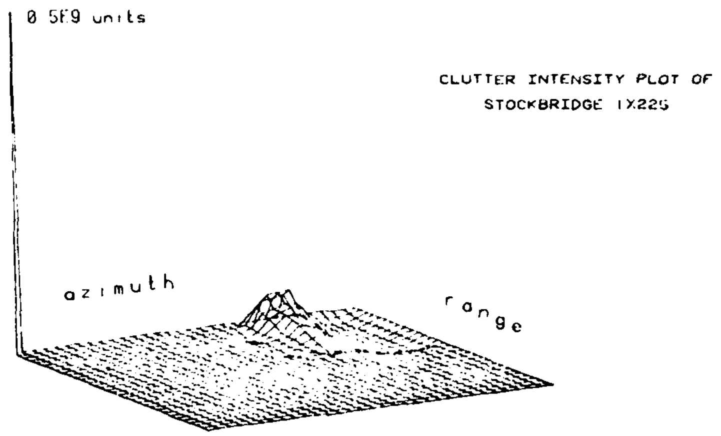
0 5E9 units
CLUTTER INTENSITY PLOT OF
STOCKBRIDGE 1X225
azimuth
range

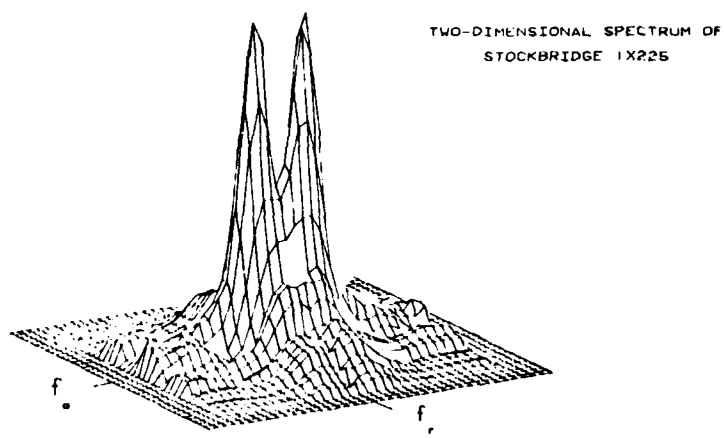
TWO-DIMENSIONAL SPECTRUM OF
STOCKBRIDGE 1X225

FIGURE 5.1.44

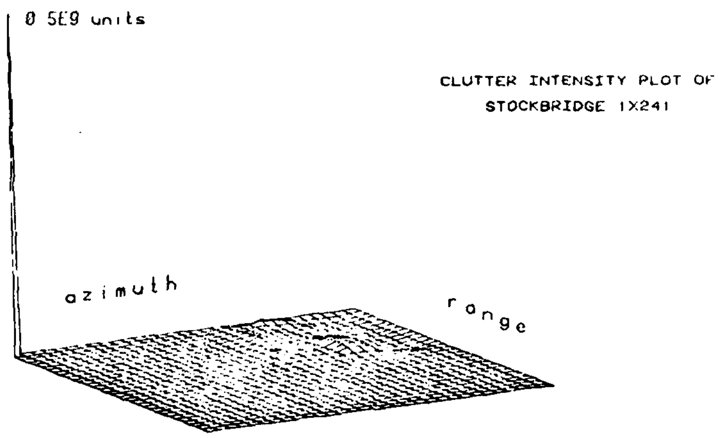
0 5E9 units
CLUTTER INTENSITY PLOT OF
STOCKBRIDGE 1X241
azimuth
range

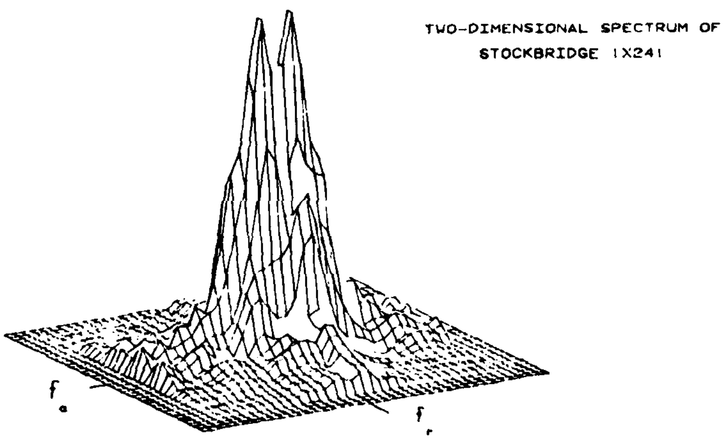
TWO-DIMENSIONAL SPECTRUM OF
STOCKBRIDGE 1X241
f_a
f_r

FIGURE 5 1 45

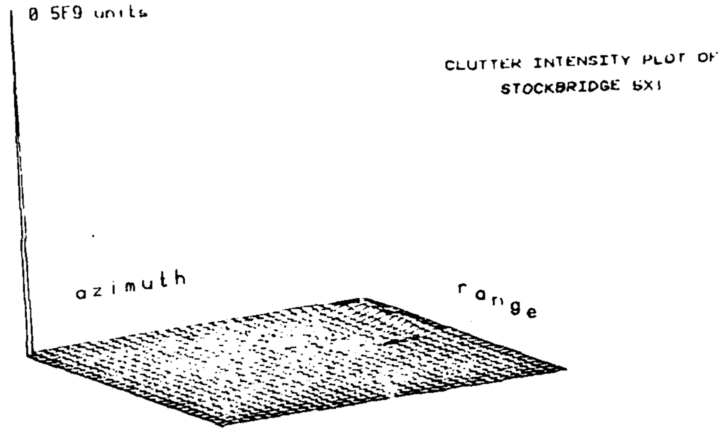
0 5E9 units
CLUTTER INTENSITY PLOT OF
STOCKBRIDGE 6X1
azimuth
range

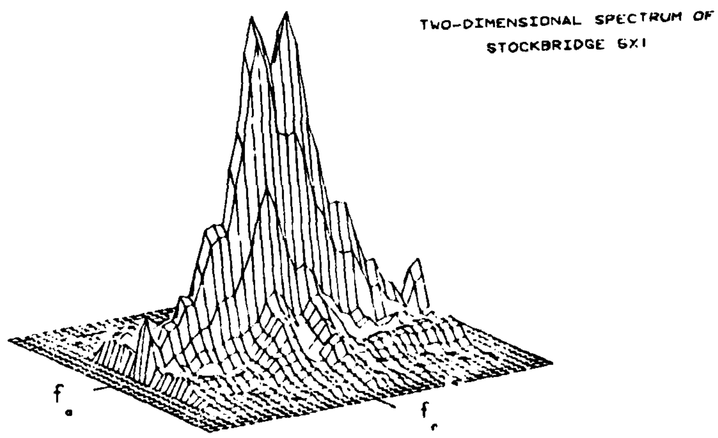
TWO-DIMENSIONAL SPECTRUM OF
STOCKBRIDGE 6X1
f_a
f_r

FIGURE 5 1 46

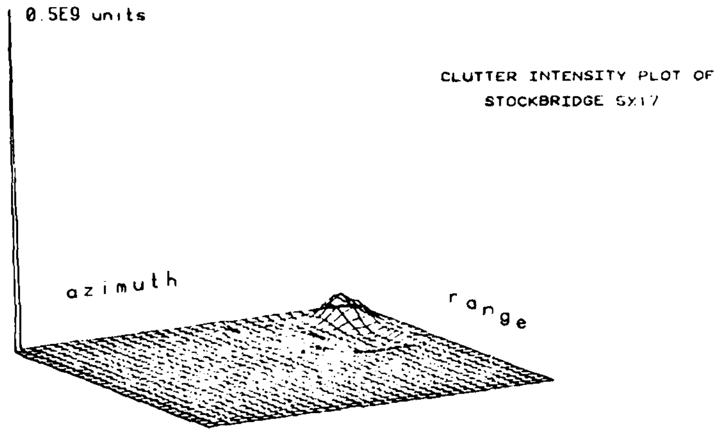
0.5E9 units
CLUTTER INTENSITY PLOT OF
STOCKBRIDGE SX17
azimuth
range

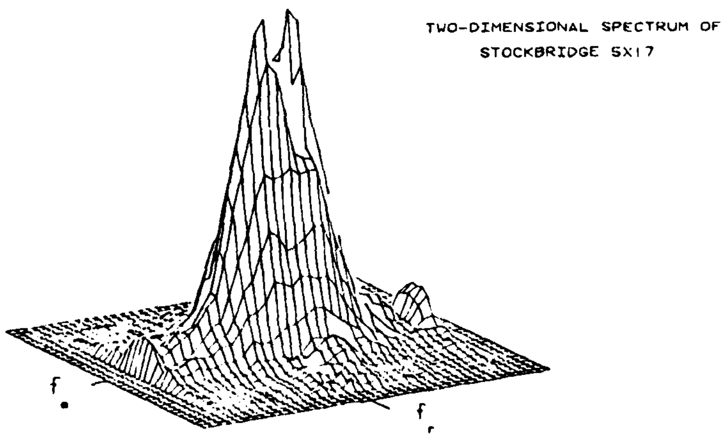
TWO-DIMENSIONAL SPECTRUM OF
STOCKBRIDGE SX17
f_a
f_r

FIGURE 5.1.47

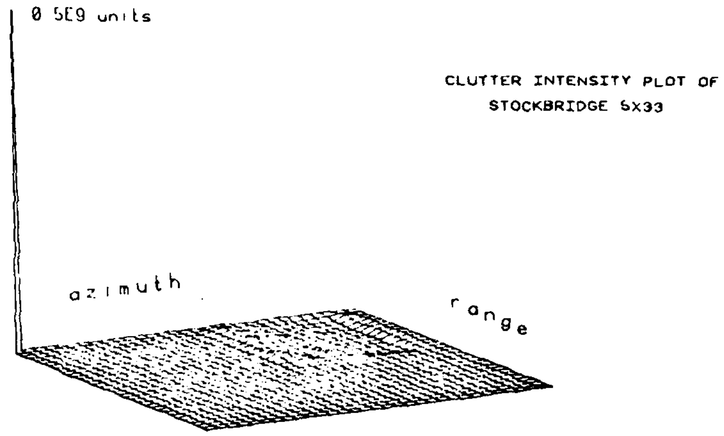
0 5E9 units
CLUTTER INTENSITY PLOT OF
STOCKBRIDGE 5X33
azimuth
range

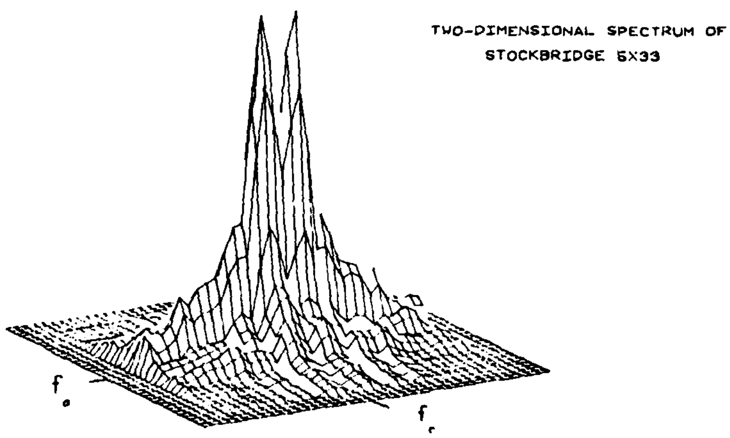
TWO-DIMENSIONAL SPECTRUM OF
STOCKBRIDGE 5X33
f_a
f_r

FIGURE 5.1.48

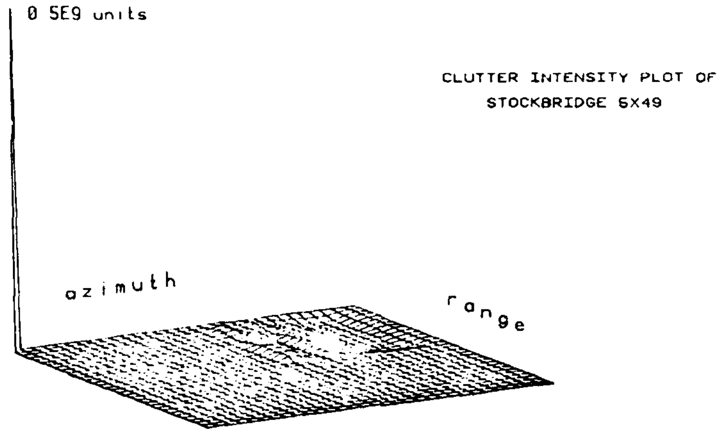
0 5E9 units
CLUTTER INTENSITY PLOT OF
STOCKBRIDGE 5X49
azimuth
range

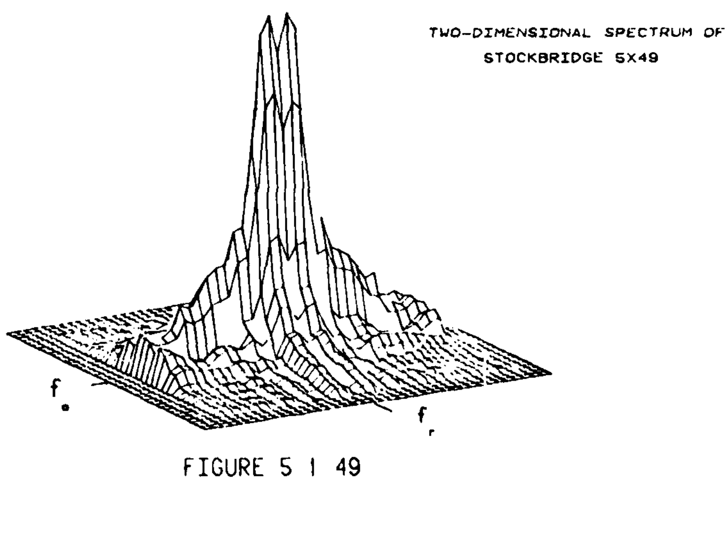
TWO-DIMENSIONAL SPECTRUM OF
STOCKBRIDGE 5X49
f_a
f_r

FIGURE 5 1 49

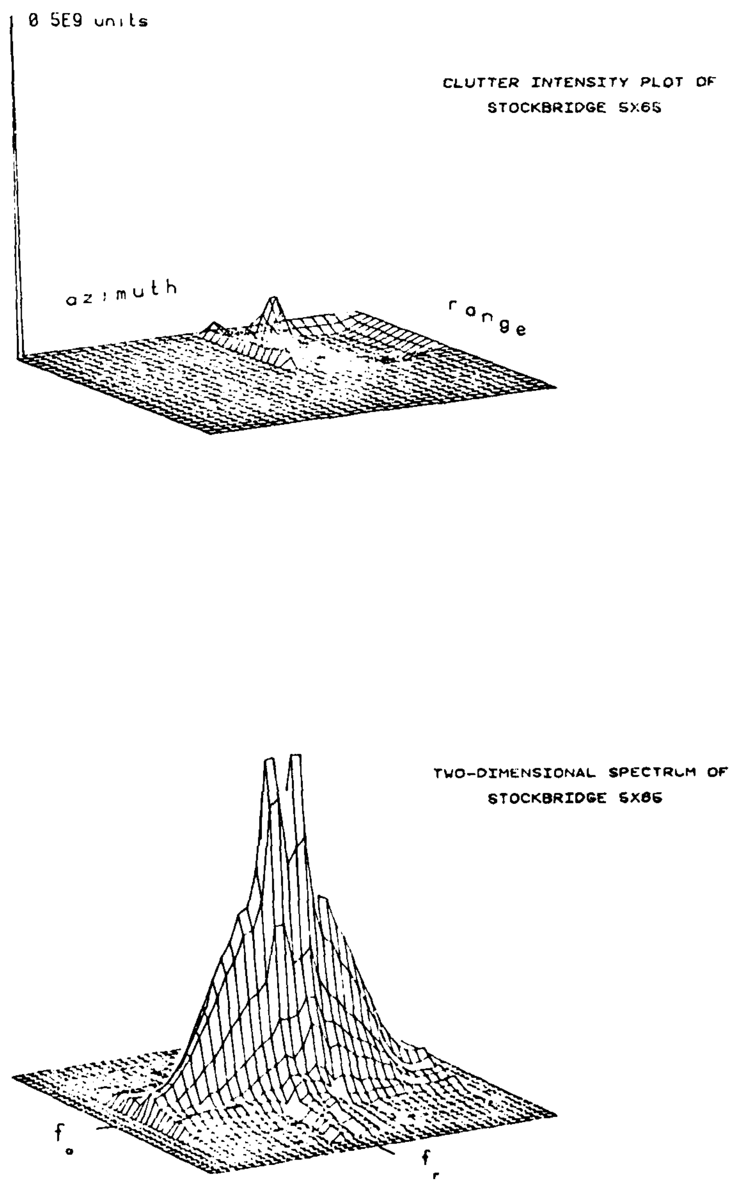
0 5E9 units
CLUTTER INTENSITY PLOT OF
STOCKBRIDGE SX65
azimuth
range
TWO-DIMENSIONAL SPECTRUM OF
STOCKBRIDGE SX65
f_a
f_r

FIGURE 5 1 50

AD-A113 384 CLARKSON COLL OF TECHNOLOGY POTSDAM NY F/G 20/14
DEFINITION AND LOCATION OF HOMOGENEOUS REGIONS IN RADAR BACKSCA--ETC(U)
FEB 82 B A BLACK, M AROZULLAH, S T CUMMINGS F30602-80-C-0192

UNCLASSIFIED RADC-TR-82-10 NL

2 OF 2
AD A
113384

END
DATE
FILMED
05-82
DTIC

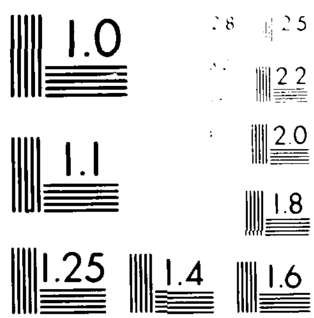
1.0
2.5
2.2
2.0
1.1
1.8
1.25
1.4
1.6

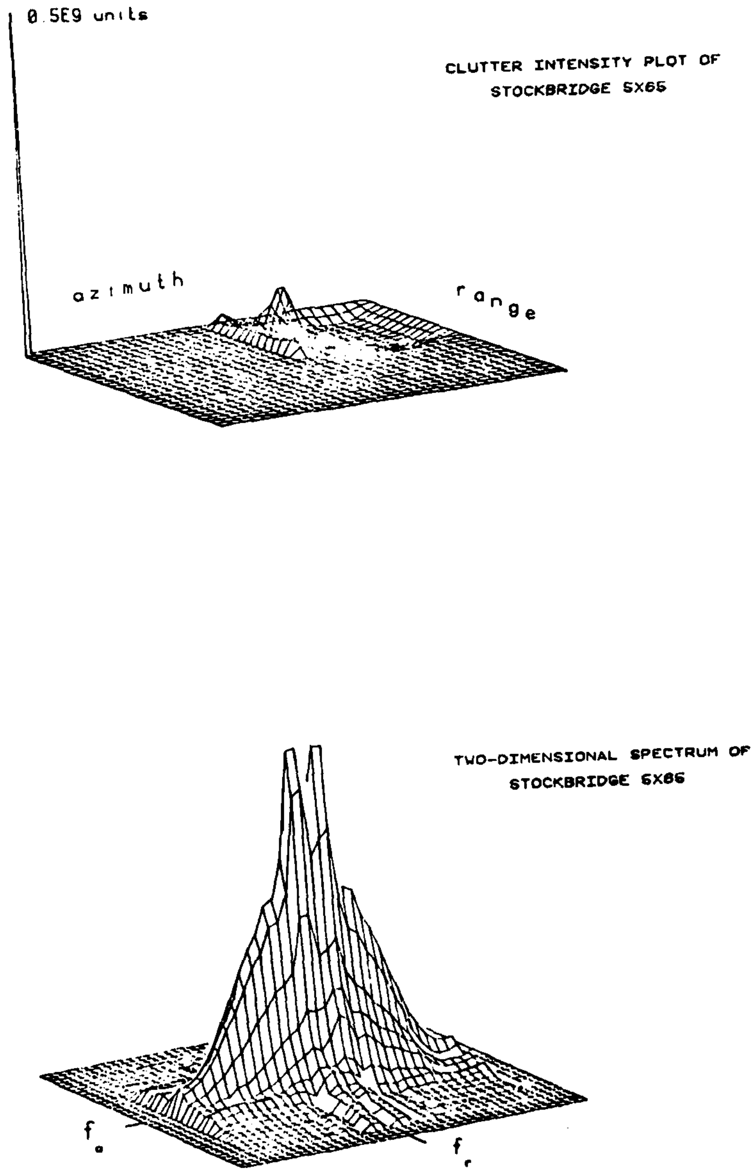
0.5E9 units
CLUTTER INTENSITY PLOT OF
STOCKBRIDGE 5X65
azimuth
range
TWO-DIMENSIONAL SPECTRUM OF
STOCKBRIDGE 6X86
f_a
f_r

FIGURE 5.1.50

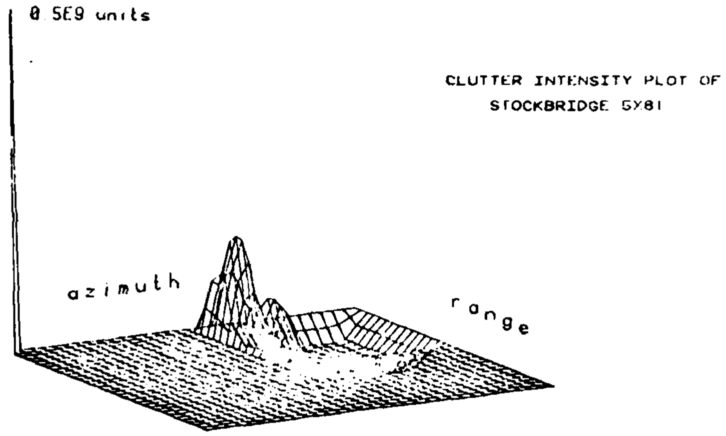

0.5E9 units
CLUTTER INTENSITY PLOT OF
STOCKBRIDGE 5X81
azimuth
range

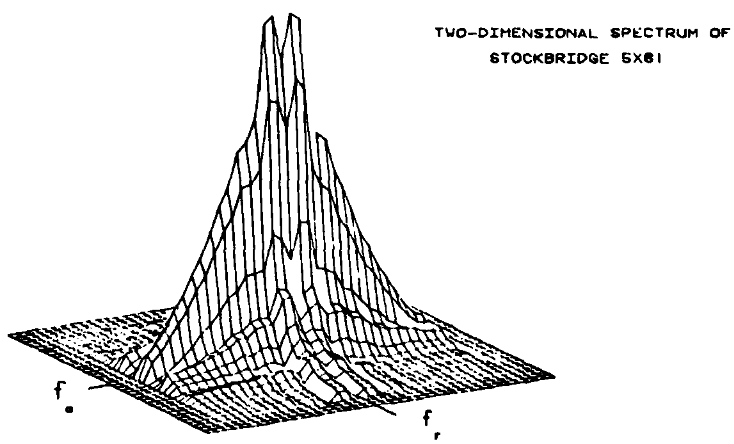

TWO-DIMENSIONAL SPECTRUM OF
STOCKBRIDGE 5X81
f_a
f_r

FIGURE 5.1.51

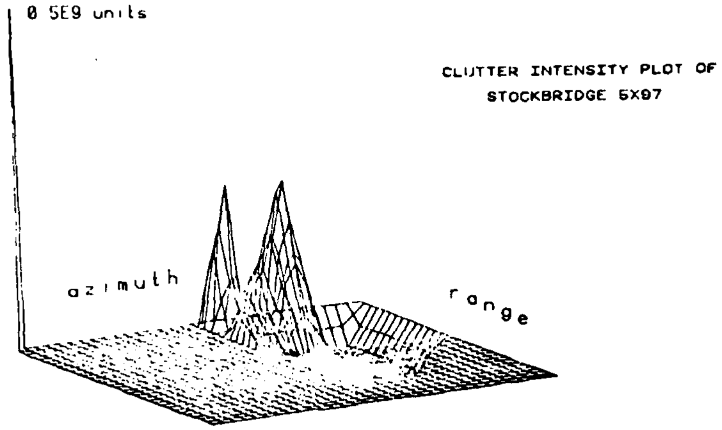
0 5E9 units
CLUTTER INTENSITY PLOT OF
STOCKBRIDGE 5X97
azimuth
range

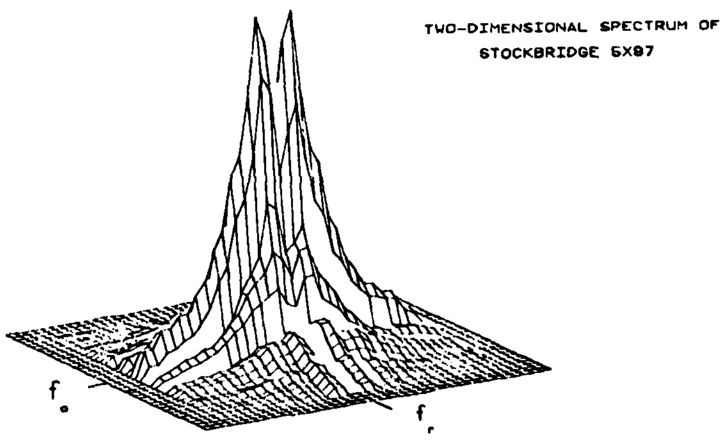
TWO-DIMENSIONAL SPECTRUM OF
STOCKBRIDGE 5X97
f_a
f_r

FIGURE 5.1 52

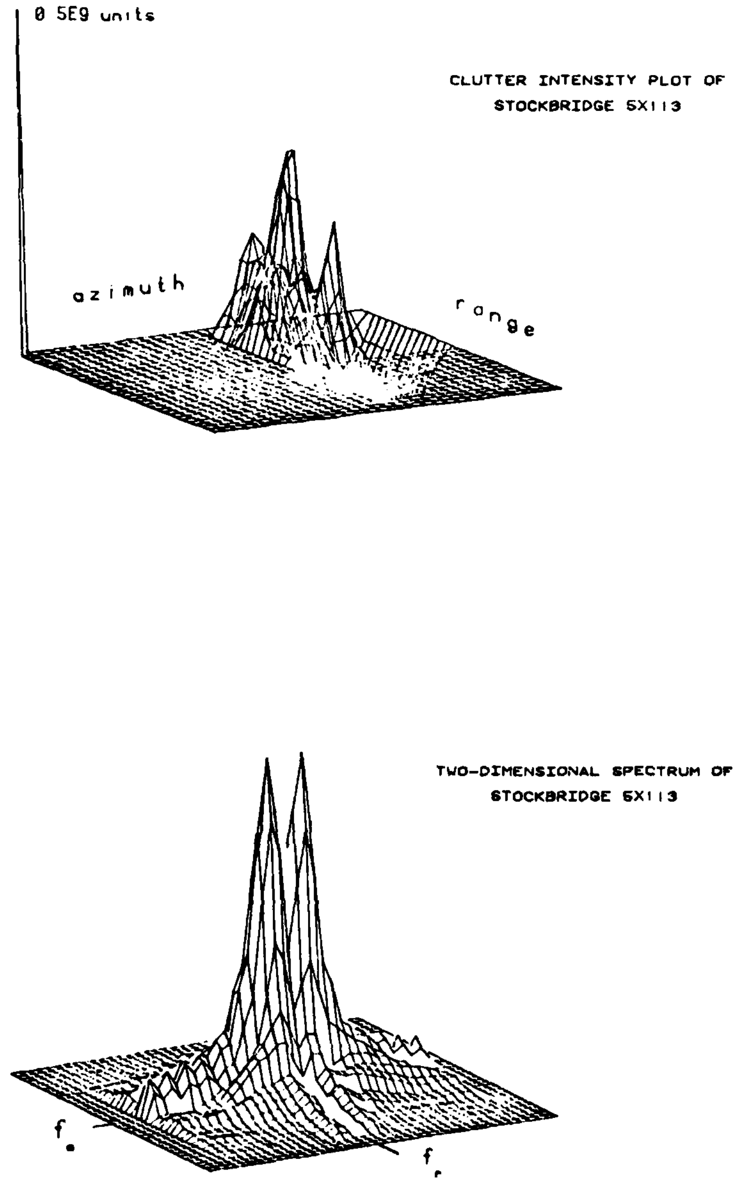
0 5E9 units
CLUTTER INTENSITY PLOT OF
STOCKBRIDGE 5X113
azimuth
range
TWO-DIMENSIONAL SPECTRUM OF
STOCKBRIDGE 5X113

FIGURE 5.1.53

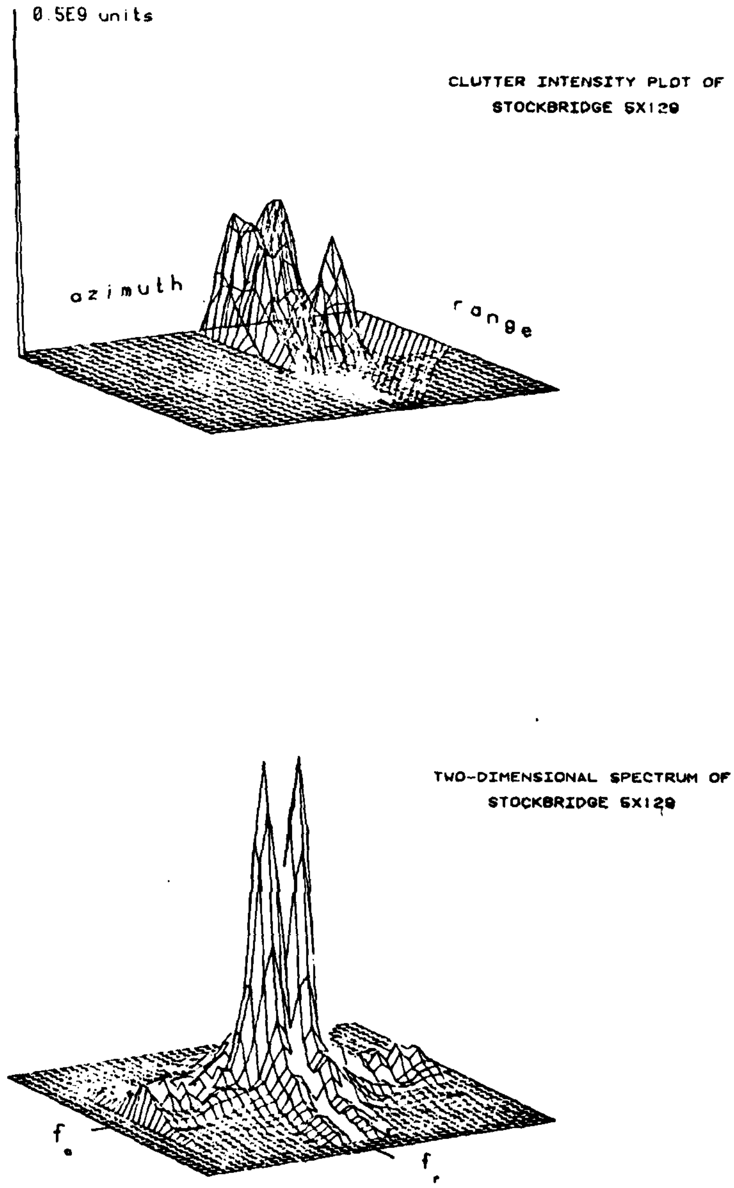
0.5E9 units
CLUTTER INTENSITY PLOT OF
STOCKBRIDGE 6X120
azimuth
range
TWO-DIMENSIONAL SPECTRUM OF
STOCKBRIDGE 6X120
f_a
f_r

FIGURE 5.1.54

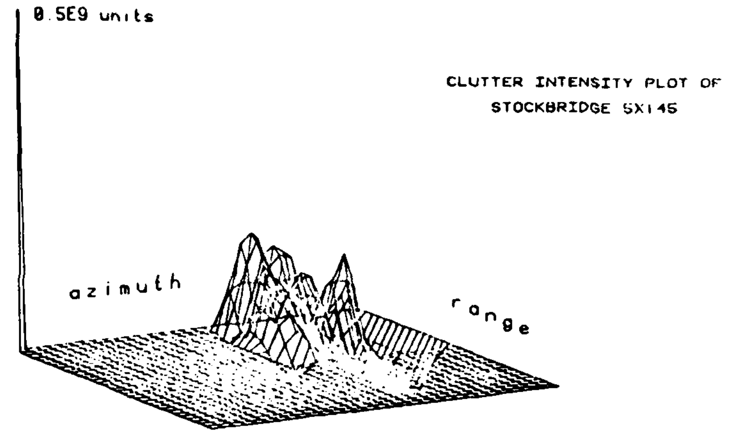
0.5E9 units
CLUTTER INTENSITY PLOT OF
STOCKBRIDGE 5X145
azimuth
range

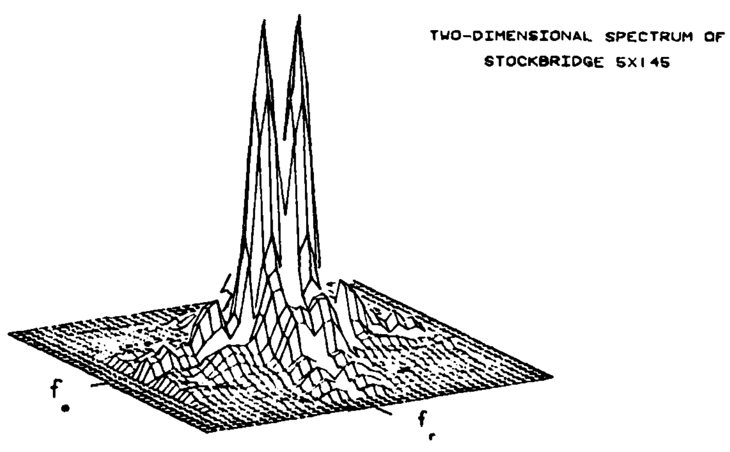
TWO-DIMENSIONAL SPECTRUM OF
STOCKBRIDGE 5X145
f_a
f_r

FIGURE 5.1 S5

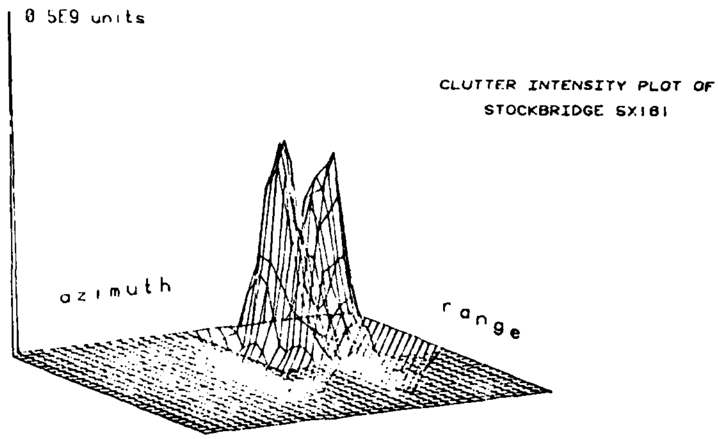
0 5E9 units
CLUTTER INTENSITY PLOT OF
STOCKBRIDGE 5X181
azimuth
range

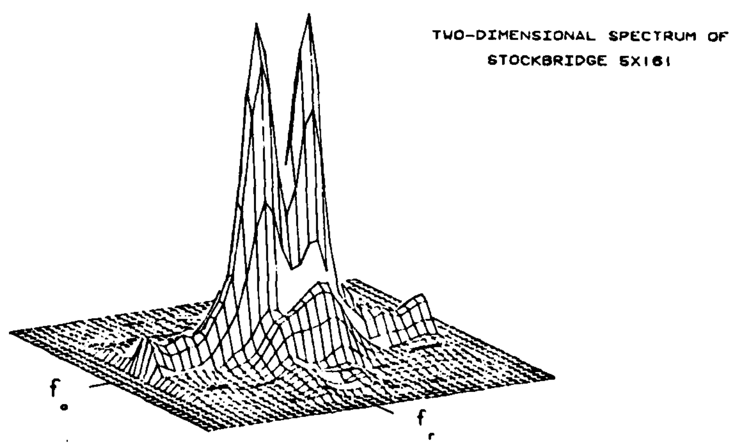
TWO-DIMENSIONAL SPECTRUM OF
STOCKBRIDGE 5X181
f_r

FIGURE 5 1 56

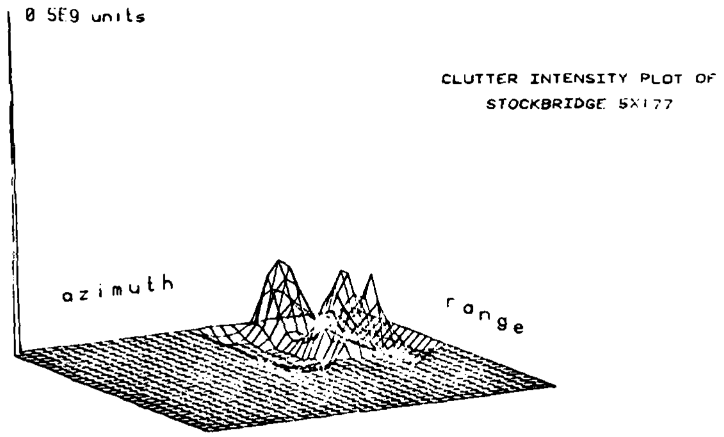
0 5E9 units
CLUTTER INTENSITY PLOT OF
STOCKBRIDGE 5X177
azimuth
range

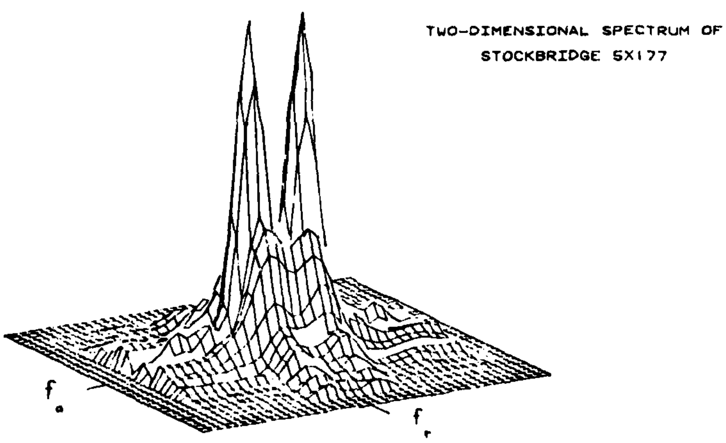
TWO-DIMENSIONAL SPECTRUM OF
STOCKBRIDGE 5X177
f_a
f_r

FIGURE 5.1.57

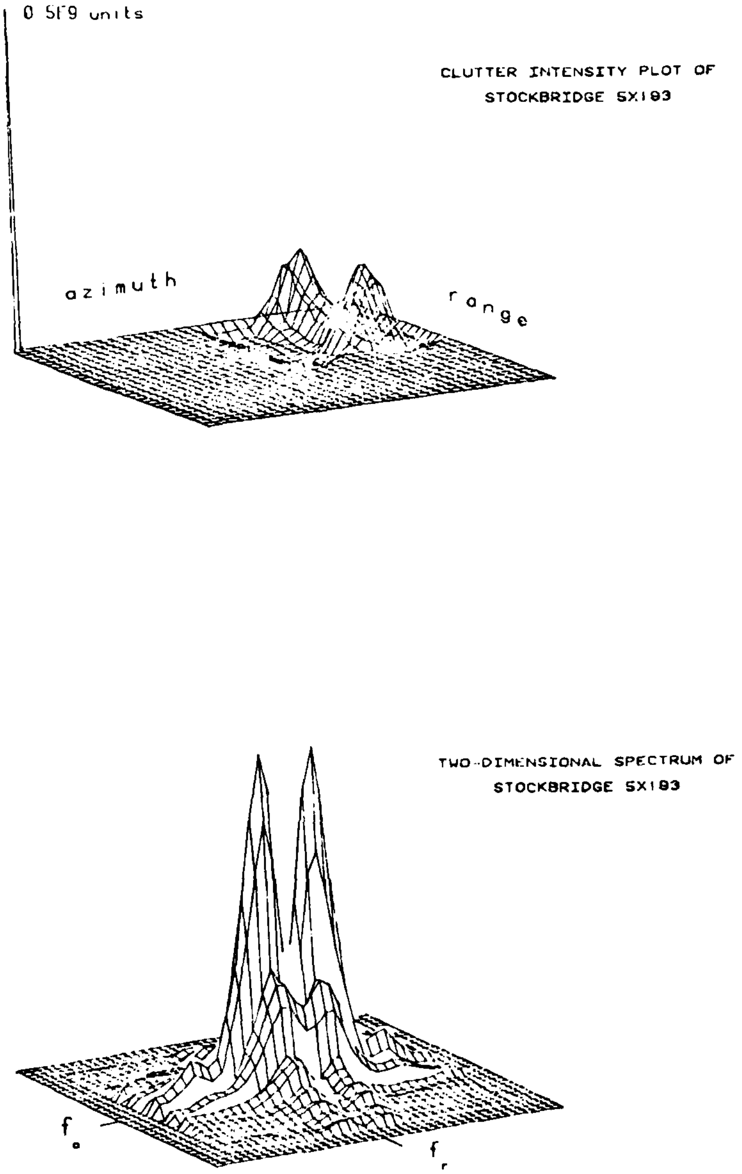
0 5E9 units
CLUTTER INTENSITY PLOT OF
STOCKBRIDGE 5X183
azimuth
range
TWO-DIMENSIONAL SPECTRUM OF
STOCKBRIDGE 5X183
f_a
f_r

FIGURE 5 1 58

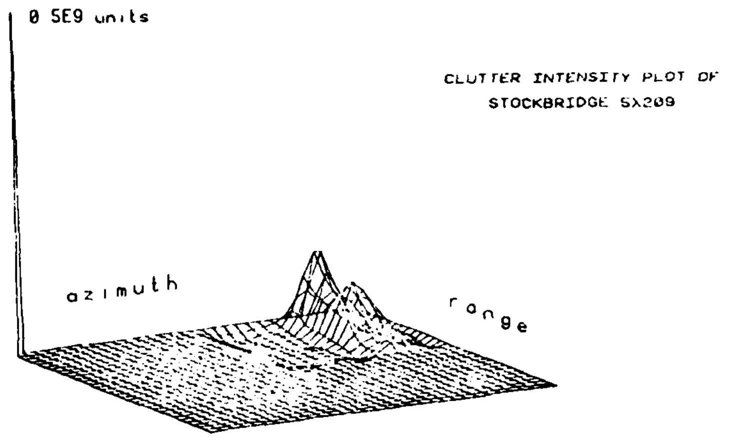
0 5E9 units
CLUTTER INTENSITY PLOT OF
STOCKBRIDGE 5X209
azimuth
range

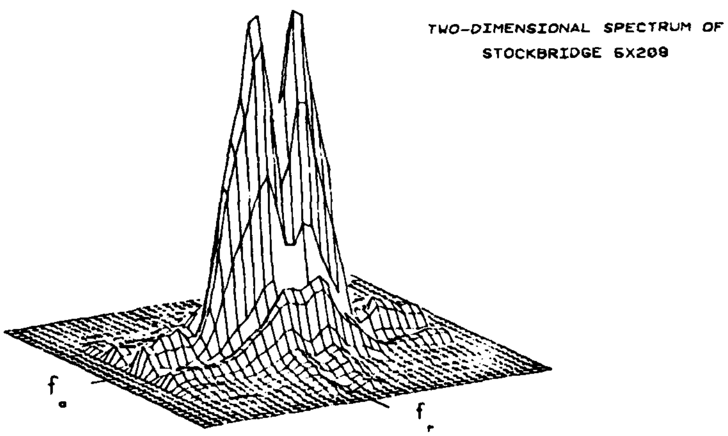
TWO-DIMENSIONAL SPECTRUM OF
STOCKBRIDGE 6X209
f_a
f_r

FIGURE 5 1.59

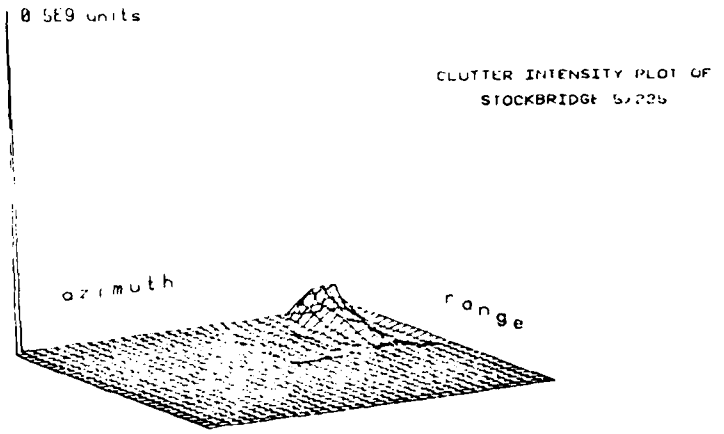
0 5E9 units
CLUTTER INTENSITY PLOT OF
STOCKBRIDGE 5X225
azimuth
range

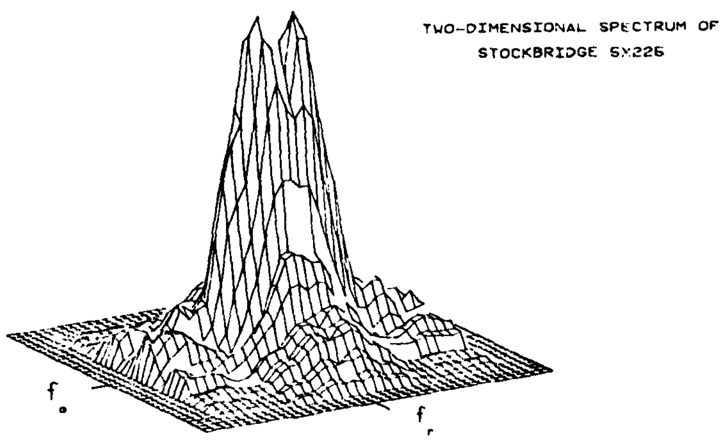
TWO-DIMENSIONAL SPECTRUM OF
STOCKBRIDGE 5X225
f
f

FIGURE 5 1 60

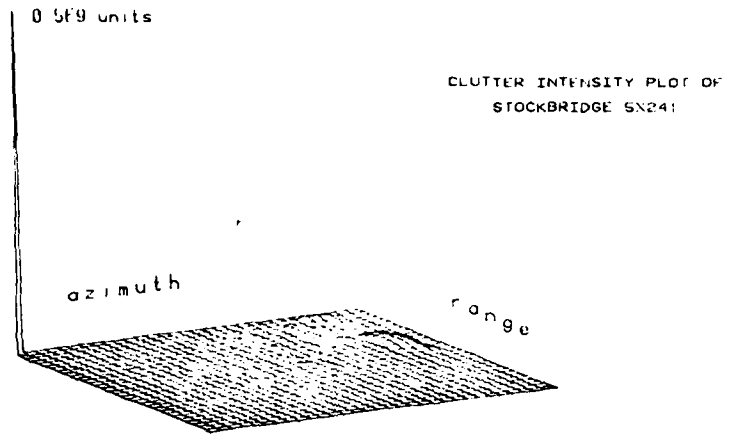
0 SF9 units
CLUTTER INTENSITY PLOT OF
STOCKBRIDGE SX241
azimuth
range

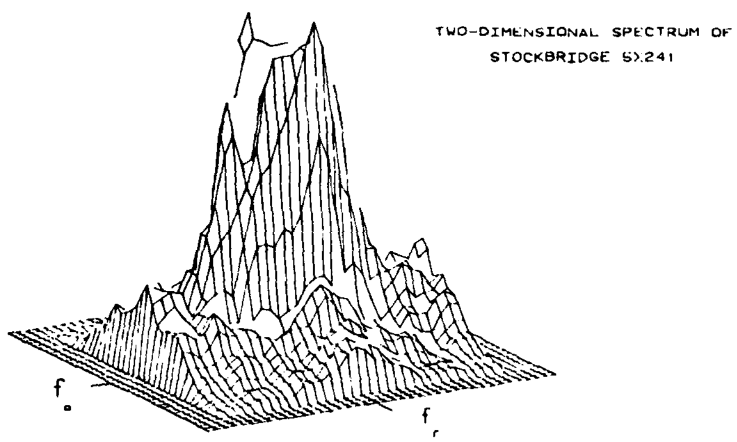
TWO-DIMENSIONAL SPECTRUM OF
STOCKBRIDGE SX241

FIGURE 5 1 61

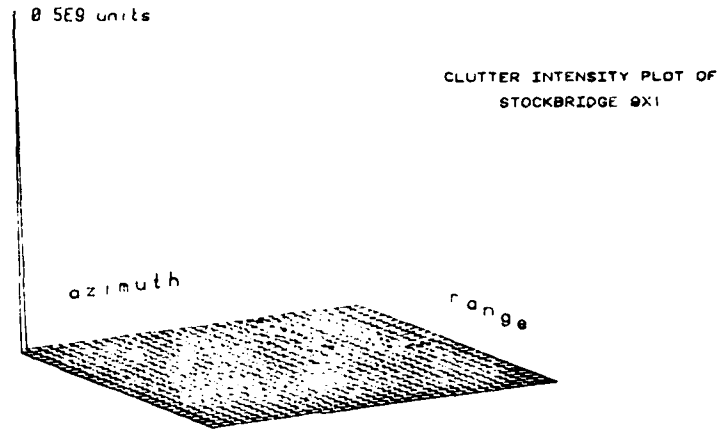
0 5E9 units
CLUTTER INTENSITY PLOT OF
STOCKBRIDGE 9X1
azimuth
range

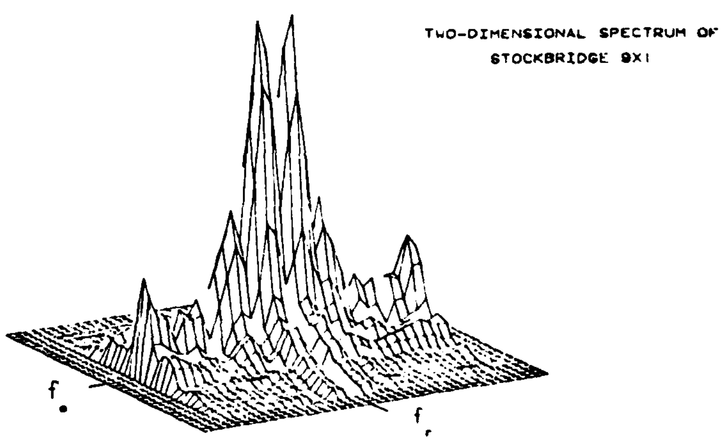
TWO-DIMENSIONAL SPECTRUM OF
STOCKBRIDGE 9X1

FIGURE 5 1 62

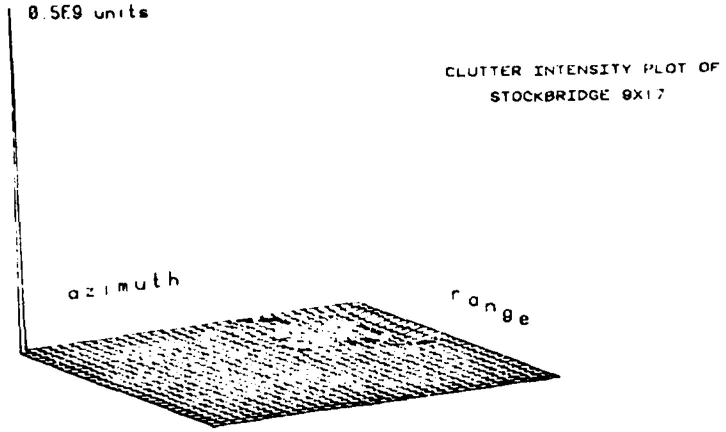
0.5E9 units
CLUTTER INTENSITY PLOT OF
STOCKBRIDGE 9X17
azimuth
range

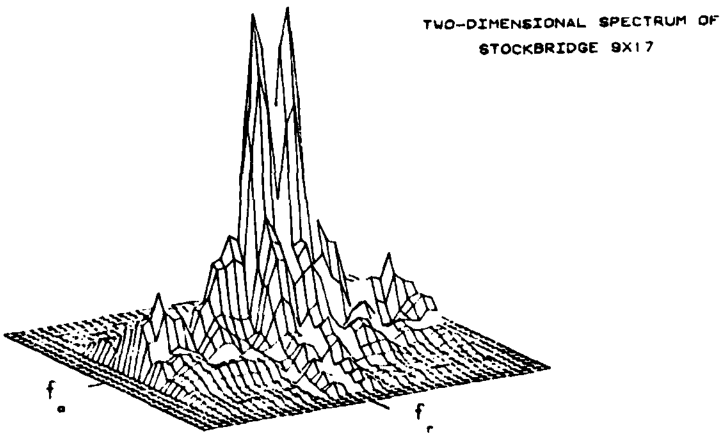
TWO-DIMENSIONAL SPECTRUM OF
STOCKBRIDGE 9X17
f_a
f_r

FIGURE 5.1.63

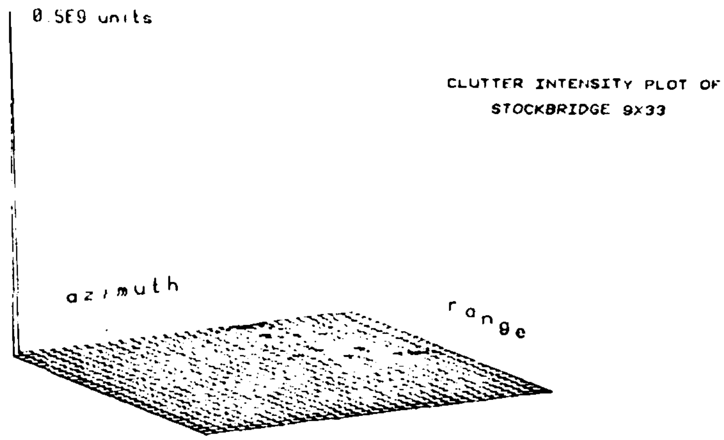

0.5E9 units
CLUTTER INTENSITY PLOT OF
STOCKBRIDGE 9X33
azimuth
range

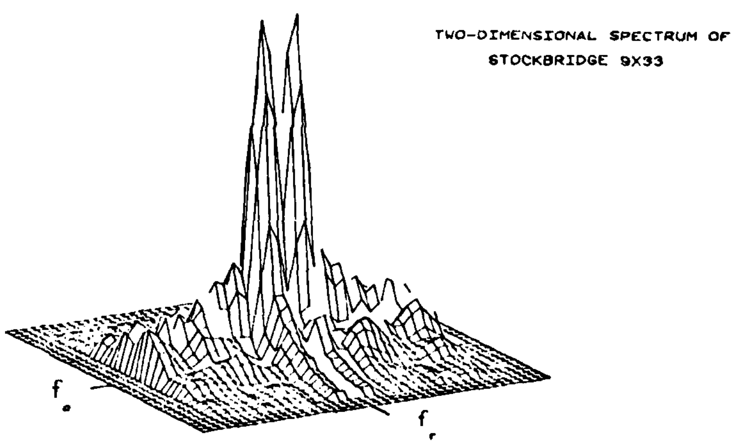

TWO-DIMENSIONAL SPECTRUM OF
STOCKBRIDGE 9X33

FIGURE 5.1.64

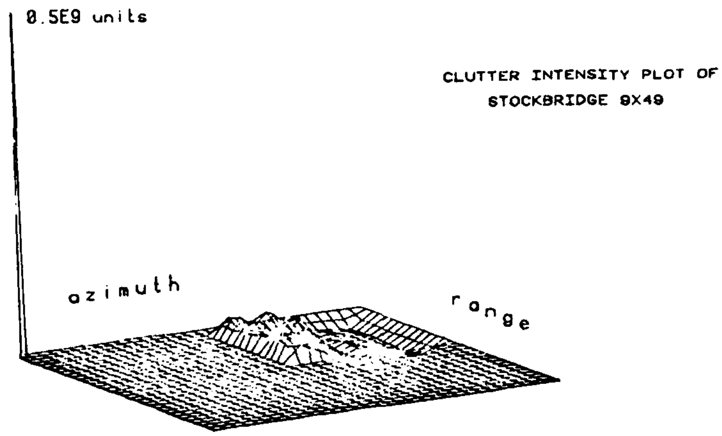
0.5E9 units
CLUTTER INTENSITY PLOT OF
STOCKBRIDGE 9X49
azimuth
range

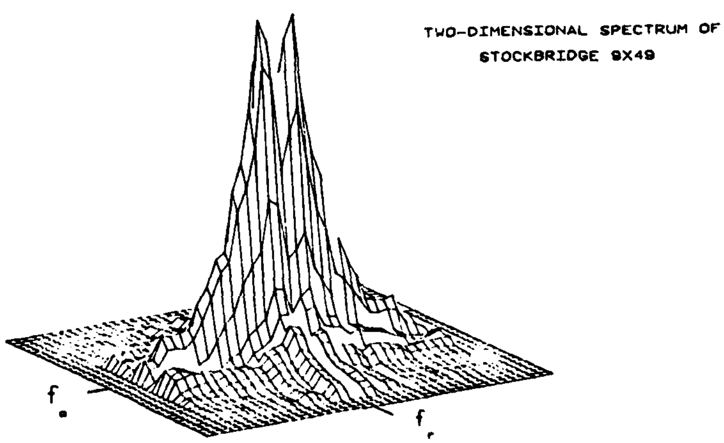
TWO-DIMENSIONAL SPECTRUM OF
STOCKBRIDGE 9X49
f_a
f_r

FIGURE 5.1.65

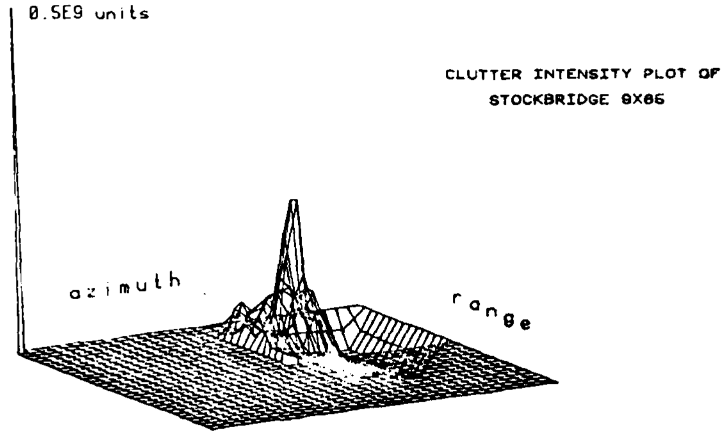
0.5E9 units
CLUTTER INTENSITY PLOT OF
STOCKBRIDGE 9X65
azimuth
range

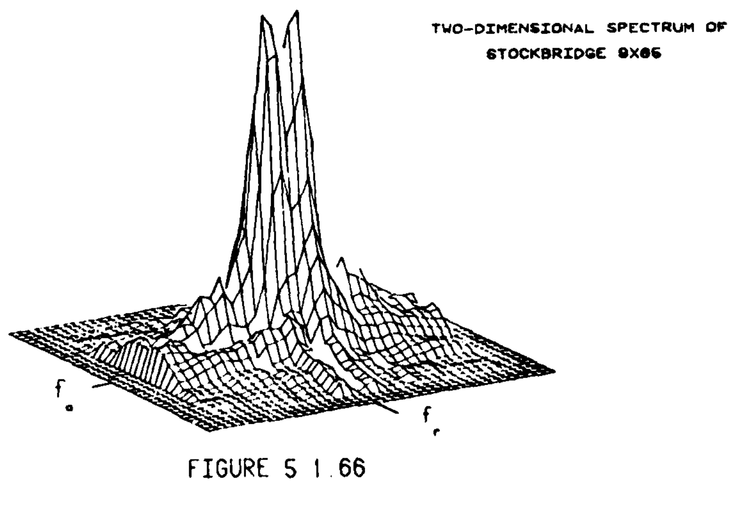
TWO-DIMENSIONAL SPECTRUM OF
STOCKBRIDGE 9X65
f_a
f_r

FIGURE 5.1.66

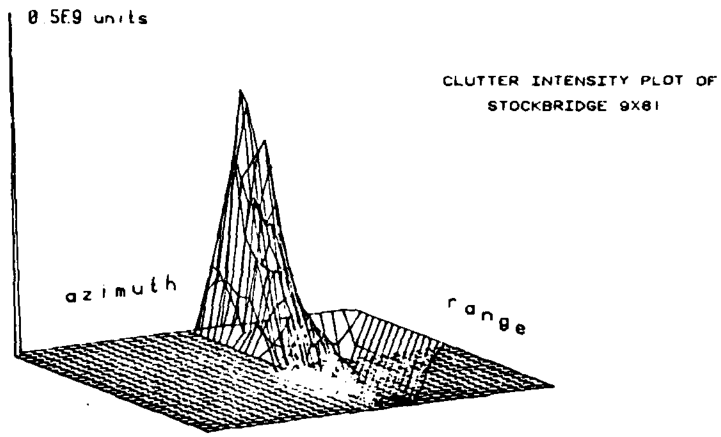
0.5E9 units
CLUTTER INTENSITY PLOT OF
STOCKBRIDGE 9X81
azimuth
range

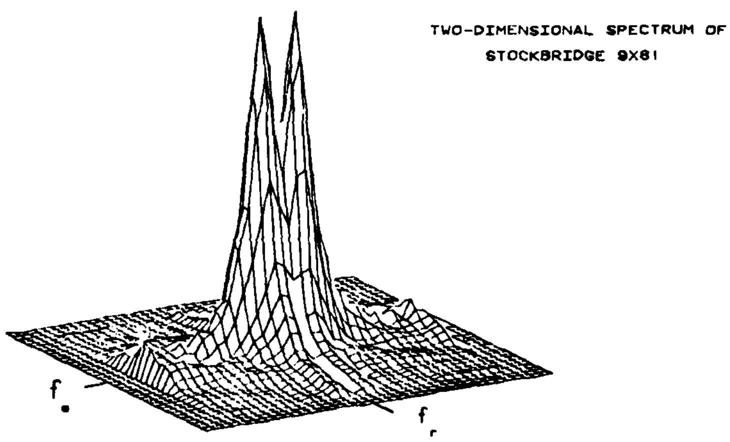
TWO-DIMENSIONAL SPECTRUM OF
STOCKBRIDGE 9X81
f_a
f_r

FIGURE 5.1.67

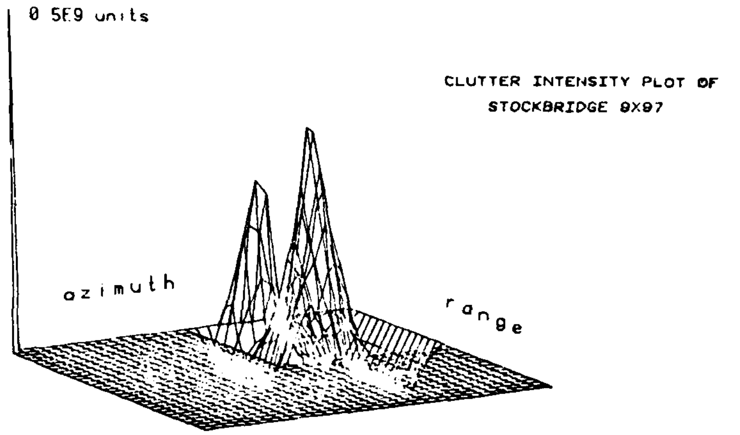
0 5E9 units
CLUTTER INTENSITY PLOT OF
STOCKBRIDGE 9X97
azimuth
range

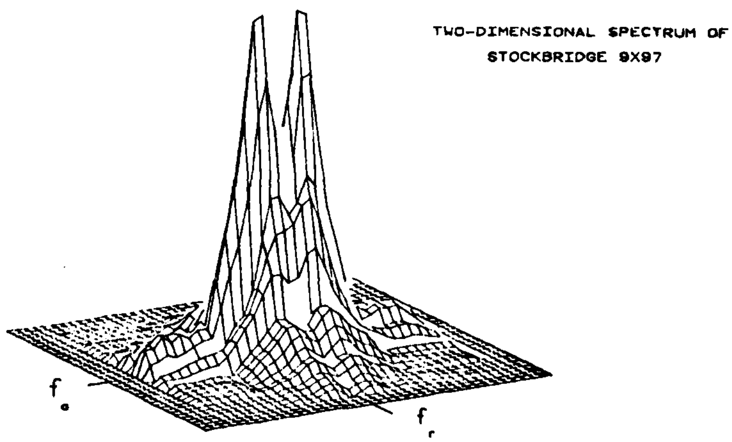
TWO-DIMENSIONAL SPECTRUM OF
STOCKBRIDGE 9X97
f_a
f_r

FIGURE 5 1.68

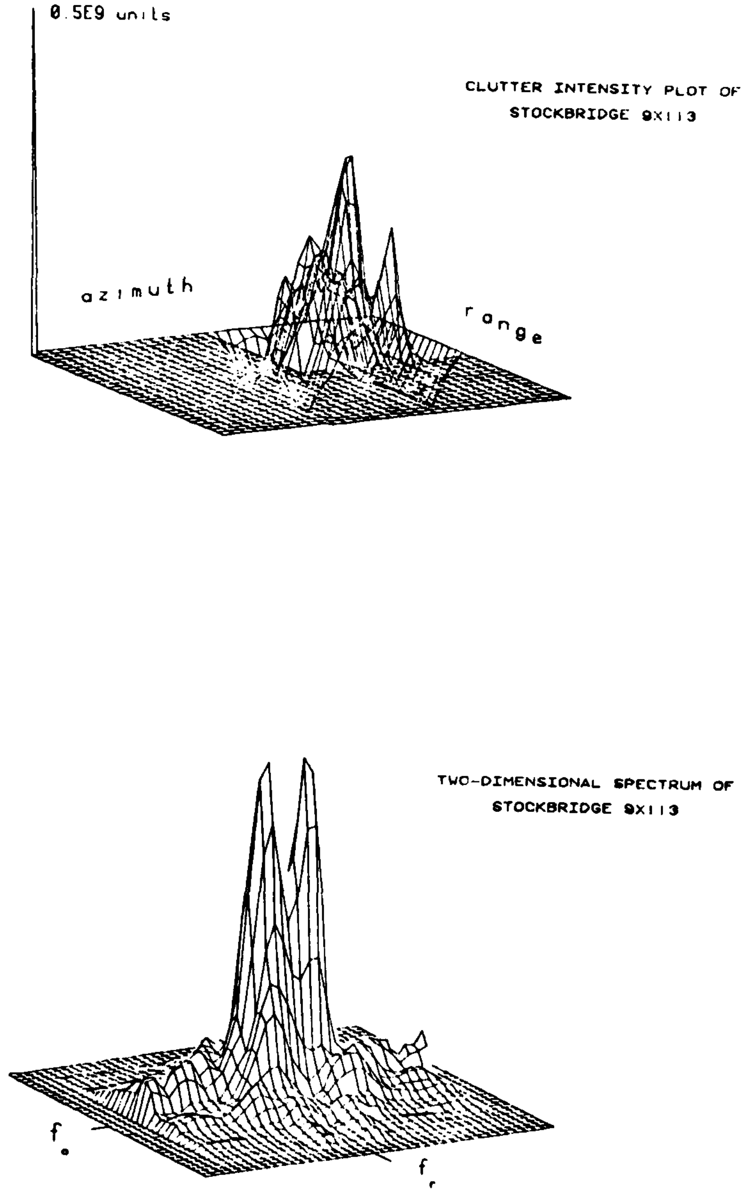
0.5E9 units
CLUTTER INTENSITY PLOT OF
STOCKBRIDGE 9X113
azimuth
range
TWO-DIMENSIONAL SPECTRUM OF
STOCKBRIDGE 9X113
f_a
f_r

FIGURE 5 I 69

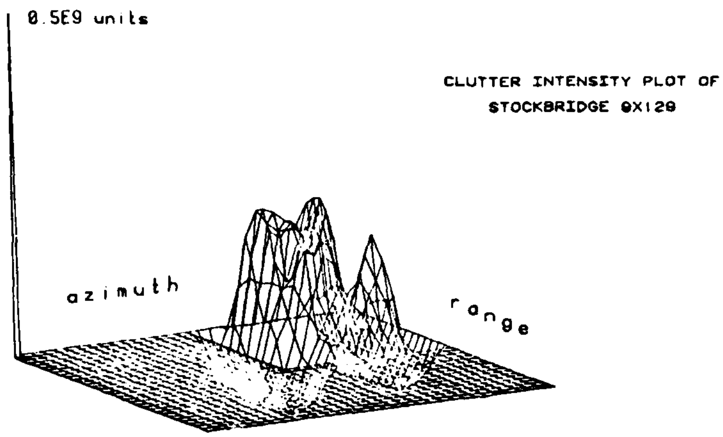
0.5E9 units
CLUTTER INTENSITY PLOT OF
STOCKBRIDGE 9X129
azimuth
range

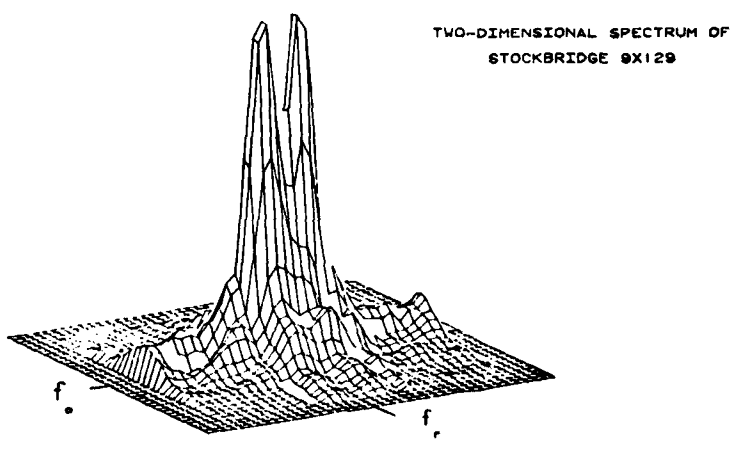
TWO-DIMENSIONAL SPECTRUM OF
STOCKBRIDGE 9X129
f_a
f_r

FIGURE 5.1 70

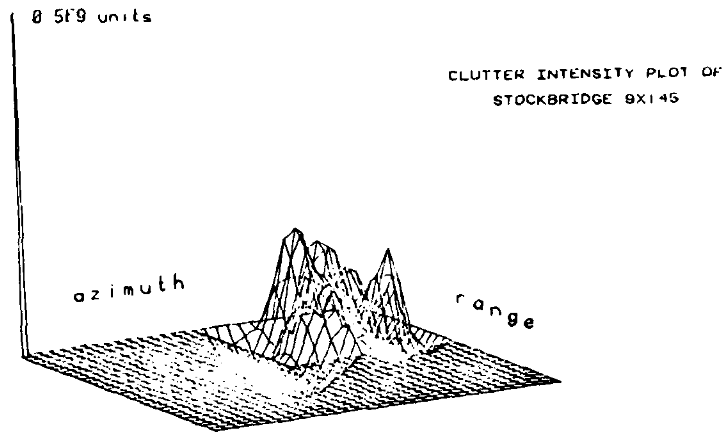
0 5E9 units
CLUTTER INTENSITY PLOT OF
STOCKBRIDGE 9X145
azimuth
range

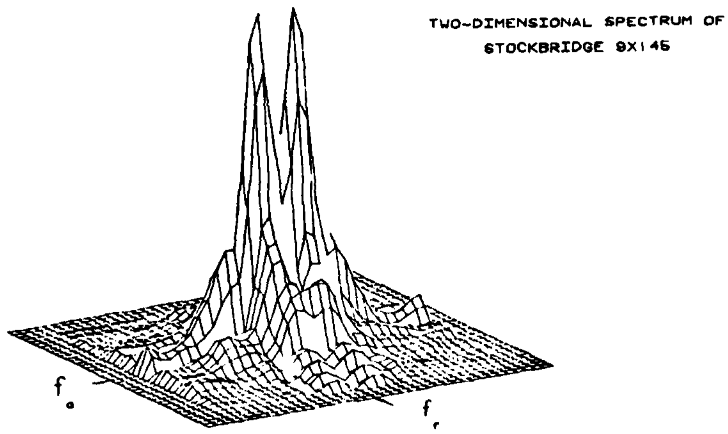
TWO-DIMENSIONAL SPECTRUM OF
STOCKBRIDGE 9X145
f_a
f_r

FIGURE 5.1.71

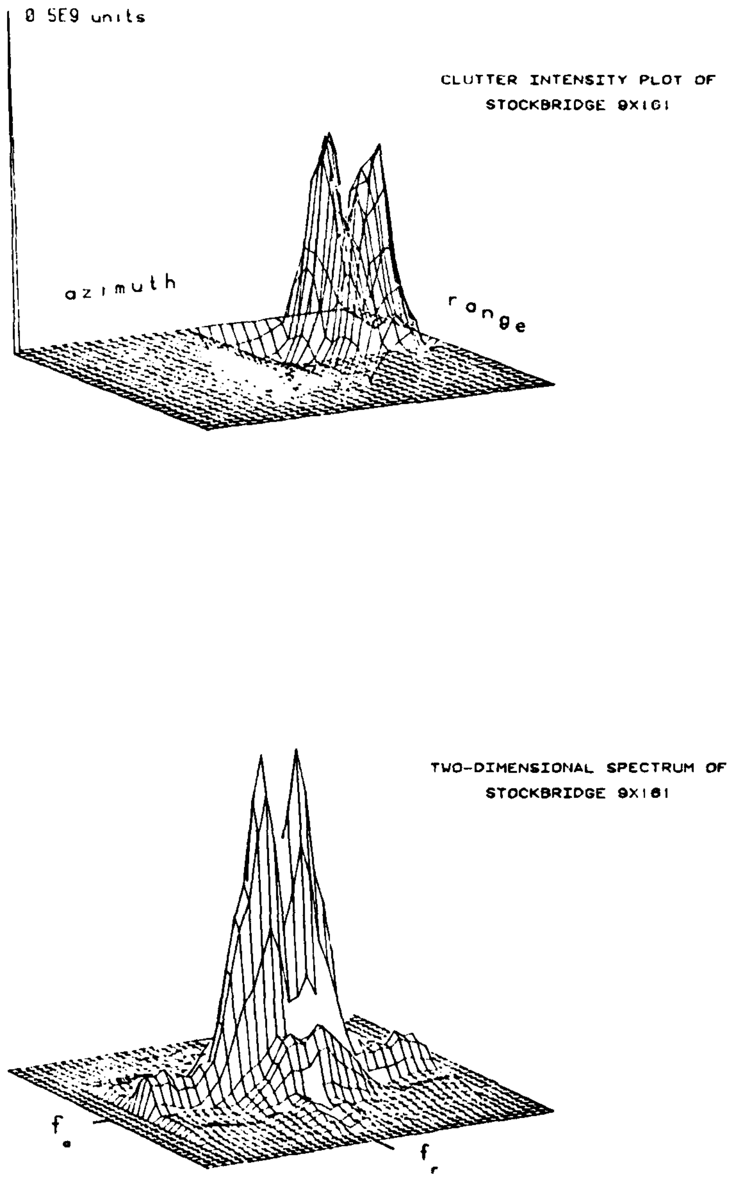
0 5E9 units
CLUTTER INTENSITY PLOT OF
STOCKBRIDGE 9X161
azimuth
range
TWO-DIMENSIONAL SPECTRUM OF
STOCKBRIDGE 9X161
f_a
f_r

FIGURE 5 1 72

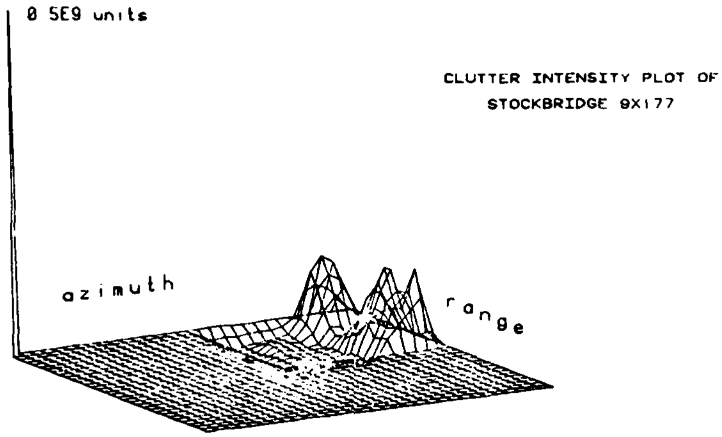

0 5E9 units
CLUTTER INTENSITY PLOT OF
STOCKBRIDGE 9X177
azimuth
range

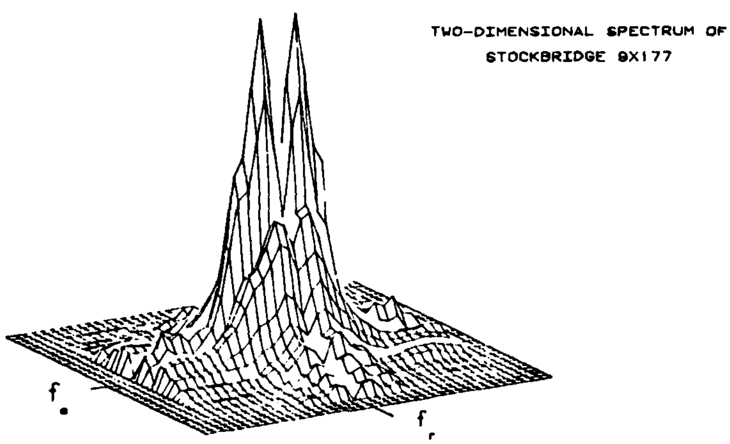

TWO-DIMENSIONAL SPECTRUM OF
STOCKBRIDGE 9X177

FIGURE 5 1 73

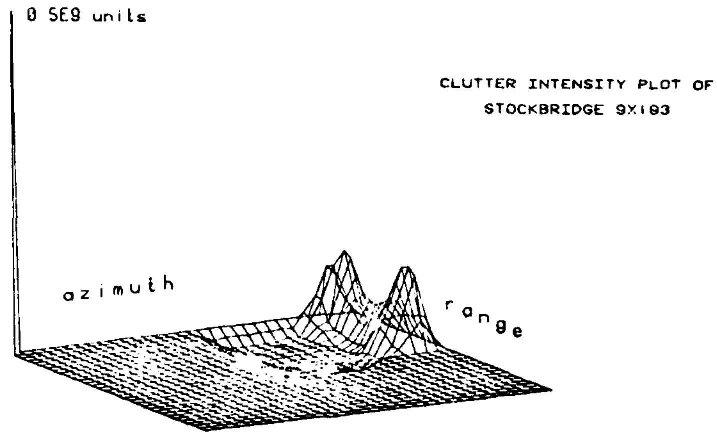
0 5E9 units
CLUTTER INTENSITY PLOT OF
STOCKBRIDGE 9X183
azimuth
range

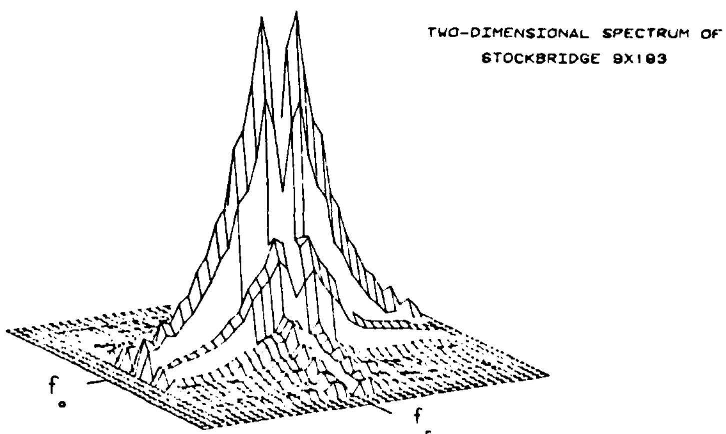
TWO-DIMENSIONAL SPECTRUM OF
STOCKBRIDGE 9X183

FIGURE 5.1.74

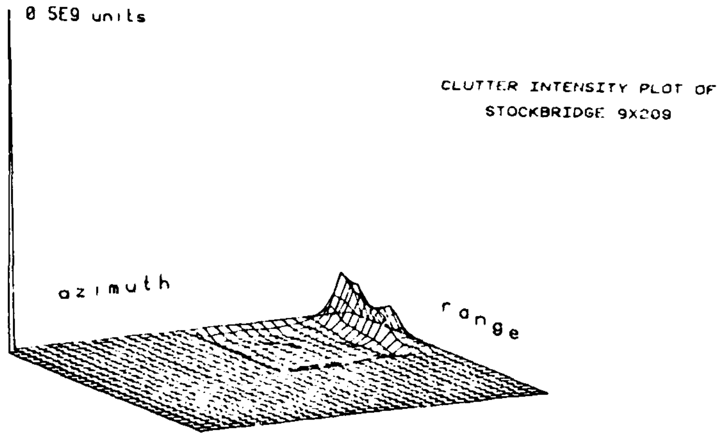
0 SE9 units
CLUTTER INTENSITY PLOT OF
STOCKBRIDGE 9X209
azimuth
range

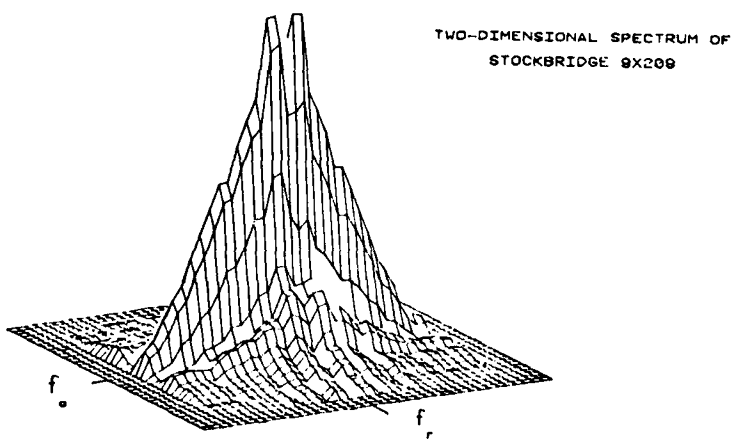
TWO-DIMENSIONAL SPECTRUM OF
STOCKBRIDGE 9X209
f_a
f_r

FIGURE 5.1 75

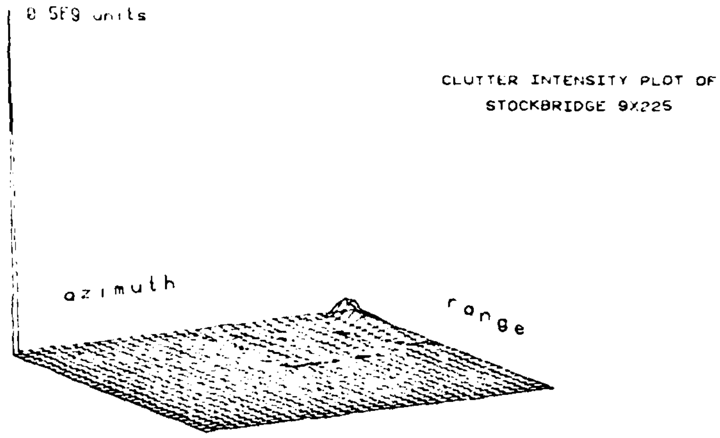

0 5E9 units
CLUTTER INTENSITY PLOT OF
STOCKBRIDGE 9X225
azimuth
range

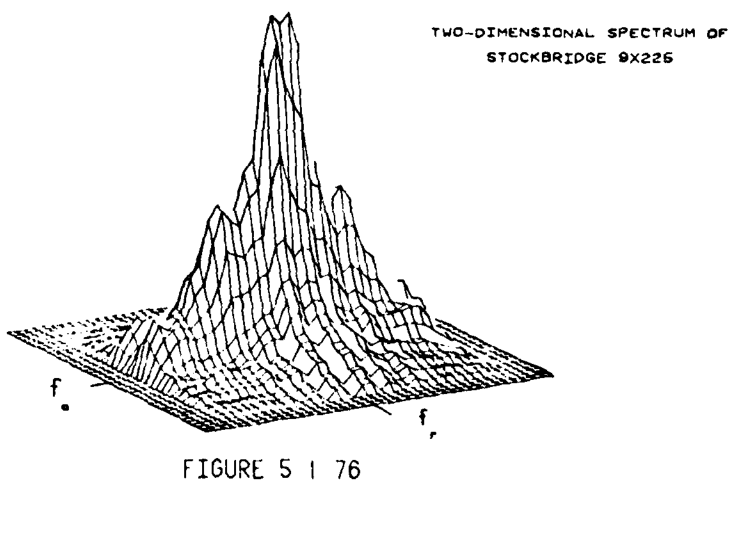

TWO-DIMENSIONAL SPECTRUM OF
STOCKBRIDGE 9X225
f_a
f_r

FIGURE 5 1 76

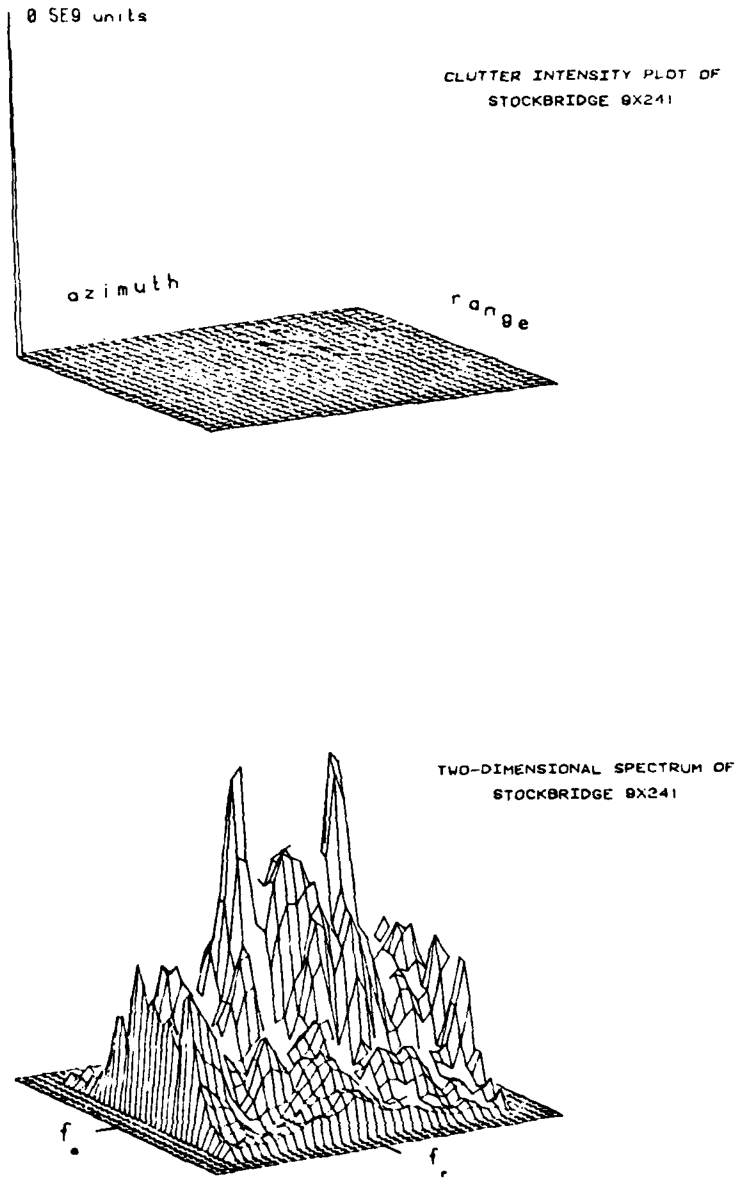
0 SE9 units
CLUTTER INTENSITY PLOT OF
STOCKBRIDGE 9X241
azimuth
range
TWO-DIMENSIONAL SPECTRUM OF
STOCKBRIDGE 9X241
f_a
f_r

FIGURE 5 1 77

SAMPLED SPECTRA OF STOCKBRIDGE AREAS

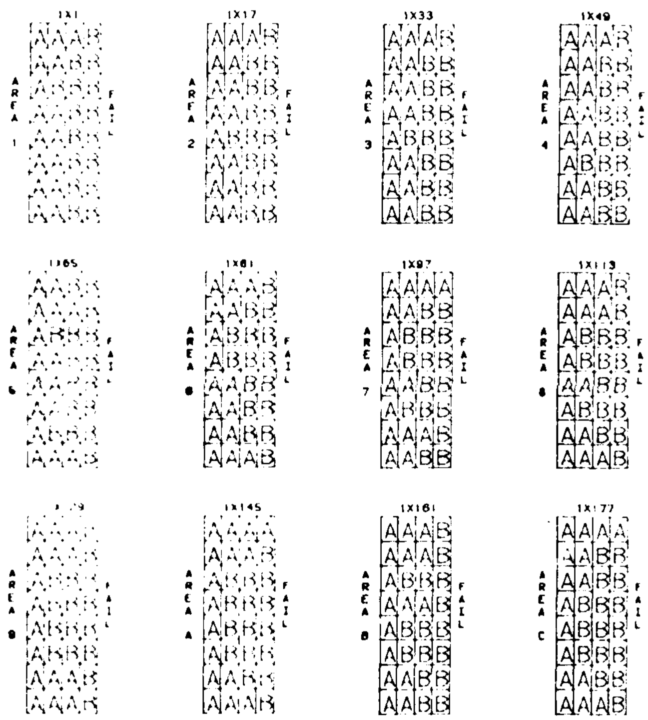

FIGURE 5.1.78

SAMPLED SPECTRA OF STOCKBRIDGE AREAS

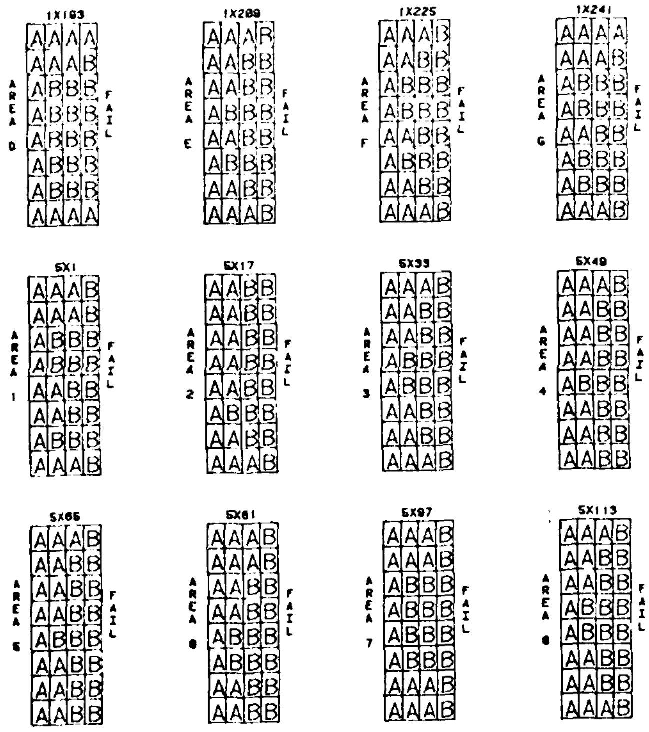

FIGURE 5 1 79

SAMPLED SPECTRA OF STOCKBRIDGE AREAS

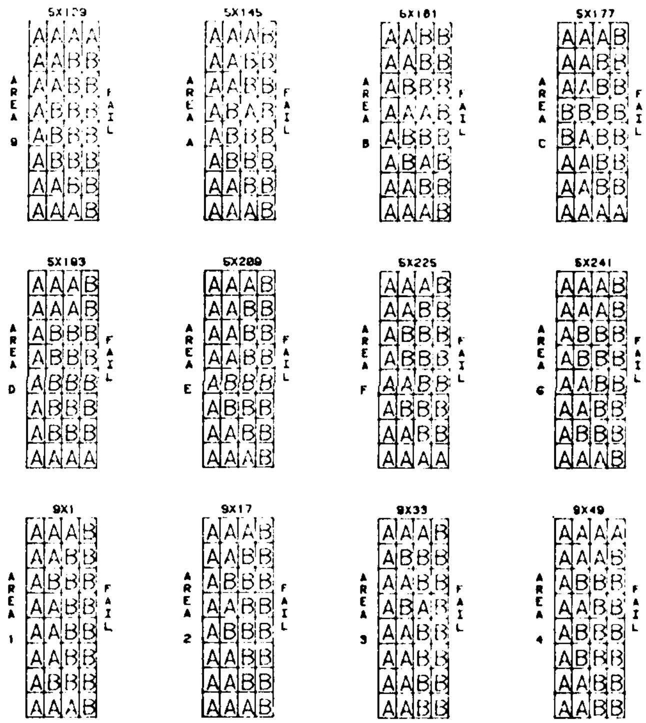

FIGURE 5 1 80

SAMPLED SPECTRA OF STOCKBRIDGE AREAS

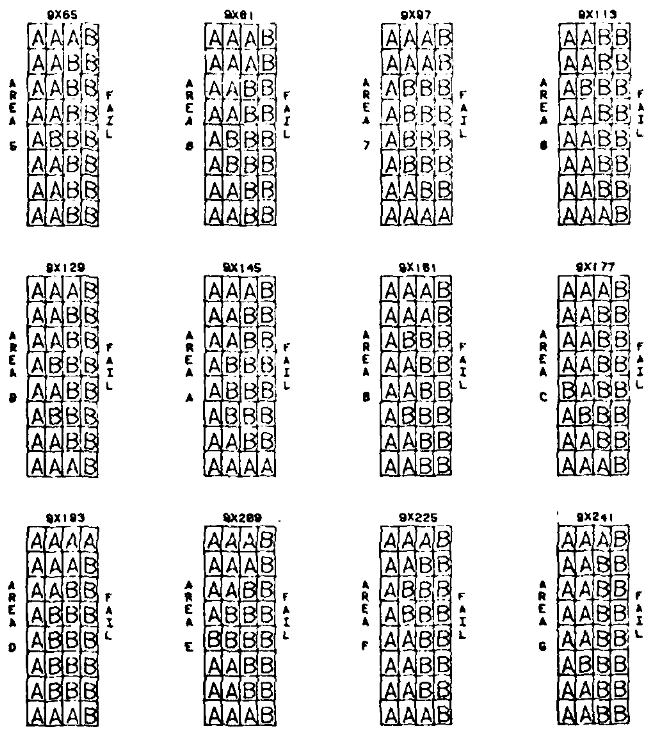

FIGURE 5 1 81

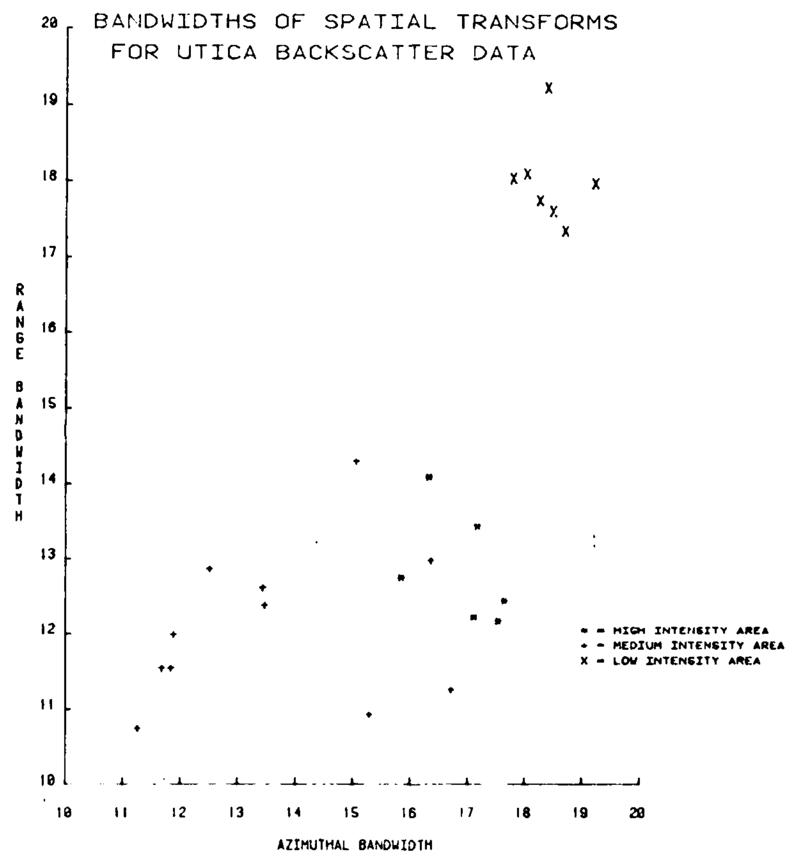

BANDWIDTHS OF SPATIAL TRANSFORMS
FOR UTICA BACKSCATTER DATA
RANGE BANDWIDTH
AZIMUTHAL BANDWIDTH
* - HIGH INTENSITY AREA
+ - MEDIUM INTENSITY AREA
X - LOW INTENSITY AREA

FIGURE 5 I 82

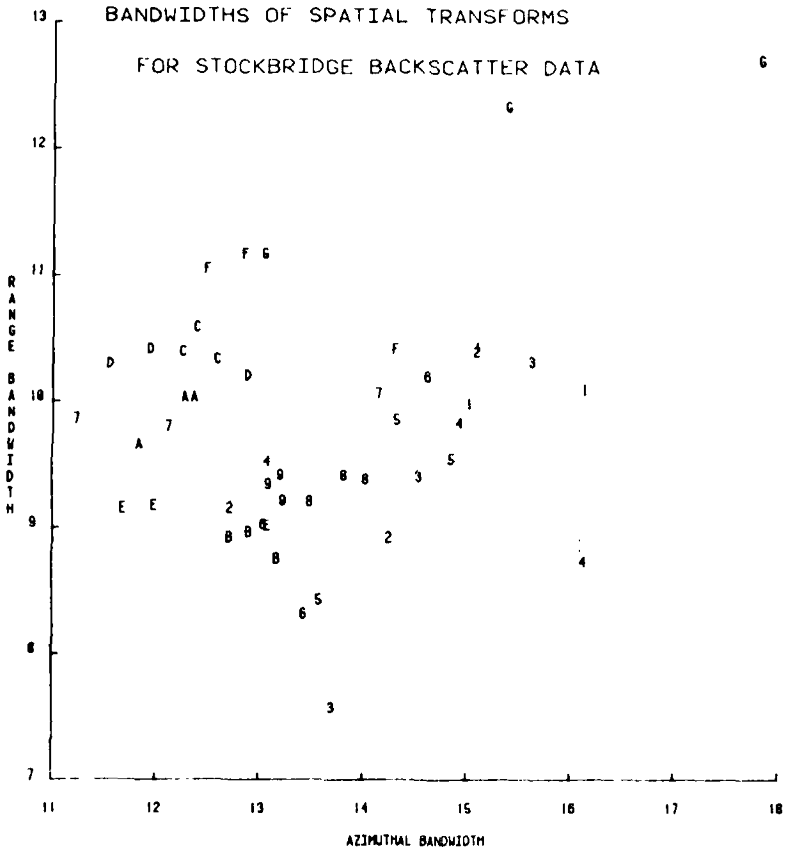
BANDWIDTHS OF SPATIAL TRANSFORMS
FOR STOCKBRIDGE BACKSCATTER DATA
RANGE BANDWIDTH
AZIMUTHAL BANDWIDTH
13
12
11
10
9
8
7
11
12
13
14
15
16
17
18

FIGURE 5.1.83

Section 5.2- The Isodistributive Definition

In attempting to locate homogeneous regions under the isodistributive definition, the researcher must be aware that the regions in question may vary from a minimum of two resolution cells to as many as are contained within the limits of the data. For the independent cells of West Stockbridge Hill, the total number of available window sizes is 1023. Clearly, a choice of window size, or sizes, must be made since running the test on the entire data set for that many windows would be prohibitive in terms of time and funding. Therefore, a few window sizes were used to find whether there are any homogeneous regions under the second definition of homogeneity. The results presented in Figure 5.2.1-5.2.6, located at the end of this section, show that homogeneous regions (crossed areas) of varying sizes can be found in the clutter data.

Figure 5.2.1 shows homogeneous regions that are two resolution cells in azimuth by two resolution cells in range. There were 256 such regions tested. Figure 5.2.1 illustrates that 135 of these proved to be homogeneous under the isodistributive definition. This confirms that homogeneous regions which are 6 degrees wide in azimuth and 120 m in range exist in great numbers in the West Stockbridge Hill data. The area covered by these regions is over 50% of the total area.

In Figure 5.2.1-5.2.4, each figure represents a doubling of the window length in range. It is apparent that a smaller ratio of homogeneous area to total area is obtained as the size of the window increases. This is not surprising if one considers that a greater number of cells per test increases the probability that at least one of the included cells' backscatter will be governed by a dissimilar probability distribution.

One feature of the results for the second definition is particularly interesting. This is that the homogeneous regions tend to be located in areas of mid-range mean value of backscatter. Regarding Figure 5.2.1 and Figure 5.1.2, and comparing (allowing for distortion between the plots), one can see that the homogeneous regions do not occur for the larger window sizes in areas of high backscatter intensity, nor do they occur in areas of low backscatter intensity. These regions of mid-range intensity correspond to the radar-facing slopes of hills as well as the backsides. No other outstanding feature of the topography of these regions is apparent.

Figure 5.2.5 shows regions which passed a two cell by two cell sliding window. The results are plotted on a radial graph like that of Figure 2.2 for easy comparison. The eight azimuths chosen for independence are plotted. The longest arcs are cells which passed the Kruskal-Wallis test in each of the four windows in which it appeared. Shorter arcs denote cells that passed three tests, two tests, and one test, with no arc at all signifying cells that failed all possible tests. Cells that are along the edges of the data sequence can appear in only two tests, except for those points located at the very corners which appear in only one test.

The largest homogeneous regions found appear in Figure 5.2.6.

These were found by testing areas selected by looking for areas in Figure 5.2.1, which are dense in terms of the cells that passed the two by two, sliding window. The areas which show the greatest concentration of small homogeneous regions were suspected of larger scale homogeneity. Again, these regions correspond to leading and trailing edges of hills that appear on the topographic maps of the West Stockbridge Hill area. As can be seen in Figure 5.2.6, one area stretches across four cells in azimuth. This region, in particular, corresponds to the radar-facing side of West Stockbridge Hill, which exhibits a very large gradient, predominantly in the radial direction as measured from the radar. The same is true of the area that overlaps the four azimuth wide region, only it is approximately twice the length in range as the previous region. The remaining two regions correspond to the backsides of two hills. The area which spans azimuths 5 and 6 is on the backside of Stockbridge Hill. The remaining area is on the backside of Eaton Hill, whose crest is just outside the area covered by the data. Eaton Hill is within the minimum range of the data and just outside the 209 degree azimuth.

The results of the second definition of homogeneity represent several runs of the Kruskal-Wallis test. The results shown in Figure 5.2.6 were tested on the basis of the previous results. This "result-guided" testing procedure was devised to find the largest areas which might pass the test. It is desirable to locate the largest regions because these areas may prove to be the most useful, since areas fitting this definition are homogeneous regions within which the statistics of the backscatter in the individual resolution cells are similar to one another. This type of information may prove to be very useful to radar system designers. In particular, the knowledge that homogeneous regions exist which are a pulse length or more in range duration will possibly aid in the design of radars employing such signal processing techniques as pulse compression and CFAR.

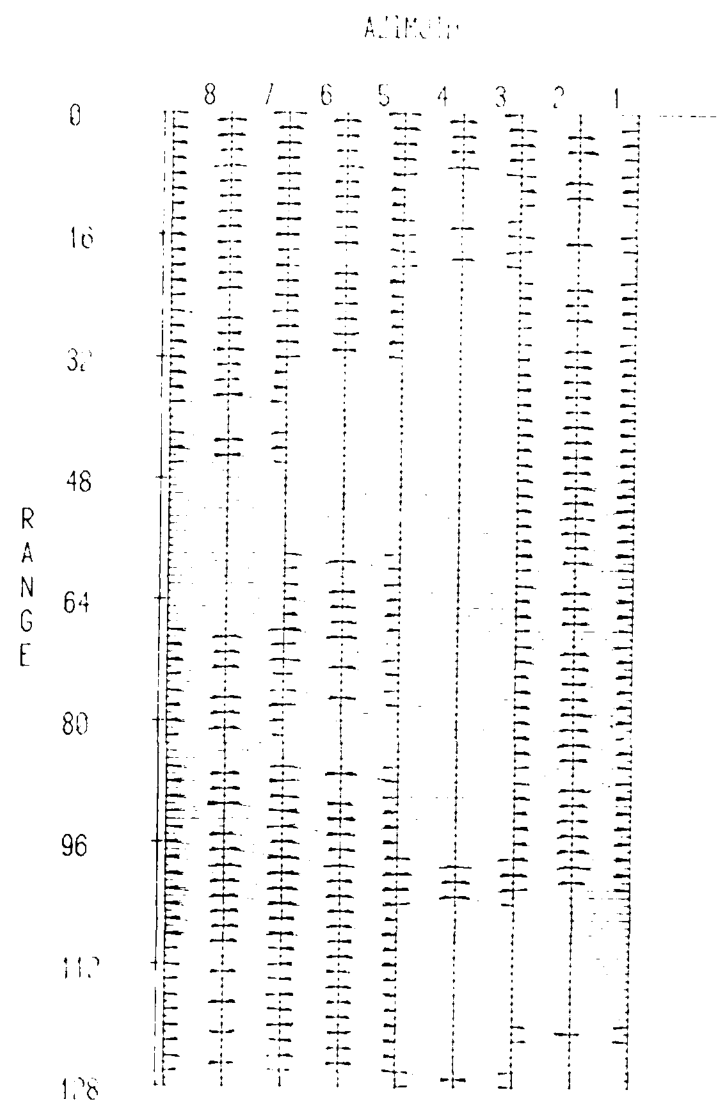

FIGURE 5.2 [illegible] CELL BY 2 CELL ISODISTRIBUTIVE REGIONS

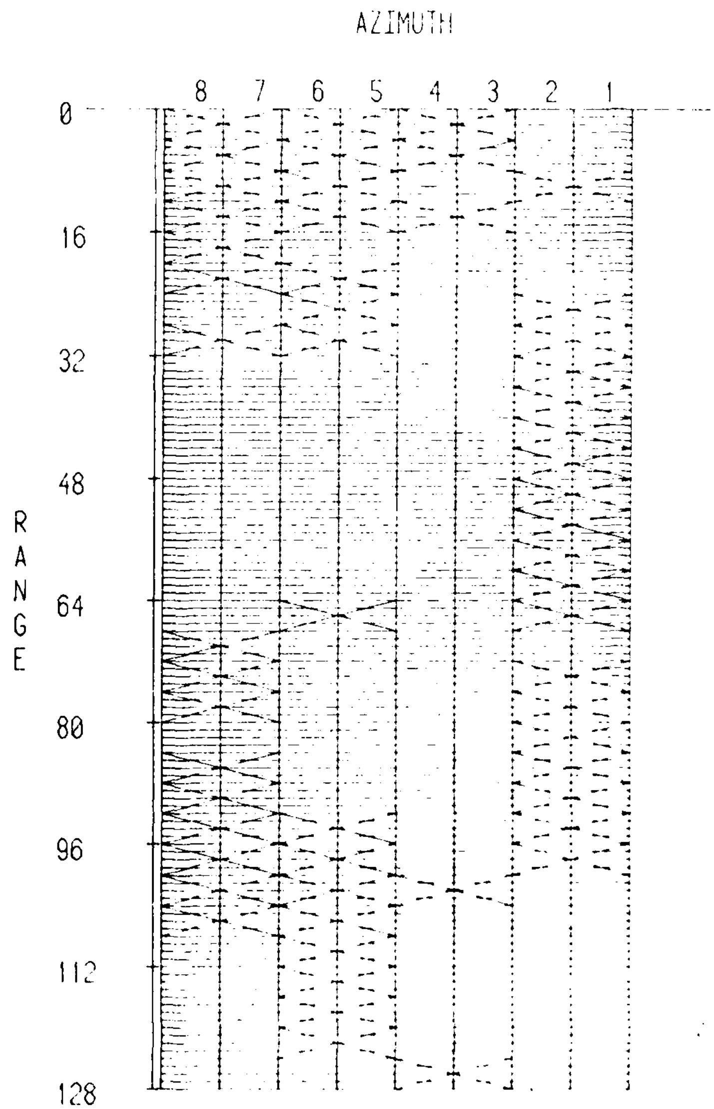

FIGURE 5 2 2- 2 CELL BY 4 CELL ISODISTRIBUTIVE REGIONS

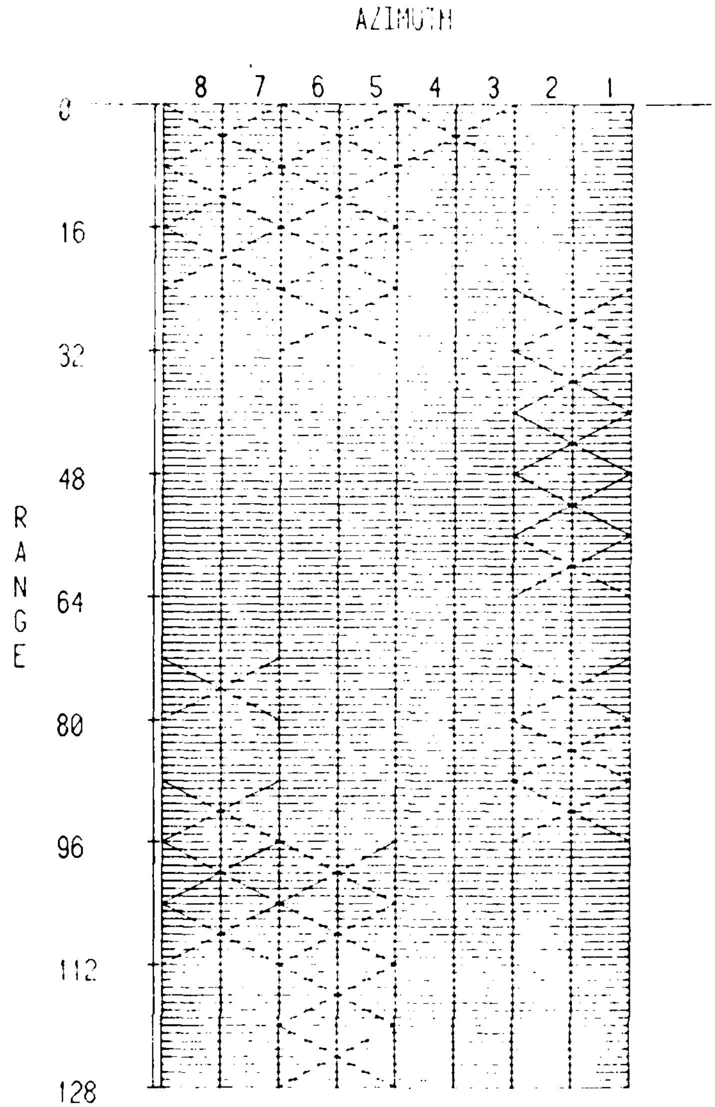

FIGURE 5 2 3- 2 CELL BY 8 CELL ISODISTRIBUTIVE REGIONS

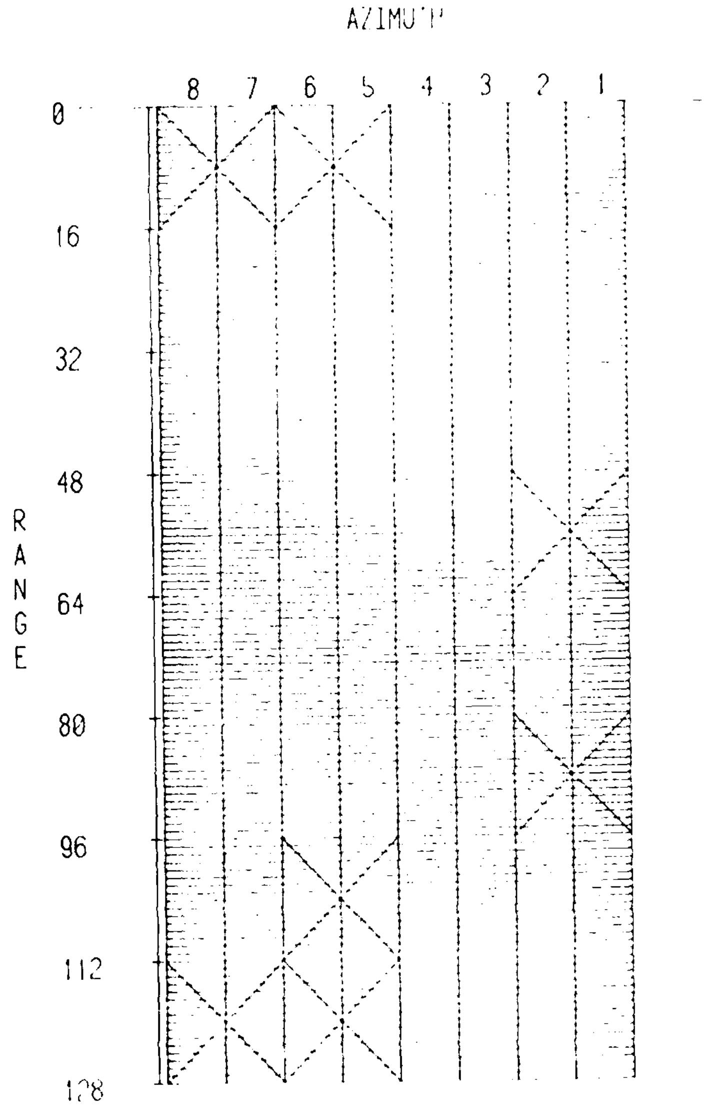

FIGURE 5.2.4 2 CELL BY 16 CELL ISODISTRIBUTIVE REGIONS

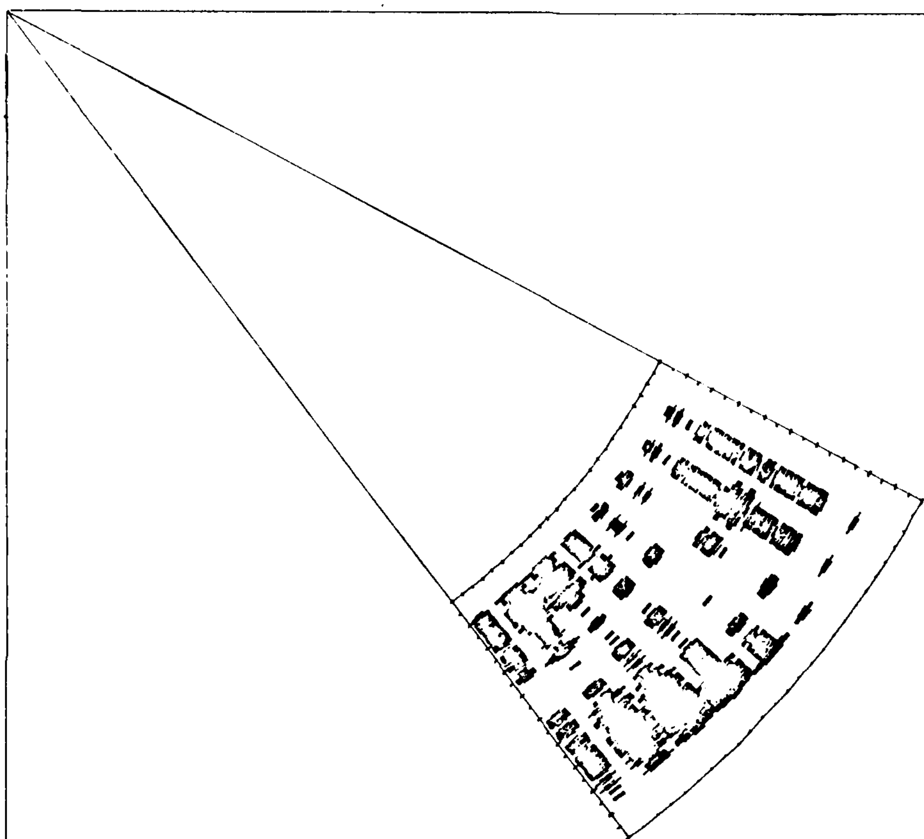

FIGURE 5 2.5- 2 CELL BY 2 CELL, OVER-LAPPING ISODISTRIBUTIVE REGIONS

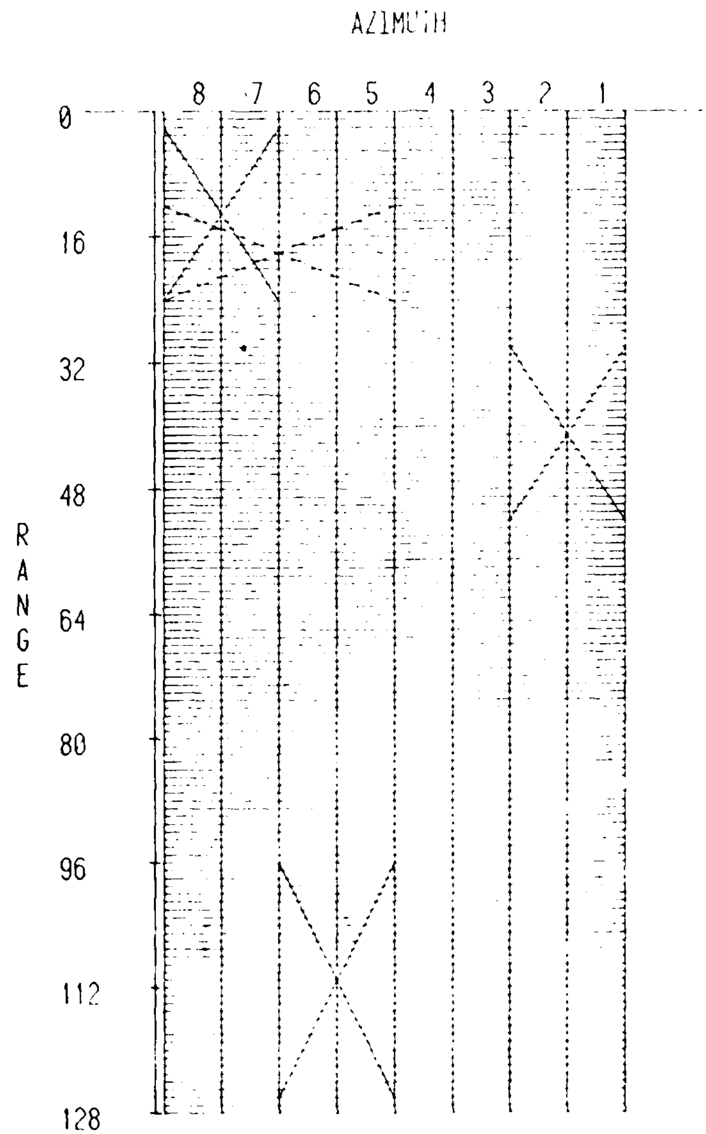

FIGURE 5.2.6- LARGEST ISODISTRIBUTIVE REGIONS LOCATED

Chapter Six- Conclusions and Suggestions for Future Work

Section 6.1- Conclusions

The overall goal of this project is to determine a relationship between the topography of the radar environment and the clutter which is perceived by either a human observer or an automatic radar. In moving towards this objective, the present study has offered an approach that begins with the separation of radar clutter into its components. These components have been designated to be homogeneous regions.

Two definitions of radar clutter homogeneity have been presented and tested for their applicability to two sets of backscatter data, the Utica and West Stockbridge Hill data sets. In keeping with Webster's definition of the word "homogeneous" [19], the two definitions of radar clutter homogeneity indicate areas in which the clutter signal possesses a uniform structure throughout the enclosed area. The rough clutter definition encompasses clutter regions which are homogeneous in the sense that the finite, two-dimensional clutter signal within the homogeneous region represents a broken, uneven surface. The isodistributive definition of radar clutter homogeneity includes regions which are homogeneous in the statistical sense, i.e., the backscatter measurements in every cell of the region can be modeled by a common probability distribution. Both definitions were successful in locating homogeneous regions. The rough clutter regions seem to correspond to ground areas which exhibit low intensity radar return which is just above the noise level in the radar receiver. The isodistributive definition has located areas that lie in the valleys between high-intensity regions.

The viability of the rough clutter definition as presented in this thesis is heavily dependent upon the radar resolution as demonstrated in Section 5.1. Three possible solutions to this problem remain to be investigated.

First, a determination of the actual beam pattern which is convolved with the ground should be made so that some form of equalization for beam effects may be attempted. However, any promising results which lie in this direction rely on both a beam pattern spectrum which is, at least, approximately invertible, and an insignificant degradation of the signal-to-noise ratio at the higher two-dimensional frequencies where beam pattern equalization would have a great effect on boosting the effect of receiver noise.

Second, an increase of the radar resolution, so that each recorded backscatter sample represents an area of ground on the order of a few square meters, would also increase the practicality of the rough clutter definition. This approach requires an increase in both range resolution and azimuthal resolution. The increased range resolution is generally attainable through pulse compression techniques, which are in general use. On the other hand, increasing the azimuthal resolution of many presently active search radars would require costly changes in their antenna structures.

The third solution is to widen the definition of homogeneity in regard to the two-dimensional frequency content of the clutter signal. It is apparent that the rough clutter definition is very stringent when applied to low resolution clutter returns. It may be sufficient to define clutter regions in which the spectral content includes a dominant frequency component which is removed from either or both frequency axes. This type of categorical definition would indicate regions whose clutter returns exhibit significant flucuations in either, or both, range and azimuth. Such homogeneous regions may be useful to radar designers who employ CFAR techniques which require a constant updating of clutter rejection thresholds. This type of undulating clutter region would disclose the rate at which the rejection threshold must be updated. Along the same lines, some promise in the application of clustering algorithms to parametric descriptions of the two-dimensional spectra of clutter regions is indicated in the results of the two-dimensional spectral spreads presented in Figures 5.1.82 and 5.1.83. With other spectral parameters such as energy content and peak spectral component location included, the parametric descriptions of the spectra might yield interesting results when processed by clustering algorithms.

The isodistributive definition appears to be useful in predicting that areas in the valleys adjacent to high-intensity regions are homogeneous in that the resolution cells in those areas exhibit locally equivalent probability distributions. Such information suggests that some common mechanism or effect is responsible for the equivalency of the cellular distributions. One possibility that may warrant further investigation is that the convolution of the compressed pulse shape with the hilltops produces notable sidelobes which may cause homogeneous clutter distributions within the resolution cells wherein the sidelobes reside.

Further testing of the isodistributive definition is necessary. Additional backscatter data sets of West Stockbridge Hill, as well as other similarly hilly areas, are required to determine whether this definition consistently corresponds to slopes of hills over temporal and spatial differences. If it proves to be consistent, then then the definition will be particularly applicable to radar signal processing techniques, such as CFAR, which utilize statistical clutter information to reject clutter.

Section 6.2- Suggestions for Future Research

Several possible new directions may be taken in solving the problem of suitably defining homogeneous regions. In Figure 6.1, the mean value of the West Stockbridge Hill data is displayed in a three-dimensional plot. Figure 6.2 shows the variance plot of the same data set. It appears that some positive spatial correlation exists between the mean and variance of the West Stockbridge Hill data set. In Figure 6.3, the normalized standard deviation is displayed, where the normalization is to the mean value of the backscatter in the resolution cell. These

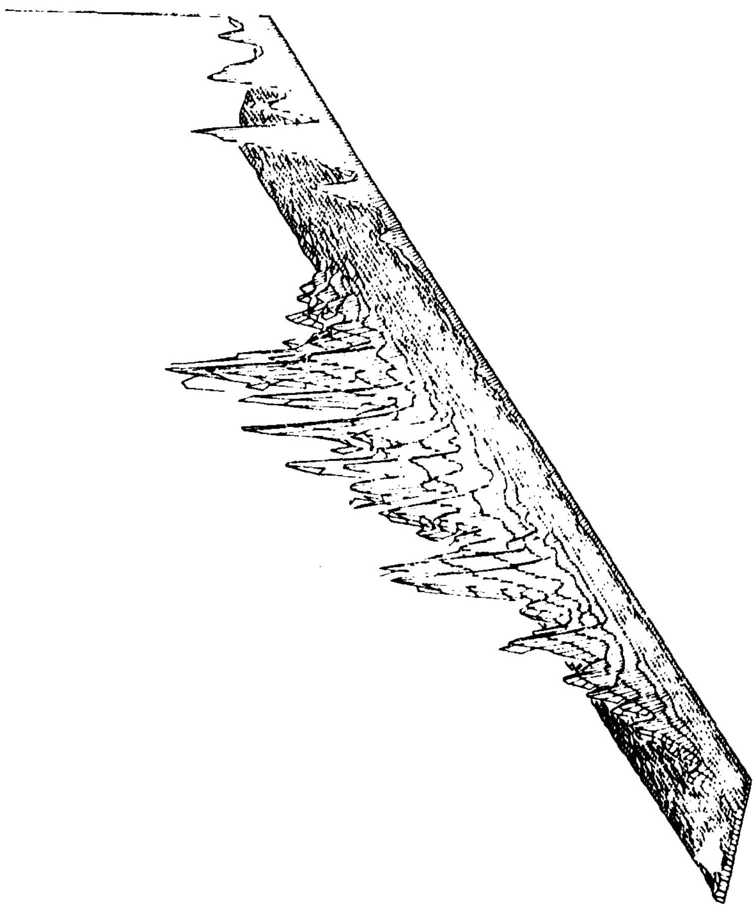

FIGURE 6.1- THREE-DIMENSIONAL PLOT OF THE WEST STOCKBRIDGE HILL MEAN VALUE DATA

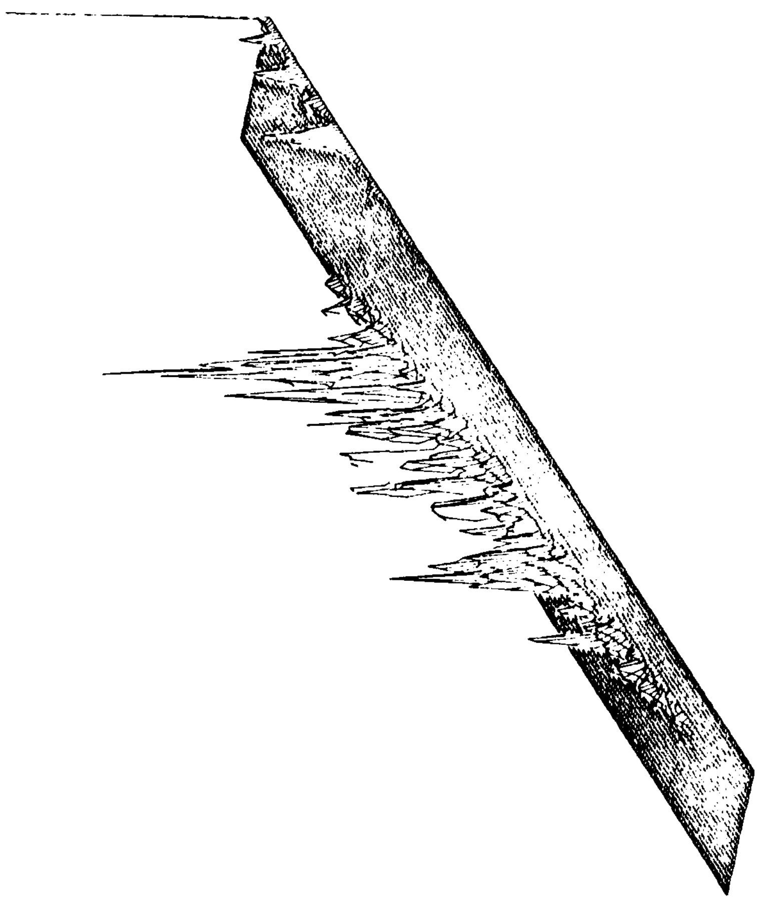

FIGURE 6 2- THREE-DIMENSIONAL PLOT OF THE WEST STOCKBRIDGE HILL SAMPLE VARIANCE

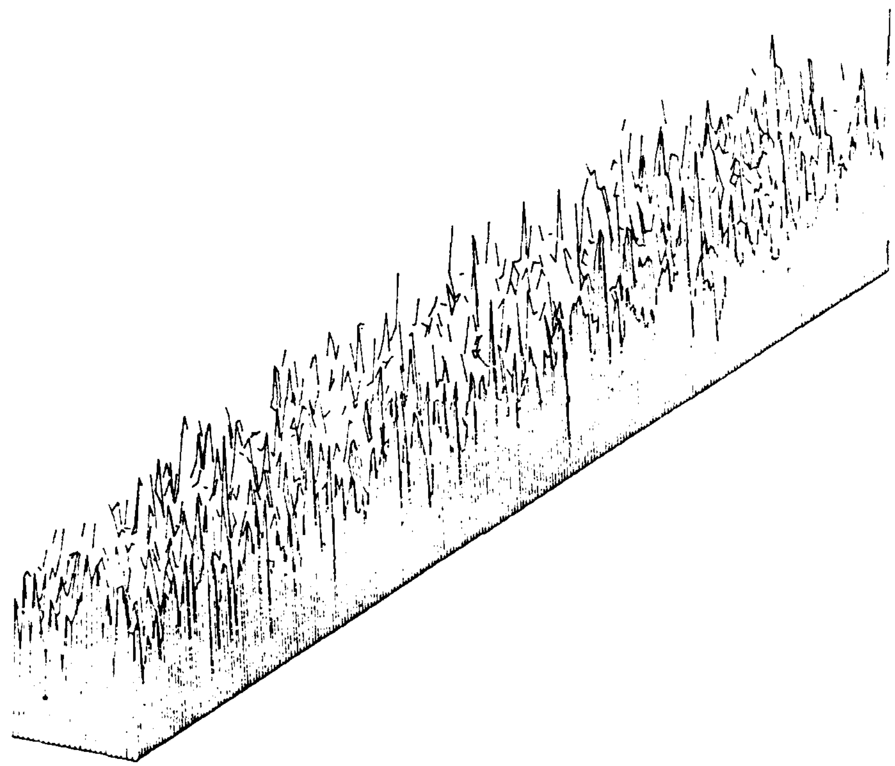

FIGURE 6 3- THREE-DIMENSIONAL PLOT OF THE WEST STOCKBRIDGE HILL NORMALIZED STANDARD DEVIATION

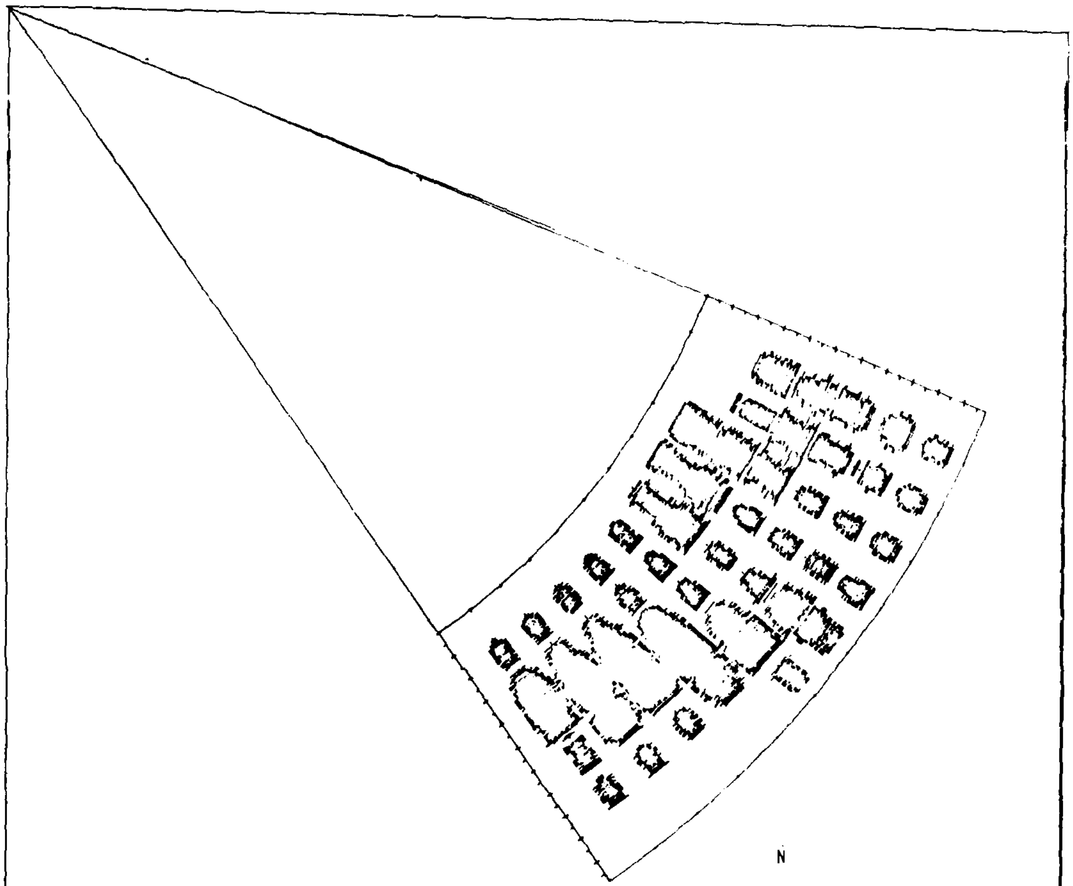

FIGURE 6 4- SIMULATED PPI DISPLAY OF DOPPLER SPREADS FOR COHERENTLY DETECTED STOCKBRIDGE DATA observations are consistent with the non-homogeneous, Rayleigh clutter model discussed by Szajnowski [12]. Further work along this line may be useful in relation to the isodistributive definition of homogeneity which requires a more formal method of preprocessing. In addition to the aforementioned processing, the third data set of coherently detected data, taken in the West Stockbridge Hill area, has been doppler processed and the corresponding doppler spreads have been computed and are shown in Figure 6.4, where long arcs on the radial graph denote large doppler spreads and short arcs indicate smaller spreads. Some correlation of the large doppler spreads with large mean backscatter return can be seen. Further work in discovering the cause of this correlation would require study of the ground cover in these areas of large doppler spread and a corresponding theoretical analysis of the doppler spreads which could be expected.

In continuing along the lines of research in the present study, the next iteration of work should include the investigation of methods for collating the topographic maps with the clutter maps so that spatially accurate comparisons of topographic features and the homgeneous regions located by both the rough clutter definition and the isodistributive definition may be made. This is by no means a simple task. The automatic collation of maps remains as one of the unsolved problems in pattern recognition. As a practical example of this problem, attempts to find a point of reference in the West Stockbridge Hill clutter data failed. There are several large radio towers on the crest of the hill which should be easily detectable through the fact that their backscatter returns should be of high mean value and low variance. However, no such points could be successfully located. The solution to this map collation problem may lie in the utilization of digitized maps. Such maps include specific location information and, in some cases, also contain a great deal of topographic information. These maps would prove useful in solving both the collation problem and the topography-clutter relationship problem. However, difficulties in aligning the topographic maps and the clutter maps may still occur and by no means are digitized maps the complete solution to the topography-clutter relationship problem.

The solution to the topography-clutter problem lies in the successful collaboration of researchers who *approach the problem from* the direction taken in this work and those who attempt to statistically model the radar environment and formulate backscatter models.

Appendix A

The derivation of the equivalent noise bandwidth for the two-dimensional lag window is given in the following.

It is desired that the expected value of the spectral estimate be equal to the actual spectral value:

$$E[C(k,\ell)] = \Gamma(k,\ell). \tag{A.1}$$

The windowed spectral estimate is

$$E[\overline{C}(k,\ell)] = E[C(k,\ell)]*W(k,\ell). \tag{A.2}$$

Substituting (A.1) in (A.2), we have the desired result

$$E[\overline{C}(k,\ell)] = \Gamma(k,\ell)*W(k,\ell). \tag{A.3}$$

Expanding the discrete two-dimensional convolution, we obtain

$$\Gamma(k,\ell)*W(k,\ell) = \sum_{\eta=-\infty}^{\infty} \sum_{\nu=-\infty}^{\infty} \Gamma(\nu,\eta)W(k-\nu,\ell-\eta). \tag{A.4}$$

Now, we desire that

$$\Gamma(k,\ell)*W(k,\ell) = \Gamma(k,\ell). \tag{A.5}$$

Assuming that the bandwidth of the window is narrow compared to the actual spectrum, we may treat Γ as a constant, so that

$$\Gamma \sum_{\eta=-\infty}^{\infty} \sum_{\nu=-\infty}^{\infty} W(k-\nu,\ \ell-\eta) = E[\overline{C}(k,\ell)]. \tag{A.6}$$

This implies that

$$\sum_{\eta=-\infty}^{\infty} \sum_{\nu=-\infty}^{\infty} W(k-\nu,\ell-\eta) = 1 \tag{A.7}$$

which is to say that the volume under our two-dimensional two-dimensional window should be equal to unity. The equivalent window should be a right circular cylinder of radius B and height given by

$$W^2(0,0) = \frac{1}{\pi B^2}\ . \tag{A.8}$$

To obtain the equivalent noise bandwidth, B, of the window, we use the expression

$$\pi B^2 = \frac{\frac{1}{N^2} \sum_{k=1}^{N} \sum_{\ell=1}^{N} W^2(k,\ell)}{\frac{1}{N^2} W^2(0,0)} . \tag{A.9}$$

Using Parseval's theorem and substituting for $W^2(0,0)$, (A.9) becomes

$$\pi B^2 = \frac{1}{N^2 \sum_m \sum_n w^2(m,n)} . \tag{A.10}$$

But we note from (A.7) that

$$w(0,0) = \frac{1}{N^2} \sum_k \sum_\ell W(k,\ell) = \frac{1}{N^2} . \tag{A.11}$$

Since in our case $W(0,0)=1$. We must multiply the entire sequence in (A.10) by $1/N^2$, so that finally

$$B = \left| \frac{N^2/\pi}{\sum_{m=1}^{N} \sum_{n=1}^{N} w^2(m,n)} \right|^{1/2} \tag{A.12}$$

In our case $2B=3.13$.

A three-dimensional plot of the two-dimensional lag window for a length of 2 points, which is that utilized in this thesis, is displayed in Figure A.1.

FIGURE A 1

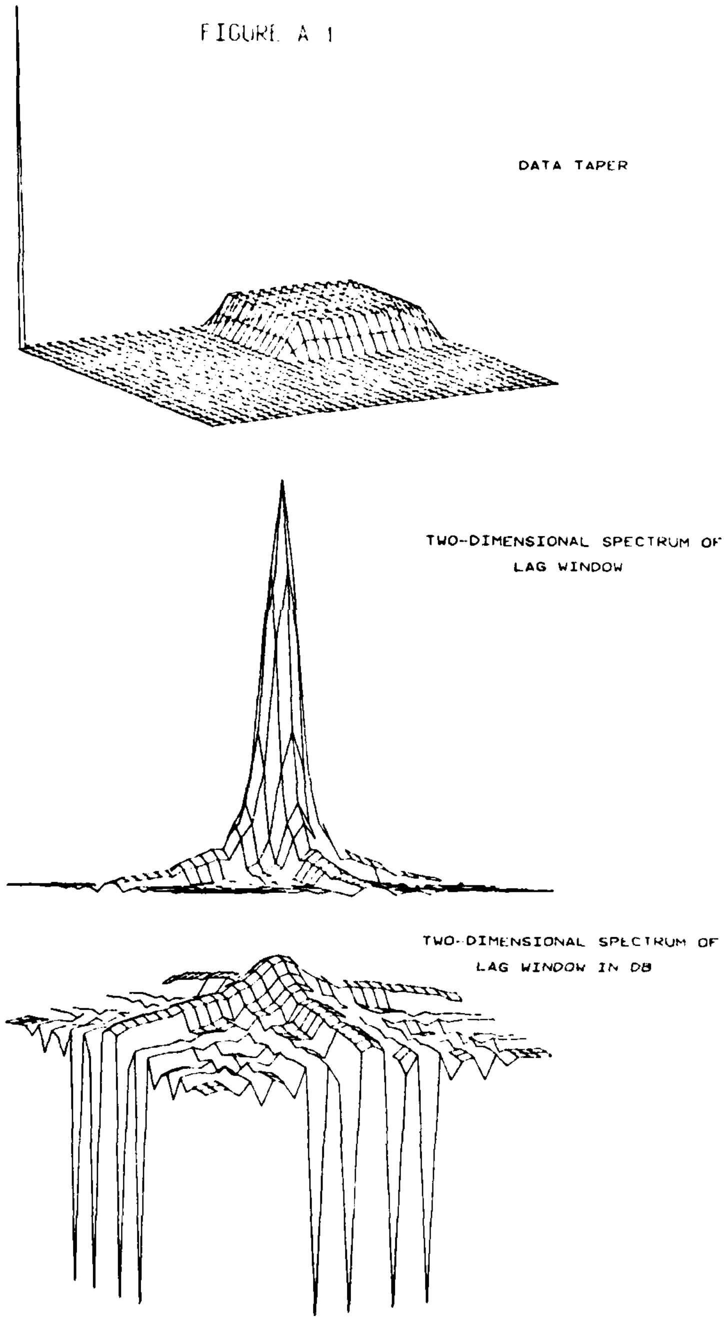
DATA TAPER
TWO-DIMENSIONAL SPECTRUM OF
LAG WINDOW
TWO-DIMENSIONAL SPECTRUM OF
LAG WINDOW IN DB

Appendix B

The following is a brief explanation of the chi-squared approximation to the null distribution of the test statistic H used in the Kruskal-Wallis test.

Non-parametric tests tend to use information that is strictly sample-related. Therefore, the null hypothesis, and the assumptions which are tested, are indirectly related to a population-related hypothesis. This hypothesis may be logically connected to the null, or sample-related, hypothesis. In the present situation, the population-related hypothesis is that the C populations, from which the C sets of samples are drawn, are identically distributed. The sample-related hypothesis is that there are equal a priori probabilities for each of the distinguishable divisions of the N ranks into C columns of R ranks per column. The total number of such divisions is given by:

$$D= N!/(R!)^{C} \tag{B.1}$$

from the rules for permutations and combinations [13].

It is desirable for the test statistic to include information supplied by the column rank sums. Let us choose

$$H' = \sum_{i=1}^{C} R_i \overline{T}_i \qquad (B.2)$$

as the variable part of the test statistic. Furthermore, let us assume that the R_i are all equal. Equation (B.2) becomes

$$H' = \sum_{i=1}^{C} R \overline{T}_i^{\,2} \ . \qquad (B.3)$$

Now, T_i is the sum of R observations made on a finite population, the ranks from 1 to N. The mean of this finite population is

$$\mu = \frac{N+1}{2} \qquad (B.4)$$

and the population variance is

$$\sigma^2 = \frac{N^2-1}{12} \qquad (B.5)$$

Under the null hypothesis, the R observations, which sum to T_i, will be randomly drawn without replacement from the finite population of ranks. In this situation, T_i as a variate will have a mean given by

$$\mu_s = \frac{R(N+1)}{2} \qquad (B.6)$$

and a variance

$$s^2 = \frac{R(N^2-1)}{12}\,\frac{(N-R)}{(N-1)} \tag{B.7}$$

where the final fraction in equation (B.7) is the correction factor for sampling without replacement. By virtue of the Central Limit Theorem, the distribution of the variate, T_i, will approach a normal distribution as R increases. The quantity

$$\frac{T_i - [R(N+1)/2]}{\sqrt{[R(N^2-1)/12][N-R)/(N-1)]}}$$

may be treated as a variate with normal distribution, N(0,1). The sum of the squares of C of the above unit normal variates would be distributed as chi-squared with C degrees of freedom. However, only C-1 of the rank sums are independent, since the last T_i is determined by elimination of the ranks summing to the previous T_i´s. Therefore, only C-1 of the T_i considered may be regarded as independent. Hence, C-1/C of the sum of the squares of T_i is distributed as chi-squared with C-1 degrees of freedom as in

$$\chi^2 \cong \frac{C-1}{C}\sum_{i=1}^{C}\frac{\{T_i-[R(N+1)/2]\}^2}{R(N+1)(N-R)/12} \tag{B.8}$$

Rearranging equation (B.8), we have

$$x^2 \cong \frac{12(C-1)}{C(N-R)(N+1)} \sum_{i=1}^{C} \frac{\{T_i - [R(N+1)/12]\}^2}{R} \qquad (B.9)$$

Noting that

$$T_i = R\,\overline{T}_i \qquad (B.10)$$

and $$N=RC \qquad (B.11)$$

and substituting equations (B.10) and (B.11) in (B.9) we have,

$$x^2 \cong \frac{12}{N(N+1)} \sum_{i=1}^{C} R(\overline{T}_i - \frac{N+1}{2})^2 \qquad (B.12)$$

which is equal to H as in equation (B.1).

```
C*********************************************************************
C          THIS PROGRAM COMPUTES THE TWO-DIMENSIONAL POWER SPECTRUM
C OF A TWO-DIMENSIONAL INPUT SEQUENCE, XREAL.  THE INPUT SEQUENCE
C MUST CONSIST OF A REAL PART, XREAL, AND AN IMAGINARY PART, XIMAG.
C THE INPUT SEQUENCE SIZE CAN BE CHANGE WITH MINOR ALTERATIONS
C SUCH AS DIMENSION CHANGES AND SUBROUTINE ARGUMENT CHANGES.  XRIND
C WILL CONTAIN SAMPLED SPECTRAL ESTIMATES.  THE RATE OF THE SAMPLING
C MAY BE CHANGED SO AS TO ALLOW FOR DIFFERENT LAG WINDOW WIDTHS.
C XREALP AND XIMAGP ARE USED IN SUBROUTINE FFT TO HOLD THE ROWS
C AND COLUMNS OF THE COMPLEX INPUT SEQUENCE.
C*********************************************************************
      DIMENSION XREAL(32,32),XIMAG(32,32),XREALP(32),XIMAGP(32)
      DIMENSION XRIND(8,8)
      INTEGER ARRAY(240),IAZM(100),JRNG(100)
C*********************************************************************
C          ARRAY IS USED IN SUBROUTINE SQUARE TO READ IN A DATA FILE
C SO THAT THE APPROPRIATE VALUES IN THE FILE ARE SELECTED.  IAZM AND
C JRNG READ FROM UNIT 5 THE MINIMUM RANGE AND AZIMUTH COORDINATES OF
C THE AREAS TO BE PROCESSED.
C*********************************************************************
      COMMON DCVALT
      DO 1488 I=1,24
      READ(5,1489) IAZM(I),JRNG(I)
1489  FORMAT(2I4)
1488  CONTINUE
      PI=3.141593
```

```
C*****************************************************************
C        THE LOOP IN WHICH THE POWER SPECTRUM IS COMPUTED BEGINS.
C*****************************************************************
      DO 9999 III=1,24
      DCVAL=0.0
      DCVALT=0.0
      IAZMTH=IAZM(III)
      JRANGE=JRNG(III)
      WRITE(6,2838)
2838  FORMAT('1')
      WRITE(6,1477) IAZMTH,JRANGE
      WRITE(6,2837)
2837  FORMAT(' ')
1477  FORMAT(' STARTING AZIMUTH AND RANGE: ',2I4)
      CALL SQUARE(XREAL,IAZMTH,JRANGE,16,32)
      CALL PAD(XREAL,16,32)
      CALL PLOT(XREAL,32,32)
      CALL DC(XREAL,16,32)
C*********************************************************
C         THE FOLLOWING NESTED LOOP SETS THE IMAGINARY PART OF
C THE INPUT SEQUENCE TO ZERO AND REMOVES THE DC VALUE
C OF THE INPUT SEQUENCE.
C*********************************************************
      DO 46 I=1,32
      DO 46 J=1,32
      XIMAG(I,J)=0.0
      IF((I.GT.16).OR.(J.GT.16)) GO TO 46
      XREAL(I,J)=XREAL(I,J)-DCVALT
46    CONTINUE
      CALL DC(XREAL,32,32)
      CALL TAPER(XREAL,2,16,32)
C*********************************************************
C   THE FOLLOWING CODE PERFORMS THE IN-PLACE CALCULATION OF
C THE POWER SPECTRUM.  AT THE CALL TO WINDOW XREAL CONTAINS
C THE AUTOCORRELATION SEQUENCE OF THE INPUT SEQUENCE.
```

```
C*****************************************************************
      CALL DC(XREAL,32,32)
      CALL FFT2D(XREAL,XIMAG,32,0,2)
      CALL FFT2D(XREAL,XIMAG,32,1,0)
      CALL WINDOW(XREAL,16,0,16,32)
      CALL FFT2D(XREAL,XIMAG,32,0,0)
C***************************************************************
C     THIS NESTED LOOP PERFORMS THE SPECTRAL SAMPLING.  BY CHANGING
C THE DIMENSIONS OF XRIND AND THE STATEMENTS THAT INCREASE JCOL
C AND IROW, THE RATE OF SAMPLING CAN BE CHANGED.
C***************************************************************
      IROW=1
      DO 63 I=1,8
      JCOL=1
      DO 64 J=1,8
      XRIND(I,J)=XREAL(I+IROW,J+JCOL)/1024.0
      JCOL=JCOL+3
64    CONTINUE
      IROW=IROW+3
63    CONTINUE
C*****************************************************************
C     THE FOLLOWING PAIR OF NESTED LOOPS REARRANGES THE SPECTRUM
C SO THAT DC APPEARS AT XREAL(17,17).
C*****************************************************************
      DO 4321 I1=1,16
      DO 4321 J1=1,16
      I2=I1+16
      J2=J1+16
      XHOLD=XREAL(I1,J1)
      XREAL(I1,J1)=XREAL(I2,J2)
      XREAL(I2,J2)=XHOLD
4321  CONTINUE
      DO 8765 I1=1,16
      DO 8765 J1=17,32
      I2=I1+16
      J2=J1-16
      XHOLD=XREAL(I1,J1)
      XREAL(I1,J1)=XREAL(I2,J2)
      XREAL(I2,J2)=XHOLD
```

```
8765  CONTINUE
      QMAX=0.0
      DO 1111 I=1,32
      DO 1111 J=1,32
      IF(QMAX.GT.XREAL(I,J)) GOTO 1111
      IPEAK=I
      JPEAK=J
      QMAX=XREAL(I,J)
1111  CONTINUE
C*************************************************************
C     THE FOLLOWING LINES OF CODE COMPUTE THE SPECTRAL SPREADS
C OF THE POWER SPECTRUM.
C*****************************************************************
      XSUMPT=0.0
      XSUMIT=0.0
      DO 9878 I=1,17
      XSUMI=0.0
      DO 9876 J=1,32
      XSUMI=XSUMI+XREAL(I,J)
9876  CONTINUE
      XSUMIT=XSUMIT+XSUMI*(I-17)**2
      XSUMPT=XSUMPT+XSUMI




9878  CONTINUE
      APRIME=2*SQRT(XSUMIT/XSUMPT)
      XSUMPT=0.0
      XSUMJT=0.0
      DO 9879 J=1,17
      XSUMJ=0.0
      DO 9877 I=1,32
      XSUMJ=XSUMJ+XREAL(I,J)
9877  CONTINUE
      XSUMJT=XSUMJT+XSUMJ*(J-17)**2
      XSUMPT=XSUMPT+XSUMJ
9879  CONTINUE
```

```
      BPRIME=2*SQRT(XSUMJT/XSUMPT)
      PRATIO=(XSUMPT-XREAL(17,17))/XREAL(17,17)
      DO 43 I=1,32
      DO 43 J=1,32
      IF(XREAL(I,J).LE.0) GO TO 555
      XREAL(I,J)=10.0*ALOG10(XREAL(I,J)/QMAX)
      GO TO 43
555   XREAL(I,J)=-1000.0
43    CONTINUE
      WRITE(6,2838)
      WRITE(6,2836) IRANGE,JRANGE
2836  FORMAT(' TWO-DIMENSIONAL SPECTRUM OF ',I4,I4)
      WRITE(6,2837)
      WRITE(6,1357) IPEAK,JPEAK
      WRITE(6,2837)
1357  FORMAT(' PEAK FREQ VALUE AT ',I4,I4)
      WRITE(6,9873) APRIME,BPRIME
      WRITE(6,2837)
9873  FORMAT(' BANDWIDTHS AZIMUTH-RANGE: ',F15.2,F15.2)
      CALL PLOT(XREAL,32,32)
      DO 88 I=1,8
      WRITE(6,7777) (XRIND(I,J),J=1,4)
7777  FORMAT(4E15.8)
88    CONTINUE
      REWIND 1
9999  CONTINUE
      WRITE(6,999)
999   FORMAT(' FINISSIMO ')
200   FORMAT(64F10.3)
      STOP
      END
```

```
C**************************************************************
C    SUBROUTINE PAD PADS THE INPUT SEQUENCE TO THE DESIRED LENGTH.
C NSIZE IS THE LENGTH OF THE INPUT SEQUENCE AND NSQR IS THE LENGTH
C OF THE PADDED SEQUENCE.
C******************************************************************
      SUBROUTINE PAD(XR,NSIZE,NSQR)
      DIMENSION XR(NSQR,NSQR)
      NQ=NSIZE+1
      DO 40 I=NQ,NSQR
      DO 40 J=1,NSQR
      XR(I,J)=0.0
40    CONTINUE
      DO 41 I=1,NSIZE
      DO 41 J=NQ,NSQR
      XR(I,J)=0.0
41    CONTINUE
      RETURN
      END


C*************************************************************
C    SUBROUTINE TAPER TAPERS THE INPUT SEQUENCE SO THAT THE EFFECTS
C OF THE FINITE LENGTH DATA WINDOW ARE REDUCED.  THE TAPER USED
C IS A RAISED COSINE. THE WIDTH IS VARIABLE BY CHANGING NWIDTH.
C NSIZE IS THE INPUT SEQUENCE LENGTH.  THE TAPER IS APPLIED IN A
C RECTANGULAR FASHION TO ALL FOUR EDGES OF THE SEQUENCE.
C NSQR IS THE LENGTH OF THE PADDED SEQUENCE.
C*****************************************************************
      SUBROUTINE TAPER(XR,NWIDTH,NSIZE,NSQR)
      DIMENSION XR(NSQR,NSQR)
      PI=3.141593
      DO 28 I=1,NWIDTH
      RSDCOS=0.5+0.5*COS((I-1)*PI/NWIDTH+PI)
      DO 33 J=1,NSIZE
      XR(I,J)=RSDCOS*XR(I,J)
      K=NSIZE-I+1
```

```
      XR(K,J)=RSDCOS*XR(K,J)
35    CONTINUE
25    CONTINUE
      DO 24 J=1,NWIDTH
      RSDCOS=0.5+0.5*COS((J-1)*PI/NWIDTH+PI)
      DO 34 I=1,NSIZE
      XR(I,J)=RSDCOS*XR(I,J)
      K=NSIZE-J+1
      XR(I,K)=RSDCOS*XR(I,K)
34    CONTINUE
24    CONTINUE
      RETURN
      END
C*****************************************************************
C  SUBREROUTINE SQUARE READS IN A SQUARE SECTION OF THE RADAR
C CLUTTER MAP.  ARRAY MAY BE CHANGED FROM REAL TO INTEGER OR
C VICE VERSA SO THAT THE INPUT FILE MAY BE READ IN THE APPROPRIATE
C FORMAT.  SQUARE READS IN EVERY AZIMUTH AND PLACES THOSE VALUES
C THAT ARE BETWEEN ISTART, IEND, JSTART AND JSTART+NSIZE.
C ISTART AND JSTART ARE THE MINIMUM AZIMUTH AND RANGE CELL
C IN THE DESIRED SEQUENCE. NSIZE IS THE LENGTH OF THE
C INPUT SEQUENCE AND NSQR IS THE PADDED SEQUENCE LENGTH.
C*****************************************************************
      SUBROUTINE SQUARE(XR,ISTART,JSTART,NSIZE,NSQR)
      DIMENSION XR(NSQR,NSQR)
      INTEGER ARRAY(240)
      IEND=ISTART+NSIZE
      ISTRT=ISTART-1
      JSTRT=JSTART-1
      DO 26 I=1,81
      READ(1,100) (ARRAY(J),J=1,240)
100   FORMAT(20I4)
      IF((I.LT.ISTART).OR.(I.GE.IEND)) GO TO 26
      DO 26 J=1,NSIZE
      XR(I-ISTRT,J)=(ARRAY(JSTRT+J))/1.0
26    CONTINUE
      RETURN
      END
```

```
C*************************************************************
C    SUBROUTINE VAR COMPUTES THE MEAN AND VARIANCE OF A SQUARE
C SEQUENCE OF LENGTH NSQR.
C*************************************************************
      SUBROUTINE VAR(XR,NSQR)
      DIMENSION XR(NSQR,NSQR)
      TAVG=0.0




      DO 55 I=1,NSQR
      PAVG=0.0
      DO 56 J=1,NSQR
56    PAVG=PAVG+XR(I,J)
      TAVG=TAVG+PAVG/(NSQR*NSQR)
55    CONTINUE
      TVAR=0.0
      DO 57 I=1,NSQR
      PVAR=0.0
      DO 58 J=1,NSQR
58    PVAR=PVAR+(XR(I,J)-TAVG)*(XR(I,J)-TAVG)
      TVAR=TVAR+PVAR/(NSQR*NSQR-1)
57    CONTINUE
      WRITE(6,333) TAVG,TVAR
333   FORMAT(' MEAN= ',E16.8,' VARIANCE= ',E16.8)
      RETURN
      END
C***********************************************************
C     SUBROUTINE WINDOW APPLIES A RAISED COSINE LAG WINDOW TO
C THE TWO-DIMENSIONAL AUTOCORRELATION FUNCTION.  THE WINDOW
C IS ROTATED AROUND THE LAG PLANE ORIGIN. THE WIDTH OF THE
C WINDOW IS CONTROLLED BY WIDTH. NSIZE IS THE INPUT SEQUENCE
C LENGTH AND NSQR IS THE PADDED SEQUENCE LENGTH.
C***********************************************************
      SUBROUTINE WINDOW(XR,WIDTH,NSIZE,NSQR)
      DIMENSION XR(NSQR,NSQR)
      PI=3.141593
```

```
      NG=NSIZE+1
      DO 23 I=1,NSIZE
      DO 23 J=1,NSIZE
      RANGE=((I-1)**2+(J-1)**2)**0.5
      RSDCOS=0.5+0.5*COS(RANGE*PI/WIDTH)
      IF(RANGE.GE.WIDTH) RSDCOS=0.0
      K=NSQR-I+2
      L=NSQR-J+2
      XR(I,J)=RSDCOS*XR(I,J)
      IF((K.EQ.NQ).OR.(L.EQ.NQ)) RSDCOS=0.0
      IF((K.GT.NSQR).OR.(L.GT.NSQR)) GO TO 23
      XR(I,L)=RSDCOS*XR(I,L)
      XR(K,L)=RSDCOS*XR(K,L)
      XR(K,J)=RSDCOS*XR(K,J)
23    CONTINUE
      RETURN
      END
C***********************************************************
C     SUBROUTINE DC COMPUTES THE DC VALUE OF A SEQUENCE, XR.
C ALL OR PART OF THE SEQUENCE MAY BE CONSIDERED IN THE
C CALCULATION.  NSIZE IS THE LENGTH THAT WILL BE CONSIDERED
C AND NSQR IS THE DIMENSION OF THE SQUARE ARRAY.
C***********************************************************
      SUBROUTINE DC(XR,NDCVAL,NSQR)
      DIMENSION XR(NSQR,NSQR)
      COMMON DCVALT
      DCVAL=0.0
      DCVALT=0.0
      SIZE=FLOAT(NDCVAL)**2
      DO 25 I=1,NDCVAL
      DO 35 J=1,NDCVAL
35    DCVAL=DCVAL+XR(I,J)
      DCVALT=DCVALT+DCVAL/SIZE
      DCVAL=0.0
```

```
2,    CONTINUE
995   FORMAT(' DCVAL= ',F15.3)
      RETURN
      END
C*****************************************************************
C     THIS PLOTTING ROUTINE IS AN EIGHT LEVEL GRAY-SCALE, LINE
C PRINTER PLOT GENERATOR.  IT MAY BE REPLACED WITH PLOT3D WHICH
C IS AVAILABLE ON MUSIC OR ANY OTHER APPROPRIATE PLOT ROUTINE.
C*****************************************************************
      SUBROUTINE PLOT(XLINE,MAXV,MAXH)
C  GRAY SCALE PROGRAM...
      INTEGER*2 GRAY
      REAL*4 XLINE(MAXV,MAXH),THRESH(8)
      IMID=MAXH/2+1
111   FORMAT(' XREAL(1,1)= ',E16.8,' XREAL(33,33)= ',E16.8)
      LOGICAL*1 SCALE(8),PLINE(64)
C READ IN THE GRAY SCALE SYMBOLS...
      READ(5,5)(SCALE(I),I=1,8)
5     FORMAT(8A1)
C
C
C  READ THE LOWEST VALUE FOR EACH GRAY LEVEL.
      DO 10 I=2,8
      READ(5,100) THRESH(I)
      II=I-1
      WRITE(6,101) SCALE(II),THRESH(I)
1     CONTINUE
      WRITE(6,102) SCALE(8),THRESH(8)
C  READ MAX HORIZ. AND VERT. AXIS VALUES. (<= 128; <= 64)
      WRITE(6,201) MAXV,MAXH
      WRITE(6,999)
9..   FORMAT('      ',8('0123456789'))
      DO 20 I=1,MAXV
      DO 30 J=1,MAXH
      GRAY=1
      DO 40 K=2,8
      IF (XLINE(I,J) .LT. THRESH(K)) GO TO 40
```

```
      GRAY=K
4     CONTINUE
      PLINE(J)=SCALE(GRAY)
3     CONTINUE
      WRITE(6,400) I,(PLINE(J),J=1,MAXH)
2     CONTINUE
100   FORMAT(F16.1)
101   FORMAT(' SYMBOL''',A1,''' <',F16.1)
102   FORMAT(' SYMBOL''',A1,'''=>',F16.1)
201   FORMAT(' MAXV=',I4,' MAXH=',I4,/)
200   FORMAT(2I4)
400   FORMAT(' ',I4,64A1)
300   FORMAT(64F15.1)
      RETURN
      END
C***************************************************************
C     SUBROUTINE FFT PERFORMS A FAST FOURIER TRANSFORM OF THE
C ROWS AND COLUMNS OF XREAL AND XIMAG.  IT IS CALLED FROM FFT2D.
C THIS FFT ROUTINE WAS OBTAINED FROM DR. MEYER.
C****************************************************************
      SUBROUTINE FFT(C,D,N,NEWI,NSTUE,IK)
      DIMENSION C(128),D(128)
      DIMENSION CO(128),SI(128)
      INTEGER P




      PI2=8.0*ATAN(1.0)
      DO 13 J=1,9
      M=J
      IF(N-2**M)13,12,13
   13 CONTINUE
   12 CONTINUE
      IF(IK.NE.1) GO TO 433
  434 FORMAT(1H0,'*****   INVERSE TRANSFORM   *****')
  433 CONTINUE
```

```
      NN=1
      NA=N/2
      XN=N
      NB=NA
      CU 16 I=1,N
      IA=0
      IC=I-1
      DO 15 J=1,M
      P=M-J
      F=2**F
      IB=IC/P
      IC=IC-IB*P
      F=2**(J-1)
 15   IA=IA+IB*P
      IA=IA+1
      IF(I.GE.IA) GO TO 166
      A=C(I)
      B=D(I)
      C(I)=C(IA)
      C(IA)=A
      D(I)=D(IA)
      D(IA)=B
 166  CONTINUE
 16   CONTINUE
      X=N
      X=PI2/X
      CO(1)=1.0
      SI(1)=0.0
      DC 3 J=1,M
      IF(NN.EQ.1)GO TO 5
      DC 6 L=1,NC
      I=NC-L+1
      K=2*I-1
      CO(K)=CO(I)
 6    SI(K)=SI(I)
      P=0
      DO 1 L=1,NC
      P=P+NE
      U=CCS(X*P)
```

```
      V=-SIN(X*P)
      IF(IK.EQ.1)V=-V
      IA=2*L
      CC(IA)=U
      SI(IA)=V
    1 P=P+NB
    5 P=1
      II=0
      DO 2 I=1,NA
      II=II+1
      KKK=P+NN
      A=C(KKK)*CC(II)-D(KKK)*SI(II)
      B=C(KKK)*SI(II)+D(KKK)*CC(II)



      C(KKK)=C(P)-A
      D(KKK)=D(P)-B
      C(P)=C(P)+A
      D(P)=D(P)+B
      IF(II.LT.NN)GO TO 77
      II=0
      P=P+NN
   77 P=P+1
    2 CCNTINUE
      NC=NN
      NB=NB/2
      NN=2*NN
    3 CCNTINUE
      RETURN
      END
```

```
C*****************************************************************
C     SUBROUTINE FFT2D PERFORMS THE TWO-DIMENSIONAL FOURIER
C TRANSFORM OF THE SQUARE SEQUENCE AR.  THIS IS DONE BY
C APPLYING SUBROUTINE FFT TO THE ROWS AND COLUMNS OF AR.
C FFT2D WAS WRITTEN BY WILLIAM LADEW.
C************************************************************************
      SUBROUTINE FFT2D(AR,AI,N,IK,IM)
      REAL AR(N,N),AI(N,N),XR(128),XI(128)
C
C ARRAY AR(N,N) IS REAL PART OF NUMBERS
C ARRAY AI(N,N) IS IMAGINARY PART.
C N IS LENGTH OF SQUARE ARRAY
C N MUST BE LESS THAN OR EQUAL TO 128
C
C IK =0 IS FFT
C IK =1 IS INVERSE FFT
C IK =1 ALSO INFLICTS A DIVIDE BY N**2 ON THE DATA AFTER THE FFT
C
C IM =0 NORMAL FFT
C IM =1 RETURNS MAGNITUDE OF WHOLE THING (IMAG. PART SET TO 0.)
C
C
C TRANSFORM ROW BY ROW
C
      DO 10 I=1,N
         DO 20 J=1,N
            XR(J) = AR(I,J)
            XI(J) = AI(I,J)
20          CONTINUE
         CALL FFT(XR,XI,N,0,0,IK)
         DO 30 J=1,N
            AR(I,J) = XR(J)
            AI(I,J) = XI(J)
30          CONTINUE
10       CONTINUE
```

```
C
C TRANSFCRM CULUMN EY COLUMN
C
      DO 40 J=1,N
         DO 50 I=1,N
            XR(I) = AR(I,J)
            XI(I) = AI(I,J)
50          CONTINUE
         CALL FFT(XR,XI,N,0,0,IK)
         DC 60 I=1,N
            AR(I,J) = XR(I)



            AI(I,J) = XI(I)
6           CCNTINUE
40       CONTINUE
      IF (IK .NE. 1) GO TO 1CC
      DC 90 I=1,N
      DC 9C J=1,N
      AR(I,J) = AR(I,J)/(N**2)
      AI(I,J) = AI(I,J)/(N**2)
90    CCNTINUE
100   CONTINUE
      IF (IM .EQ. C) RETURN
      DC 200 I=1,N
      DC 2CC J=1,N
      AR(I,J) = SQRT(AR(I,J)**2 + AI(I,J)**2)
      AI(I,J) = 0.
200   CCNTINUE
      RETURN
      END
```

```
C**********************************************************
C    KRUSKALRPT PERFORMS THE KRUSKAL-WALLIS TEST ON THE
C THREE-DIMENSIONAL RADAR DATA.
C    SUBROUTINE SQUARE READS THE BACKSCATTER VALUES FROM
C THE DATA FILE THAT APPEAR IN A WINDOW SIZE DETERMINED
C BY IAZMTH AND JRANGE.
C    THE DATA SHOULD ALREADY HAVE BEEN SAMPLED FOR SA
C INDEPENDENCE BEFORE KRUSKALRPT PROCESSES IT.
C**********************************************************
      SUBROUTINE SQUARE(XR,ISTART,JSTART,NAZMTH,NRANGE)
      DIMENSION XR(8,10,10),ARRAY(128)
      IEND=ISTART+NAZMTH
      ISTRT=ISTART-1
      JSTRT=JSTART-1
      DO 26 I=1,8
      DO 26 L=1,10
      READ(1,101) (ARRAY(J),J=1,128)
101   FORMAT(E16.8)
      IF((I.LT.ISTART).OR.(I.GE.IEND)) GO TO 26
      DO 26 J=1,NRANGE
      XR(I-ISTRT,L,J)=ARRAY(JSTRT+J)/1.0
26    CONTINUE
      RETURN
      END
C**********************************************************
C  TH  ARRAY CLTTR HOLDS THE VALUES WHICH APPEAR IN THE
C WINDOW AS IT PASSES OVER THE DATA.  T HOLDS THE COLUMN
C SUMS.
C**********************************************************
      DIMENSION CLTTR(8,10,10),T(10,10)
      DO 1111 II=1,8,2
      DO 2222 JJ=1,128,2
      WRITE(6,1234) II,JJ
1234  FORMAT(' AZIMUTH, RANGE STARTING POINT:',I4,I4)
      CALL SQUARE(CLTTR,II,JJ,2,2)
      DO 5 I=1,2
      DO 5 J=1,10
      WRITE(6,222) (CLTTR(I,J,K),K=1,2)
222   FORMAT(2E16.8)
```

```
5     CONTINUE
      GMAX=0.0
      NAZMTH=2
      NRANGE=2
      N=2*2*10
      DO 2 L=1,N
      QMAX=0.0
C**************************************************************
C  THE FOLLOWING SET OF NESTED LOOPS RANKS THE BACKSCATTER
C VALUES.
C*****************************************************************
      DO 1 I=1,NAZMTH
      DO 1 J=1,10
      DO 1 K=1,NRANGE
      IF(GMAX.GT.CLTTR(I,J,K)) GOTO 1
      GMAX=CLTTR(I,J,K)
      IMAX=I
      JMAX=J
      KMAX=K
1     CONTINUE
      CLTTR(IMAX,JMAX,KMAX)=-L
2     CONTINUE




      DO 3 I=1,NAZMTH
      DO 3 J=1,10
      DO 3 K=1,NRANGE
      CLTTR(I,J,K)=N+1+CLTTR(I,J,K)
3     CONTINUE
C************************************************************
C   THE FOLLOWING WRITE THE VALUES AND THEIR RANKS IN
C A T BLE.
C***************************************************************
      DO 4 I=1,NAZMTH
      WRITE(6,100) I
100   FORMAT(' AZIMUTH # ',I2)
```

```
      DO 4 J=1,10
      WRITE(6,111) (CLTTR(I,J,K),K=1,2)
111   FORMAT(2F16.1)
4     CONTINUE
C*****************************************************************
C   THE FOLLOWING COMPUTES THE COLUMN SUMS AND THEIR SQUARES.
C*****************************************************************
      TSUMSQ=0.0
      DO 7 I=1,NAZMTH
      DO 7 K=1,NRANGE
      CSUM=0.0
      DO 8 J=1,10
      CSUM=CSUM+CLTTR(I,J,K)
8     CONTINUE
      T(I,K)=CSUM
      WRITE(6,777) I,K,T(I,K)
777   FORMAT(' COLUMN SUM(',I2,',',I2,')=',F16.8)
      TSUMSQ=TSUMSQ+T(I,K)**2
7     CONTINUE
C******************************************************
C   THE TEST STATISTIC IS COMPUTED IN H.
C******************************************************
      H=(-3.*(N+1)+(12./(N*(N+1)*10))*TSUMSQ)
      WRITE(6,333) TSUMSQ
333   FORMAT(' TSUMSQ=',F16.8)
      WRITE(6,888)
888   FORMAT(/)
      WRITE(6,999) H
999   FORMAT(' H=',F16.8)
      REWIND 1
2222  CONTINUE
1111  CONTINUE
      STOP
      END
```

References

1. David K. Barton, Radars- Volume 5- Radar Clutter, Dedham, MA: Artech House, Inc., 1975.
2. Merrill I. Skolnik, Introduction to Radar Systems, New York: McGraw-Hill, Inc., 1962.
3. H. E. King, C. J. Samites, D. E. Snow , and R. I. Collinton, "Terrain Backscatter Measurements at 40 to 90 GHz", IEEE Trans. on Antennas and Propagation, vol. 18, no. 6, Nov. 1970.
4. H. Krason and G. Randig, "Terrain Backscatter Characteristics at Low Grazing Angles for X- and S-band", Proc. IEEE, vol. 54, no. 12, Dec. 1966.
5. R. L. Cosgriff, W. H. Peake, and R. C. Taylor, "Terrain Scattering Properties for Sensor System Design (Terrain Handbook II)", Engineering Experiment Station Bulletin No. 181, The Ohio State University, Columbus, OH, May 1960.
6. F. M. Dickey et. al., "Moisture Dependency of Radar Backscatter from Irrigated and Non-irrigated Fields",IEEE Trans. on Geophysics and Electronics, vol. 12, no. 1, Jan. 1974.

7. S. Rosenbaum and L. W. Bowles, "Clutter Return from Vegetated Areas", IEEE Trans. on Antennas and Propagation, vol. 22, no. 2, May 1974.

8. S. B. Kesler and S. Haykin, "The Maximum Entropy Method Applied to the Spectral Analysis of Radar Clutter", IEEE Trans. on Information Theory, vol. 24, no. 2, 1978.

9. S. Haykin, "Spectral Classification of Radar Clutter Using the Maximum Entropy Method", NATO Advanced Study on Pattern Recognition and Signal Processing, Series #E-29, 1978.

10. F. E. Nathanson and J. P. Reilly, "Clutter Statistics Which Affect Radar Performance Analysis", IEEE Trans. on Aerospace and Electronic Systems, vol. 3, no. 6 (Eastcon Suppl.), Nov. 1967.

11. L. M. Spetner, I. Katz, "Two Statistical Models for Radar Terrain Returns", IRE Trans. on Antennas and Propagation, vol. 8, no. 3, May 1960.

12. W. J. Szajnowski, "Testing the Independence of Non-homogeneous Rayleigh Clutter", IEEE Trans. on Aerospace and Electronic Systems , vol. 16, no. 3, May 1980.

13. J. V. Bradley, Distribution-Free Statistical Tests, Englewood Cliffs, NJ: Prentice-Hall, Inc., NJ, 1968.

14. Klauder et. al., "The Theory and Design of Chirp Radars", BSTJ, vol. 39, no. 4, July 1960.

15. A. Hald, Statistical Theory with Engineering Applications, New York: Jchn Wiley & Sons, Inc., 1952.

16. G. M. Jenkins and D. G. Watts, Spectral Analysis and its applications, San Francisco: Holden-Day, Inc., 1968.

17. T. S. Huang, "Two-dimensional Windows", IEEE Trans. on Audio Electroacoust., vol. 20, no. 1, 1972.

18. W. Kruskal and W. A. Wallis, "Use of Ranks in One-Criterion Variance Analysis", Journal of the American Statistical Association, vol. 47, pp. 583-621, 1952.

19. Webster's New Collegiate Dictionary, Springfield, MA: G. &C. Merriam Co., 1980.

MISSION
of
Rome Air Development Center

RADC plans and executes research, development, test and selected acquisition programs in support of Command, Control Communications and Intelligence (C^3I) activities. Technical and engineering support within areas of technical competence is provided to ESD Program Offices (POs) and other ESD elements. The principal technical mission areas are communications, electromagnetic guidance and control, surveillance of ground and aerospace objects, intelligence data collection and handling, information system technology, ionospheric propagation, solid state sciences, microwave physics and electronic reliability, maintainability and compatibility.

END

DATE
FILMED

05-82

DTIC